Long-Term Change of the Secchi Disk Depth in Indonesian Lakes Shown by Landsat TM and ETM+ Data

January 2021

Fajar Setiawan

Long-Term Change of the Secchi Disk Depth in Indonesian Lakes Shown by Landsat TM and ETM+ Data

A Dissertation Submitted to
the Graduate School of Life and Environmental Sciences,
the University of Tsukuba
in Partial Fulfillment of the Requirements
for the Degree of Doctor of Philosophy
(Doctoral Program in Integrative Environment and Biomass Sciences)

Fajar Setiawan

Abstract

Most of Indonesia's lakes face environmental problems such as eutrophication, sedimentation, and depletion of dissolved oxygen. The water quality database for supporting lake management in Indonesia is very limited due to financial constraints. The remote sensing technique shows great potential to retrieve water quality data from space to address this issue.

I made two efforts to improve the robustness of the Secchi Disk Depth (SD) estimation model using Landsat TM & ETM+. First, I carried out image preprocessing, which includes removing contaminated water pixels, filtering images to reduce noise effects, and mitigating atmospheric effects before using Landsat data. For removing contaminated water pixels, I used a 90 m buffer to avoid adjacency effects from land and reflectance effects from the lake bottom. I also further removed clouds and cloud shadows by combining two water indices, Normalized Different Water Index (NDWI) and Modified Normalized Different Water Index (MNDWI). After that, the data quality of Landsat was improved by iteratively applied a median filter. For mitigating atmospheric effects, I used a two-step atmospheric correction method to avoid the requirement of ancillary data for correcting aerosol effects. In the first step, I carried out a Rayleigh scattering correction using the Second Simulation of the Satellite Signal in the Solar Spectrum (6S) radiative transfer model. In the second step, I further mitigated aerosol scattering pixel-by-pixel by subtracting the minimum of the Rayleigh-corrected-reflectance at the near-infrared or middle-infrared bands from those at the visible bands.

In the second effort, I selected two-band ratios (TM1/TM2 and TM3/TM2) as SD predictors (i.e., model BF). This selection differs from previous studies' recommendations. To develop SD estimation models, I used the preprocessed Landsat data and in situ-measured SD collected from nine Indonesian lakes/reservoirs (SD values 0.5–18.6 m) and a regression/multiple-regression analysis technique. In total, 42 SD estimation models were obtained (three single-band models, six band-ratios models, 18 band-ratios and single-bands

models, and 15 two-band ratios models). After excluding the estimation models with lower performance (R^2 <0.9 and RMSE >2.5 m), the remained 17 models were validated using in situ data collected from Lake Maninjau (SD ranged from 0.5 to 5.8 m, n = 74). To select an SD estimation model with the best performance, I used the Taylor diagram to show the standard deviation, correlation (r), and root means square error (RMSE) simultaneously in one diagram. As a result, I found the Model BF is the best SD estimation model, which retrieved SD values with an R^2 of 0.60 and the RMSE of 1.01 m in Lake Maninjau. In addition, since water-leaving reflectance at the green band (TM2) does not change as much as that at the blue and red bands (TM1 and TM3) in various waters, the use of this value to normalize water-leaving reflectance at blue and red bands can avoid a large of fluctuation ratios.

Then, I applied the selected Model BF to 23 Indonesian lakes, which were investigated in the 1990s by other researchers, and 14 Indonesian lakes, which I investigated between 2014 and 2018, to further confirm the performance of the Model BF. The results showed that the estimated SD from Landsat data using the Model BF generated reasonable SD values, except for lakes with inferior image quality and a large time gap between satellite acquirements and in situ measurements. The SD estimations in high and extreme turbid lakes were reasonable but slight underestimations in clear lakes. These results increase the confidence in applying the developed model to other lakes and periods.

As showcases, I applied the Model BF to Lake Maninjau, Lake Singkarak, and Lake Toba for generating a long-term SD database from Landsat time-series data. The visual comparison of the in situ-measured and satellite estimated SD values and several events (e.g., algal bloom, water management, and fish culture). The Landsat-based SD estimations well captured the change tendency of water transparency in three lakes. These results further demonstrate the developed model's reliability to generate a long-term SD database from the Landsat series.

Finally, I generated a database to show the long-term change of the SD in Indonesian lakes with area > 10 km^2 (35 lakes). I found three patterns of SD changing trend: 13 lakes with significantly increased SD, eight lakes with significantly decreased SD, and 14 lakes with no significant changed during 2000-2019. This database is expected to provide useful information for lake managers and policymakers to support inland water sustainable management.

Keywords: water transparency; historical Landsat data; empirical model; Indonesian lakes; atmospheric correction

List of Contents

List of Tables

List of Figures

List of Symbols

a, b, and c	=	model coefficients obtained using the calibration data
$B_{rescale}$	=	band-specific rescaling bias factor from Chander et al. (2009)
c	=	beam attenuation coefficient (m^{-1})
$G_{rescale}$	=	band-specific rescaling gain factor from Chander et al. (2009)
Kd	=	vertical diffuse attenuation coefficient (m^{-1})
ln (SD)	=	natural Logarithm transformed Secchi Disk Depth
L_λ	=	spectral radiance at the sensor's aperture [$W/(m^2 \cdot sr \cdot \mu m)$]
n	=	number of samples
P	=	p-value
QCAL	=	quantized calibrated pixel value [DN]
R	=	correlation coefficient
R^2	=	determination coefficient
$R_c(\lambda)$	=	atmospherically corrected reflectance
$R_{rc}(\lambda)$	=	Rayleigh corrected reflectance
$R_{rc}(4)$	=	Rayleigh corrected reflectance at Landsat TM/ETM+ Band 4
$R_{rc}(5)$	=	Rayleigh corrected reflectance at Landsat TM/ETM+ Band 5
xa, xb, and xc	=	coefficients calculated using 6S code
dgreen	=	DN values at the green band
dNIR	=	DN values at the Near Infrared band
dSWIR	=	DN values at the Short Wave Infrared band

List of Abbreviations

6S	=	Second Simulation of the Satellite Signal in the Solar Spectrum
BQA	=	Band Quality Assessment
Chl-a	=	Chlorophyll-a concentration
DN	=	Digital Number
ETM+	=	Enhanced Thematic Mapper plus
GCP	=	Ground Control Point
GOCI	=	Geostationary Ocean Color Imager
GPS	=	Global Positioning System
LIPI	=	Indonesian Institute of Science
LOESS	=	Locally Weighted Scatterplot Smoothing
MERIS	=	Medium Resolution Imaging Spectrometer
MNB	=	Mean Normalized bias
MNDWI	=	Modified Normalized Different Water Index
MODIS A	=	Moderate Resolution Imaging Spectroradiometer Aqua
MTL	=	Metadata File
n.d.	=	not defined
NDWI	=	Normalized Different Water Index
nm	=	nano meter
NMAE	=	Normalized Mean Absolute Error
NSME	=	Nash–Sutcliffe Model Efficiency
OLI	=	Operational Land Imager (Landsat 8^{th} generation)
(R)	=	Reservoir
RCL	=	Research Center for Limnology
RMS	=	Root Mean Square

RMSE	=	Root Means Square Error
S2	=	Sentinel-2
S3	=	Sentinel 3
SD	=	Secchi Disk Depth
SeaWIFS	=	Sea-viewing Wide Field-of-view Sensor
SLC	=	Scan Line Corrector
SNR	=	signal-to-noise ratio
TM	=	Thematic Mapper
TM1	=	preprocessed Landsat TM/ETM+ band 1
TM2	=	preprocessed Landsat TM/ETM+ band 2
TM3	=	preprocessed Landsat TM/ETM+ band 3
TSS	=	total suspended solid
USGS	=	United States Geological Survey
WIA	=	Willmott Index of Agreement

Chapter I General Introduction

Lakes are essential for humans as they provide water for domestic, industrial, and agricultural use and provide food. Despite their fundamental importance to humans, freshwater systems, including lakes, have been affected by anthropogenic disturbances. The disturbances caused eutrophication, acidification, and contamination by toxic substances. This problem is predicted to increase, especially in developing countries where the developments prioritize other than environmental conservation (Brönmark et al., 2002).

Indonesia has 1034 lakes identified from Landsat data (Hamzah, 2019). There are 60 lakes with an area larger than 10 km^2, including 50 natural lakes and ten reservoirs. These lakes are used as essential water resources for domestic life, industry, agriculture, transportation, energy, fisheries, and tourism (Sulastri, 2006). However, most of these waters face environmental problems such as eutrophication, sedimentation, and dissolved oxygen depletion. These problems are due mainly to untreated domestic/industrial/agricultural waste, deforestation in watersheds, and fish cultures in lakes (Ministry of Environment of the Republic Indonesia, 2011). Thus, it is crucial to routinely monitor the water quality in these lakes and reservoirs to obtain scientific data for their sustainable use.

1.1 Water Quality Database of Indonesian Lakes

A time series of water quality data (database) is critical to investigate how the water quality of lakes is changing over the years. Water quality data can be used as a benchmark for environmental management projects (plan-action-evaluation cycle). However, there is no existing water quality database for Indonesian lakes. As a result, it is not easy to evaluate the lakes objectively.

The available water quality data supporting lake management in Indonesia are very limited due to financial constraints. In 2011, the Indonesian government started a 5-year joint project to determine effective management policies for sustainable use of lakes (Ministry of Environment of the Republic Indonesia, 2011). The Ministry of Environment selected the 15 lakes with the most urgent situations. Lake Maninjau is one of the 15 priority lakes. With a total of 186 Secchi disk depth (SD) measurements taken during 2001–2018, Lake Maninjau has the greatest amount of available water quality data in Indonesia. Except for this dataset, only fragmentary water quality data exist for a few Indonesian lakes and reservoirs (Ruttner., 1930; Lehmusluoto et al., 1997).

1.2. Water Quality Monitoring Methods

Water quality data can be directly measured in a lake by performing a field survey or estimated using remote sensing data. By conducting field surveys, we can measure high accuracy data at each layer of water. However, this conventional method is time-, labor-, and cost-consuming. The other disadvantages are the limited temporal and spatial coverages. As a consequence, the amount of in situ water quality data is limited.

On the other hand, satellite remote sensing has been recognized as a supportive and powerful tool for collecting spatial and temporal water quality data, especially for lakes without available in situ data (Blondeau et al., 2014; Bonansea et al., 2015; Dörnhöfer et al., 2016; Gholizadeh et al., 2016; Giardino et al., 2001; Kloiber et al., 2002; Kutser., 2012; Olmanson et al., 2008; Olmanson et al., 2011; Olmanson et al., 2016; Oyama et al., 2009; Zheng et al., 2015). Remote sensing data can address the limitation of temporal and spatial coverages. The historical data archive is the other advantage. The use of remote sensing techniques can thus provide opportunities to generate a water-quality database for Indonesian lakes and reservoirs.

1.3. Remote Sensing Data Source for Water Quality Estimation

The first requirement for generating a water quality database from space is the availability of satellite data. Since no operational ocean color sensors are available before 1997 (Blondeau-Patissier et al., 2014) and all ocean color sensors have relatively coarse spatial resolutions (>300 m), Landsat TM/ETM+ data (obtained since 1984 with 30 m spatial resolutions) are often used to estimate the long-term changes of inland waters' water-quality parameters (Olmanson et al., 2008; Oyama et al., 2009; Kutser., 2012; Zheng et al., 2015; Lobo et al., 2015).

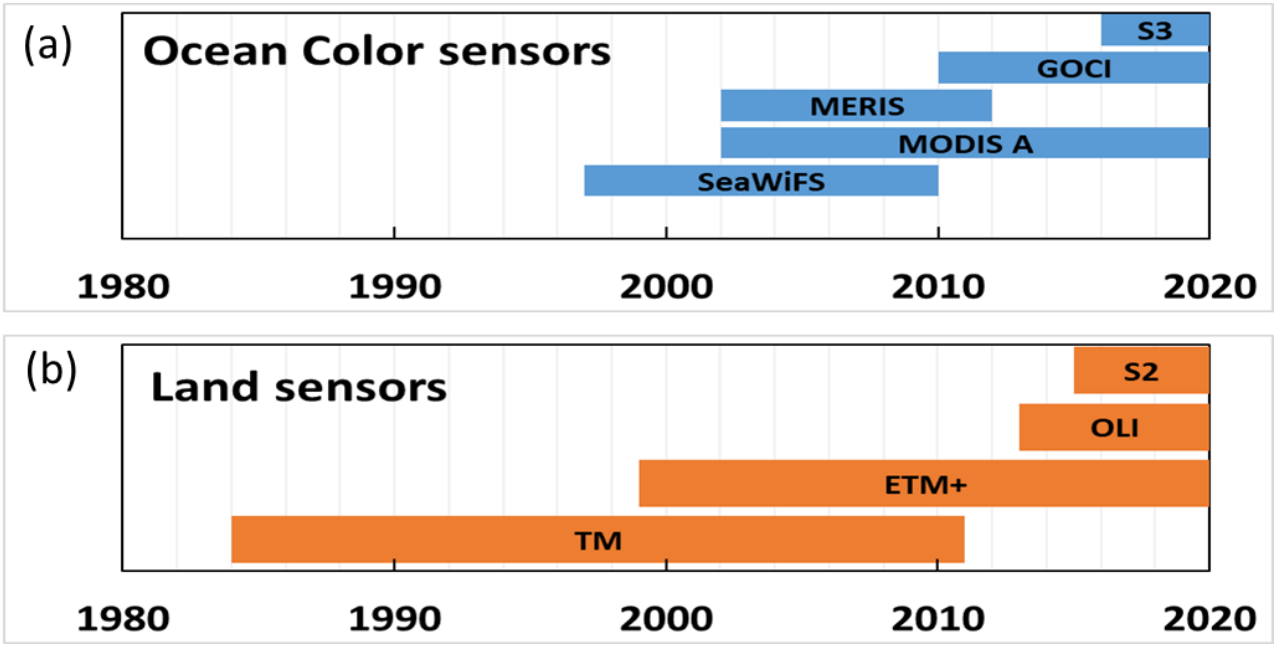

Figure 1.1. The active periods of several satellite sensors are used for studying waters, (a) Ocean Color sensors, and (b) Land sensors.

I list five primary ocean color sensors and four major land sensors that have been widely used for studying waters, as well as their active sensing periods (Figure 1.1). The ocean color sensors, including Sea-viewing Wide Field-of-view Sensor (SeaWiFS), Moderate Resolution Imaging Spectroradiometer Aqua (MODIS A), Medium Resolution Imaging Spectroradiometer (MERIS), Geostationary Ocean Color Imager (GOCI), and Sentinel-3 Ocean and Land Colour Instrument (S3-OLCI). For the land sensors including, Thematic Mapper (TM), Enhanced Thematic Mapper Plus (ETM+), Operational Land Imager (OLI), and Copernicus Sentinel-2 (S2).

The Sea-viewing Wide Field-of-view Sensor (SeaWiFS) collected data from September 1997 until the end of the mission in December 2010. The SeaWiFS were optimized for ocean color measurements. The SeaWiFS had eight spectral bands from 412 to 865 nm (central wavelengths: 412, 443, 490, 510, 555, 670, 765, and 865 nm). The SeaWiFS had a spatial resolution of 1,000 m and revisit time 1-2 days (Ocean Color-SeaWiFS, n.d.).

The Moderate Resolution Imaging Spectroradiometer Aqua (MODIS A) was launched in May 2002 (aboard the Aqua satellite MODIS A) and collecting data to present. It is a sensor for both land and water observations. The MODIS A has 36 spectral bands in total, of which nine bands are used for ocean-color remote sensing. MODIS A had a spatial resolution of 1,000 m and revisit time 1-2 days (Ocean Color-MODIS Aqua, n.d.).

The Medium Resolution Imaging Spectroradiometer (MERIS) was launched in March 2002 until December 2012. MERIS provided higher spectral and spatial resolutions but slightly lower temporal resolution and radiometric sensitivity. The spatial resolution is 300 m, and the revisit time is three days. The MERIS has 15 spectral bands in the 390-1040 nm range (The European Space Agency-MERIS, n.d). The new visible band around 620 nm and 709 nm made the MERIS useful to study alga blooms, chlorophyll-a in turbid inland and coastal waters (Kutser et al. 2006; Dall'Olmo et al. 2003; Gilerson et al. 2010; Gitelson et al. 2008; Gower et al. 2005).

The Geostationary Ocean Color Imager (GOCI) was launched in June 2010 by the Korea Aerospace Research Institute (KARI). The GOCI is a geostationary orbit sensor for monitoring ocean color from space (Ryu et al. 2012). GOCI has eight bands used for water quality monitoring. GOCI produces eight images during daylight with 500 m spatial resolution. GOCI covers only the regions of Korea, China, and Japan, and it cannot provide global data (Ocean Color-GOCI, n.d.).

The Sentinel-3 (S3) Ocean and Land Colour Instrument (OLCI) is an optical instrument used to provide MERIS data continuity. The S3-OLCI was designed to screen the ocean and land

surface and collect information related to biology (e.g., phenology of marine and terrestrial biomass). There are twin satellites of S3 (S3A and S3B). The S3A was launched in February 2016, followed by the S3B, launched in April 2018. The twin satellites were initially operated in a temporary tandem phase to allow for instrument inter-comparison. It has 21 spectral bands with a spatial resolution of 300 m and revisits time 2-3 days. The satellites provide land and ocean data, with the land data delivered by ESA (European Space Agency), while EUMETSAT (European Organization for the Exploitation of Meteorological Satellites) will be responsible for both the operation of the satellite and the processing and delivery of ocean data and additional atmosphere-related products (The European Space Agency-Sentinel-3, n.d)

The Landsat 5 Thematic Mapper (TM) was launched in March 1984 and ended the mission in November 2011. The Landsat TM has three bands in the visible range, one band in the NIR range, and two bands in the SWIR range (central wavelengths: 485, 569, 660, 840, 1676, 2223 nm). The Landsat TM spatial resolution is 30 m with 16 days revisit time. It is a sun-synchronous satellite that provides global data (Landsat Science-Landsat 5, n.d).

The Landsat 7 Enhanced Thematic Mapper Plus (ETM+) was launched in April 1999 and continuously sensing the earth until the present, despite Scan Line Corrector (SLC) failure on May 31, 2003. The ETM+ replicates the highly successful previous generation, the Thematic Mapper (TM). Like the Landsat TM, the Landsat ETM+ has three bands in the visible range, one band in the NIR range, and two bands in the SWIR range (central wavelengths: 485, 560, 662, 835, 1648, 2206 nm). The Landsat ETM+ spatial resolution is 30 m with 16 days revisit time. It is a sun-synchronous satellite that provides global data (Landsat Science-Landsat 7, n.d).

The Landsat 8 Operational Land Imager (OLI) is the successor of Landsat 5 Thematic Mapper (TM) and Landsat 7 Enhanced Thematic Mapper Plus (ETM+). The OLI was launched in February 2013. It provides coverage of the global landmass at a spatial resolution of 30 meters. The OLI collects data for two new bands, a coastal/aerosol band (band 1) and a cirrus band (band

9) and the heritage Landsat TM/ETM+. The OLI revisit time is 16 days at the equator (Landsat Science-Landsat 8, n.d).

The Copernicus Sentinel-2 (S2) are twin polar-orbiting satellites, Sentinel-2A (S2A), and Sentinel-2B (S2B), placed in the same sun-synchronous orbit, phased at 180° to each other. This setting aims to increase the revisit time (10 days at the equator with one satellite and five days with two satellites). The Sentinel-2A was launched in June 2015, followed by Sentinel-2A, which launched in March 2017. The S2 has 10 m spatial resolution for bands: B2 (490 nm), B3 (560 nm), B4 (665 nm), and B8 (842 nm). A 20 m spatial resolution for bands: B5 (705 nm), B6 (740 nm), B7 (783 nm), B8a (865 nm), B11 (1610 nm) B12 (2190 nm). A 60 m spatial resolution for bands: B1 (443 nm), B9 (940 nm), and B10 (1375 nm) (The European Space Agency-Sentinel-2, n.d).

Landsat TM/ETM+ is the most successful remote sensing satellite mission to observe the earth. Landsat has been collected and archived earth images regularly since early 1984, enabling extraction of some historical water quality information on lakes (Olmanson et al., 2008). The combination of temporal and spatial resolution and data availability makes the Landsat system particularly useful for assessing inland Lakes (Kloiber et al., 2002). Therefore, in the present study, I will use Landsat TM and ETM+ data to generate a long-term water quality database for Indonesian lakes.

1.4. Secchi Disk Depth (SD)

A key parameter to represent water quality is Secchi disk depth (SD). SD is usually measured using a white disk with a 20 to 30 cm diameter, lowered into the water until it visually disappears (Preisendorfer, 1986). SD is the most extended historical data of the water environment since the 1860s (Secchi, 1864). SD measurement method is the simplest and most often used for limnological studies because its values are easily understood (Carlson, 1977). SD represents water transparency, whose interpretation has broad applications from diverse visibility to climate change

studies (Lee et al., 2015). Generally, SD will decrease as Chl-a and suspended solid concentration increase and were used as an indirect eutrophication indicator (Karydis, 2009; Devlin et al., 2008).

Besides, unlike other water quality parameters such as chlorophyll-a concentrations, total suspended solids, and colored dissolved organic matters, SD represents the same optical properties of a waterbody as remote sensing data. Thus, it is considered the most suitable variable to be retrieved from the satellite data.

1.5. Models for Estimating SD from Remote Sensing

1.5.1. Semi-analytical Approach

The second requirement for generating a water quality database from space is the existence of estimation models. Generally, there are two types of models: empirical models and semi-analytical models (Lee et al., 2016; Rodrigues et al., 2017). The semi-analytical approach is based mainly on an underwater visibility theory. There are two main semi-analytical models for estimating SD values from remote sensing data. The first semi-analytical model was developed by Doron et al. (2011) based on a classic underwater visibility theory by Duntley (1952) used for over 60 years. In Doron et al.'s (2011) model, SD is determined by the beam attenuation coefficient *c* (m^{-1}) and the vertical coefficient Kd (m^{-1}). The second semi-analytical model was developed by Lee et al. (2015) based on a new underwater visibility theory. In Lee et al. (2015), SD is inversely proportional to the minimum value of diffuse attenuation coefficient of downwelling irradiance within the visible domain. Generally, to obtain accurate SD values in various waters, the semi-analytical approach always requires more narrow bands in the visible and near-infrared domains (Lee et al., 2016; Lee et al., 2002; Yang et al., 2013). Therefore, the semi-analytical approach is thus not suitable when using Landsat TM and ETM+ data due to their fewer available bands and broader bandwidths (>60 nm).

1.5.2. Empirical Approach

The empirical approach is based on developing bi-variate or multivariate regressions between the remotely sensed reflectance data and the in situ SD measurement. Landsat TM and ETM+ images along with empirical models have been widely used to estimate the SD in inland waters (Giardino et al., 2001; Kloiber et al., 2002; Olmanson et al., 2008; Olmanson et al., 2016; Lathrop, 1992; Lavery et al., 1993; Cox et al., 1998; Brezonik et al., 2005; Zhao et al., 2011; Sriwongsitanon et al., 2011; Bonansea et al., 2015; Butt et al., 2015). One shortcoming of the empirical approach is that in situ-measured SD data are always necessary to recalibrate the SD estimation algorithms. This shortcoming will limit satellite data to lakes with insufficient in situ data, especially in developing countries such as Indonesia.

Most Landsat-based studies use simple linear regression of a single band or band ratios to estimate SD. Landsat TM/ETM+ band 3 (TM3) is popular as an SD predictor in single band or ratio-based algorithms (e.g., Cox et al., 1998; Duan et al., 2009; Kallio et al., 2008; Lathrop., 1992; Pattiaratchi et al., 1994; Wu et al., 2008). TM3 has a positive correlation with particulate matter scattering; as the transparency (SD) decreases, TM3 brightness usually increases (Matthews, 2011). Landsat TM/ETM+ band 1 (TM1) has a smaller correlation with SD due to strong absorption in the blue domain, except for the very clear lakes (Giardino et al., 2001). Many studies achieved higher correlations by adding TM1 or TM3 to TM1/TM3 ratio in multiple regression (Lavery et al., 1993; Kloiber et al., 2002; Brezonik et al., 2005; Olmanson et al., 2008).

The advantages of using the empirical model are the simplicity of a water quality model and reasonable accuracy. Kloiber et al. (2002) mentioned that ideally, a single (standard) relatively simple equation with constant coefficient values would be useful to calculate SD or a phytoplankton abundance index. Their study indicated that if the atmospheric effects can be completely removed, then one estimation model can be applied to different images across time and space.

1.6. Objectives of the Study

Landsat TM/ETM+ data are available from 1984 with 30 m spatial resolutions. The empirical approach can also be applied to Landsat data even though it has fewer available bands and broader bandwidths (>60 nm). Therefore, I select Landsat TM/ETM+ data to show the long-term water quality change in Indonesian lakes. Accordingly, the objectives of this study were to:

1. develop a robust empirical SD estimation model for using Landsat TM & ETM+ data;
2. generate an SD database for Indonesian lakes from Landsat time series;
3. investigate the water quality changes in Indonesian lakes using the generated database.

Chapter II Develop a Robust Secchi Disk Depth Estimation Model using Landsat TM and ETM+

2.1. Introduction

A water quality database is essential to investigate how the water quality of lakes has changed over the years. However, it is difficult to provide water quality data for each Indonesian lake by performing field surveys due to financial constraints. As a result, the available water quality data for supporting lake management in Indonesia are very limited, leading to difficulties in evaluating the lakes objectively. On the other hand, the historical archive of remote sensing data provides valuable sources and opportunities to generate a water-quality database for Indonesian lakes and reservoirs.

For the creation of a water quality database from space, both the availability of satellite data and estimation models for water quality parameters are necessary. Since no operational ocean color sensors are available before 1997, and all ocean color sensors have relatively coarse spatial resolutions (>300 m), Landsat TM/ETM+ data (available from 1984 with 30 m spatial resolutions) are often used to determine the long-term changes of inland waters' water quality parameters (Kutser et al., 2012; Lobo et al., 2015; Olmanson et al., 2002; Oyama et al., 2009; Zheng et al., 2015).

In this study, I select Secchi Disk Depth (SD) as the satellite-retrieved water quality parameter because SD represents the same optical properties of a waterbody as remote sensing data. Furthermore, SD is considered as the most suitable variable retrieving from the satellite data. In addition, SD is the most available in situ data in Indonesia. For the necessary model to estimate SD using Landsat TM/ETM+, since the semi-analytical approach always requires more narrow bands in the visible and near-infrared domains (Doron et al., 2011; Lee et al., 2002, 2016; Yang et

al., 2013), semi-analytical approach not suitable when using Landsat TM and ETM+ data due to their fewer available bands and broader bandwidths (>60 nm).

Numerous studies have been used Landsat TM/ETM+ images along with empirical models to estimate SD in inland waters (Bonansea et al., 2015; Brezonik et al., 2005; Butt et al., 2015; Cox et al., 1998; Giardino et al., 2001; Kloiber et al., 2002; Lathrop., 1992; Lavery et al., 1993; Olmanson et al., 2008,2016; Sriwongsitanon et al., 2011; Zhao et al., 2011). However, I found inconsistent SD predictors and coefficients. In other words, there is no standard equation that can be directly applied to my study. For example, several researchers proposed a band-ratio of TM1/TM3 with TM1 as SD predictors (Brezonik et al., 2005; Kloiber et al., 2002; Olmanson et al., 2008; 2016). Meanwhile, Lathrop (1992) proposed the band-ratio of TM2/TM1 or TM3/TM1 as an SD predictor. Giardino (2001) introduced TM1/TM2 as an SD predictor. Lavery et al. (1993) and Bonansea et al. (2015) used the band-ratio of TM1/TM3 plus TM1 as SD predictors. In addition to inconsistent SD predictor/s, the model coefficient also changes to estimate SD on each image.

Previous researchers directly used Landsat's Digital Number data (without correction) and built an SD estimation model in each corresponding scene (Brezonik et al., 2005; Kloiber et al., 2002; Olmanson et al., 2008; 2016). This method was possible to be applied because their studies had enough in situ SD data to calibrate the model in each image. On the contrary, a similar study cannot be carried out because I do not have enough in situ SD data to calibrate the model on each Landsat scene. Therefore, I should perform corrections to produce standard Landsat data. The standardized Landsat data enlarge the possibility of building a robust SD estimation model.

Considering the broad bandwidths of Landsat TM and ETM+ sensors rather than the inherent optical properties (IOPs) of a waterbody, the different atmospheric effects on each set of historical satellite data are likely to provide a challenge to the building of a robust SD estimation model under an empirical scheme. Although not completely successful, Kloiber et al. (2002)

showed the potential to produce a standard SD estimation model for Landsat TM images acquired on different dates when the atmospheric effects in each image can be well removed in advance. Lobo et al. (2015) successfully applied a single empirical model to atmospherically corrected time-series Landsat data to estimate the concentrations of total suspended solids (TSSs) in Amazonian rivers. In addition, since the empirical approach is generally not suitable for extrapolation, a wide dynamic range of SD values is also required to develop a robust estimation model.

In addition to the atmospheric correction and SD dynamic range, observable system noise over the water surface in Landsat TM/ETM+ images due to the sensor's low signal-to-noise ratio (SNR) could well pose another difficulty in building a robust SD estimation model. Nichol and Vohora (2004) confirmed that the noise could significantly affect estimations of water quality parameters. They proposed a filtering method to smooth the Landsat TM images to improve the image quality over water areas before these images were further used.

The studies mentioned above suggested that a robust SD estimation model could probably be developed using well-preprocessed Landsat TM/ETM+ images and corresponding in situ-measured SD values with a wide dynamic range, even if an empirical approach was used. Consequently, the detailed objectives of this chapter were to:

1. develop a robust SD estimation model by using a wide range of in situ-measured SD values (0.5–18.6 m) collected from nine Indonesian lakes/reservoirs and the corresponding atmospherically-corrected and filtered Landsat TM and ETM+ images;
2. Evaluate the developed SD estimation model's performance using another in situ-measured SD dataset collected from Lake Maninjau, Indonesia.

2.2. Materials and Methods

2.2.1. Study Area

In this chapter, the study was conducted in nine Indonesian lakes. The nine Indonesian lakes are Lake Toba, Lake Maninjau, Lake Singkarak, Jatiluhur Reservoir, Saguling Reservoir,

Lake Matano, Lake Towuti, Lake Tondano, and Lake Limboto. Those nine lakes were considered to represent various water types. The water types including different lake origins (natural or human-made), a wide range of water clarity (SD values 0.5–18.6 m), depths (3 – 560 m), sizes (50 – 1,124 km^2), and altitudes (25 – 965 m above mean sea level), (Table 2.1).

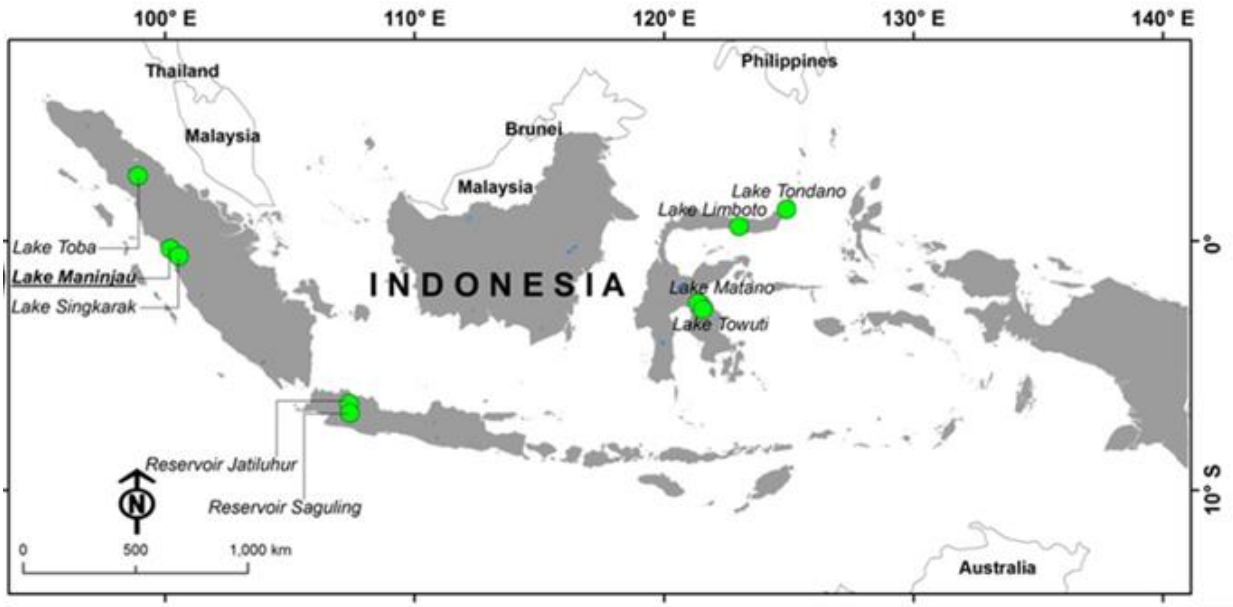

Figure 2.1. The locations of nine Indonesian Lakes

2.2.2. Data Collections

2.2.2.1. In situ Data collection

I carried out seven field surveys to collect in situ SD data during the years 2011–2014. A standard 20-cm-dia. Secchi disk painted in white and black quarters was used to measure the SD values. The locations (longitude, latitude) of the SD measurements were recorded using a GPS receiver. In total, I collected 31 in situ SD values from nine Indonesian lakes (Fig. 1b, green circles). The SD values ranged from 0.5 m to 18.6 m. Table 2.1. provides the name of the lakes, the coordinates of the collection locations, the investigation dates, and the SD values. Hereafter, I refer to this dataset as the "In situ SD Dataset I", and I used this dataset for calibrating the SD estimation models.

I also collected other in situ SD measurements from the Research Centre for Limnology (RCL), part of the Indonesian Institute of Science (LIPI). The RCL started to collect in situ SD data from

Lake Maninjau in 2001. A total of 186 SD measurements were collected from 41 field surveys from 2001 to 2018. In addition, one SD measurement was collected from Lake Maninjau by Lehmusluoto et al. (1997) in March 1992, and ten SD measurements were collected from My three field surveys (September 7, 2015: three SD measurements; September 11, 2017: four SD measurements; November 13, 2018: three SD measurements). I combined the above in situ SD data with a range of 0.50 m to 5.80 m as the "In situ SD Dataset II". I selected SD measurements with available Landsat data obtained during the same month from the "In situ SD Dataset II" and redefined these measurements as "In situ SD Dataset III". I used this dataset for validating the developed SD estimation models (n=74).

Table 2.1. The In Situ SD data of Nine Indonesian Lakes (In situ Dataset I)

No.	Name and site	Area (km^2)	Max depth (m)	Altitude (m)	Coordinate		Investigation date	SD (m)
					Longitude	Latitude		
1	Singkarak st.1	108	268	362	100.5062	-0.5432	2011-07-20	3.70
2	Singkarak st.2				100.5061	-0.5434		4.00
3	Singkarak st.3				100.5446	-0.6228		3.05
4	Singkarak st.4				100.5722	-0.6741		3.00
5	Maninjau st.1	98	165	459	100.2234	-0.2879	2011-07-21	0.90
6	Maninjau st.2				100.2173	-0.2879		0.97
7	Maninjau st.3				100.2234	-0.2879		0.91
8	Saguling st.1	53	99	645	107.4828	-6.9133	2012-07-18	0.94
9	Saguling st.2				107.4948	-6.9177		0.86
10	Saguling st.3				107.5349	-6.9333		0.88
11	Saguling st.4				107.5546	-6.9025		0.79
12	Tondano st.1	50	20	600	124.8862	1.2268	2013-03-18	2.80
13	Tondano st.2				124.8857	1.2165		2.80
14	Tondano st.3				124.8997	1.2461		2.90
15	Tondano st.4				124.9034	1.2560		2.60
16	Limboto st.1	56	3	25	122.9897	0.5877	2013-03-20	0.48
17	Limboto st.2				122.9797	0.5910		0.46
18	Limboto st.3				122.9929	0.5634		0.55
19	Toba st.1	1,124	529	905	98.6586	2.7674	2014-03-19	6.54
20	Toba st.2				98.9271	2.4147		6.50
21	Toba st.3				98.9611	2.4410		6.22
22	Jatiluhur st.1	83	105	111	107.3665	-6.5260	2014-07-15	1.37
23	Jatiluhur st.2				107.3236	-6.5393		1.83
24	Jatiluhur st.3				107.3024	-6.5805		1.74
25	Jatiluhur st.4				107.3297	-6.5139		1.71
26	Matano st.1	164	590	382	121.3001	-2.4843	2014-10-07	15.10
27	Matano st.2				121.3690	-2.4943		18.60
28	Matano st.3				121.4154	-2.5179		16.90
29	Towuti st.1	561	203	293	121.5430	-2.6990	2014-10-08	15.30
30	Towuti st.2				121.5104	-2.7989		17.10
31	Towuti st.3				121.4607	-2.8633		12.40

2.2.2.2. Satellite Data Collections

I collected satellite images that were acquired by two Landsat sensors (i.e., TM and ETM+). I used Landsat TM and ETM+ data in this study due to their high spatial resolution (30 m) and long-term data availability (since 1984). Except for a panchromatic band included in the ETM+, both sensors have a similar spectral configuration (three visible bands, three infrared bands, and one thermal infrared band, https://landsat.gsfc.nasa.gov/landsat-5/; https://landsat.gsfc.nasa.gov/landsat-7/). I did not use the thermal infrared and panchromatic bands in this study.

A total of 309 Landsat TM/ETM+ images were downloaded from the USGS website (https://earthexplorer.usgs.gov/). These satellite images include (1) seven images corresponding with in situ SD Dataset I (hereafter referred to as "Landsat Dataset I", also see Table 2.2 for details); (2) 302 images covering Lake Maninjau during the years from 2001 to 2018 (hereafter referred to as "Landsat Dataset II"). In Landsat Dataset II, 21 images corresponding to In situ SD Dataset III are referred to as "Landsat Dataset III" (see Table 2.3 for details).

Each Landsat TM/ETM+ image was bundled in a folder including three visible bands, three infrared bands, one thermal band, one panchromatic band (only for Landsat 7 ETM+), and a quality assessment band (BQA), which are all in Digital Number (DN) format. The additional files are the metadata file (_MTL.txt) and the ground control point file (_GCP.txt). For the Landsat 7 ETM+ dataset, scan line corrector (SLC) failure was also embedded with a folder containing "gap_mask" files.

Table 2.2. Seven Landsat TM/ETM+ images corresponding with In situ SD Dataset I

No	Acquisition Date	Path	Row	Sensor	Lake/Reservoir	Days between Satellite and Field Data
1	2011-07-06	127	60	5 TM	Singkarak & Maninjau	-14 & -15
2	2012-07-29	122	65	7 ETM+	Saguling	11
3	2013-03-13	111	59	7 ETM+	Tondano	5
4	2013-03-27	113	60	7 ETM+	Limboto	7
5	2014-03-30	129	58	7 ETM+	Toba	11
6	2014-07-19	122	65	7 ETM+	Jatiluhur	3
7	2014-10-08	113	62	7 ETM+	Matano & Towuti	1 & 0

Table 2.3. Twenty-one Landsat TM/ETM+ images of Lake Maninjau (Path=127, Row=60) corresponding to In situ SD Dataset III

No.	Acquisition date	Sensor	Days between Satellite and Field Data
1	2001-05-31	7 ETM+	Same month
2	2002-05-18	7 ETM+	Same month
3	2005-06-03	5 TM	Same month
4	2005-12-04	7 ETM+	Same month
5	2006-05-29	7 ETM+	Same month
6	2006-08-17	7 ETM+	Same month
7	2007-05-24	5 TM	Same month
8	2007-07-03	7 ETM+	Same month
9	2008-08-14	5 TM	Same month
10	2009-05-29	5 TM	Same month
11	2009-08-25	7 ETM+	Same month
12	2011-11-19	7 ETM+	Same month
13	2012-03-26	7 ETM+	Same month
14	2013-03-13	7 ETM+	Same month
15	2014-04-01	7 ETM+	20 days
16	2017-03-08	7 ETM+	- 9 days
17	2017-06-12	7 ETM+	Same day
18	2018-01-06	7 ETM+	-9 days
19	2018-04-28	7 ETM+	Same day
20	2018-07-17	7 ETM+	- 2 days
21	2018-09-19	7 ETM+	Same day

Note: The dates of the field surveys were not available for Landsat images Nos. 1–14.

2.2.3. Preprocessing Landsat TM and ETM+ Images

The preprocessing procedure including: (1) removing of non-water pixels, (2) reduction of noise effects, and (3) atmospheric correction. Figure 2.2. show the flowchart of the Preprocessing of the Landsat TM and ETM+ images.

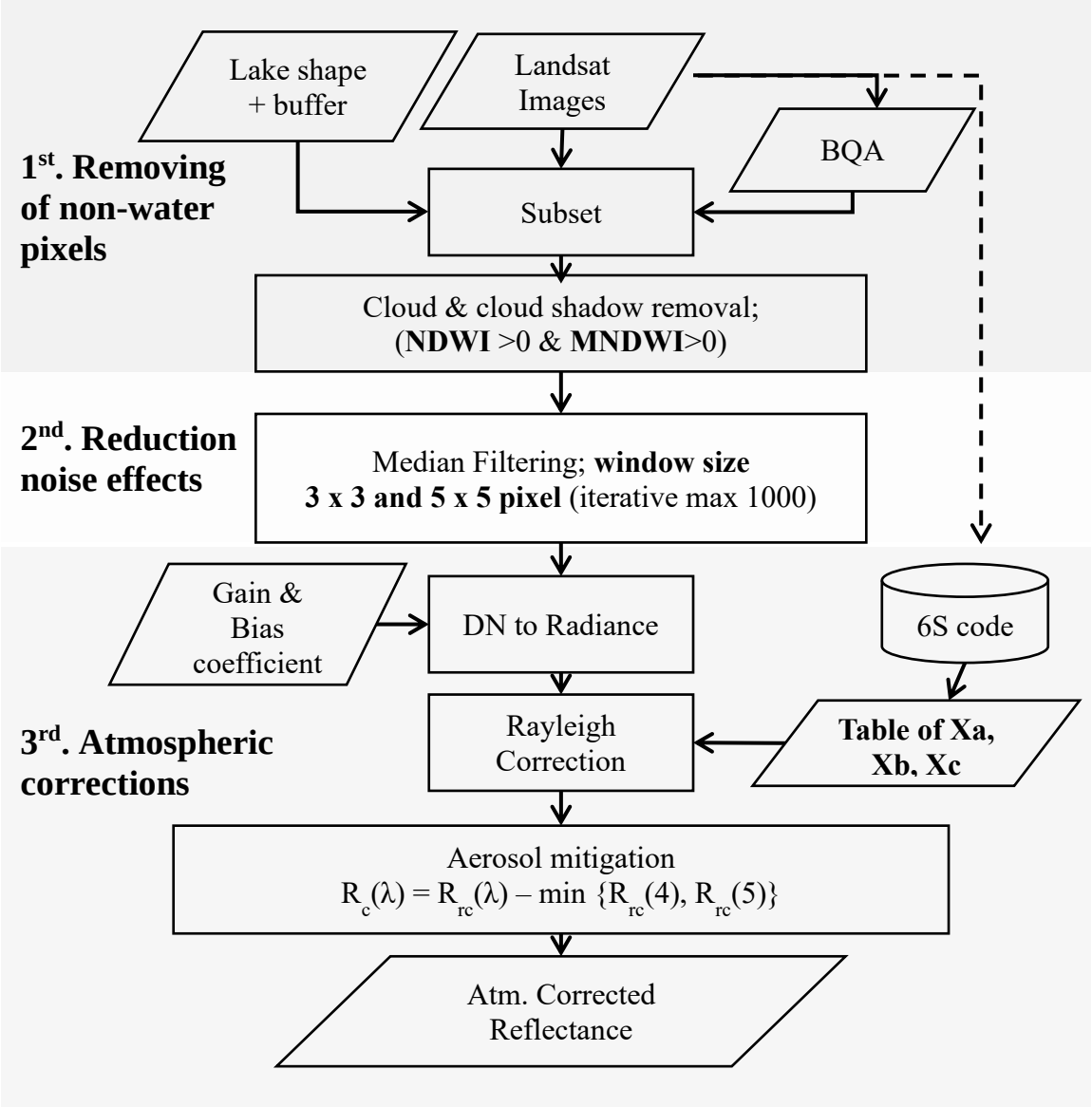

Figure 2.2. Flowchart of the Preprocessing of the Landsat TM and ETM+ Images

2.2.3.1. Removing of Non-Water Pixels

I first used lake polygons to clip water pixels and then masked the clipped water pixels with bad quality (i.e., pixels with a BQA value ≠ 672). I further removed the water pixels contaminated by clouds or cloud shadows by using the Normalized Different Water Index (NDWI, [McFeeters, 1996]) and the Modified Normalized Different Water Index (MNDWI, [Xu, 2006]). The NDWI and MNDWI values can be calculated using the following equations:

$$NDWI = (dgreen - dNIR)/(dgreen + dNIR), \quad (1)$$

$$MNDWI = (dgreen - dSWIR)/(dgreen + dSWIR), \quad (2)$$

dgreen, dNIR, and dSWIR are the DN values at the green band, near-infrared band, and shortwave infrared band. The contaminated water pixels were the pixels with both NDWI and MNDWI values <0 within the lake polygons.

2.2.3.2. Reducing Noise Effects on Water Pixels

Due to the low signal-to-noise ratios (SNRs) of the Landsat TM and ETM+ sensors, a coherent system noise pattern is observable in the images over homogeneous surfaces such as lakes (Poros and Petersen, 1985). Nichol and Vohora (2004) pointed out that the noise is serious enough to affect estimations of water-quality parameters. They proposed a method for removing the noise that uses an iterative median filtering technique in the spatial domain. In the present study, I followed Nichol and Vohora's (2004) method. I first iteratively applied a median filter with a 3-pixel by 3-pixel window to the image until no further change in pixel values was observed. I also limited the maximum iteration to 1,000 times to avoid a long computational time. I then changed the median filter size to a 5-pixel by 5-pixel window and repeated the first step.

2.2.3.3. Converting DN Values to Radiance and Minimizing Atmospheric Effects

I then converted the filtered DN values to at-sensor spectral radiance (L_λ) by using Eq. 3 (Chander et al. 2009):

$$L_\lambda = G_{rescale} * QCAL + B_{rescale}, \quad (3)$$

where L_λ is the spectral radiance at the sensor's aperture ($W/(m^2 \cdot sr \cdot \mu m)$, QCAL is the quantized calibrated pixel value (DN), $B_{rescale}$ is the band-specific rescaling bias factor from Chander et al. (2009) ($W/(m^2\ sr\ \mu m)$)/DN), and $G_{rescale}$ is the band-specific rescaling gain factor from Chander et al. (2009) ($W/(m^2\ sr\ \mu m)$).

Atmospheric correction is a crucial step in using satellite data, especially for the application of a single estimation model to different images across time and space (Kloiber et al. 2002). I proposed the use of a two-step atmospheric correction method to avoid the requirement of ancillary data for correcting aerosol effects (e.g., horizontal visibility, ratios of fine particles, and relative humidity in the atmosphere) following Wang et al. (2018). In the first step, I carried out only a Rayleigh scattering correction using the 6S (Second Simulation of the Satellite Signal in the Solar Spectrum) radiative transfer model without considering aerosol effects (Vermote et al. 1997). I selected a standard tropical atmospheric model for this correction. Table 2.4 provide detailed input for 6S software. The Rayleigh corrected reflectance (R_{rc}) for each band can be obtained using the following equations:

$$R_{rc} = y/(1.0 + xc*y), \quad (4)$$

$$y = xa * (L_\lambda) - xb, \quad (5)$$

where xa, xb, and xc are the coefficients calculated using the 6S code.

In the second step, I further mitigated the aerosol scattering effect pixel-by-pixel by subtracting the minimum of the Rayleigh corrected reflectance at the near-infrared ($R_{rc}(4)$) and middle-infrared ($R_{rc}(5)$) bands from those at the visible bands ($R_{rc}(\lambda)$):

$$R_c(\lambda) = R_{rc}(\lambda) - \min (R_{rc}(4), R_{rc}(5)), \quad (6)$$

where $R_c(\lambda)$ is the atmospherically corrected reflectance at Landsat visible bands. The second step is based on the following assumptions: (1) the water absorption at the near-infrared and middle-infrared bands is very strong, and thus the water-leaving reflectance at those bands can be considered to be zero; (2) aerosol is probably heterogeneously distributed over a lake and varies temporally; and (3) the wavelength dependence of the aerosol effect is negligible.

Table 2.4. An Example of Input for Rayleigh Scattering Correction Using 6S Radiative Transfer Model

Input data	**Explanation**	**Source of data**
7	Sensor type: Landsat TM	
03 13 1.7708 124.903 1.233	Month, date, time, longitude, latitude	Landsat meta-data file (*.MTL)
1	Tropical	User-defined
	Please leave it blank	
0	0 = no aerosol computed	User-defined
	Please leave it blank	
-1	Visibility (-1=no data)	User-defined
	Please leave it blank	
-06	Target above sea level (in negative km)	Topographical map
-1000	Sensor aboard on satellite	
	Please leave it blank	
25	Landsat TM band1	
0	Non-homogenous surface	User-defined
0	No directional effects	User-defined
4	Mean spectral value (4=lake)	User-defined
1	Request for AC (=yes)	
-0.1	Parameter of the AC (-0.1=reflectance)	
4	Ground surface is not polarized	User-defined

2.2.4. SD Estimation Model Development and Accuracy Assessment

2.2.4.1. Development of Empirical SD Estimation Models

I used In situ SD Dataset I and the preprocessed Landsat Dataset I to develop empirical SD estimation models. To reduce the impact of geometric errors associated with GPS-recorded locations of SD measurements and Landsat images, I used a 3-pixel by 3-pixel sampling window to extract the water-leaving reflectance (i.e., the preprocessed Landsat data). I averaged these values to pair them with the corresponding in situ SD measurements. I obtained a total of 31 pairs (Table 2.1). Next, to reduce the measurement errors in the in situ SD values, and by considering our finding of small variation between the SD measurements in each lake, I averaged the in situ SD values and the corresponding extracted water-leaving reflectance for each lake. The number of pairs was thus reduced from 31 pairs to nine pairs. I then used the nine natural log-transformed in situ SD values as dependent variables and various combinations of the corresponding water-leaving reflectance at the three Landsat visible bands (e.g., using single bands, band ratios, band ratios and single bands, and two-band ratios) as independent variables to develop the SD estimation models by using the regression/multiple-regression analysis technique. The general equations of the SD estimation models are as follows:

$$\ln(SD) = a + b\,(\text{single band}), \tag{7}$$

$$\ln(SD) = a + b\,(\text{band ratio}), \tag{8}$$

$$\ln(SD) = a + b\,(\text{band ratio}) + c\,(\text{single band}), \tag{9}$$

$$\ln(SD) = a + b\,(\text{band ratio 1}) + c\,(\text{band ratio 2}), \tag{10}$$

where a, b, and c are coefficients and can be obtained by fitting the calibration data. Several research groups have recommended using natural log-transformed SD values (e.g., Bonansea et al. 2015a; Brezonik et al. 2005; Kloiber et al. 2002; Olmanson et al. 2008).

Equations (7) through (10) include three single band-based (1–3), six band-ratio-based (A–F), 18 band ratio and single band-based (A1–F3), and 15 two band ratio-based (AB–EF) SD estimation models, respectively (also see Table 2.5).

2.2.4.2. Accuracy Assessment

I used three indices for assessing the accuracy of the developed models: the root means square error (RMSE), the mean normalized bias (MNB), and the normalized mean absolute error (NMAE). These indices are defined as follows:

$$\text{RMSE} = \sqrt{\frac{\sum_{i=1}^{N}(X_{esti,i}-X_{meas,i})^2}{n}}, \quad (11)$$

$$\text{MNB (\%)} = \text{mean}\ (100\times(X_{esti,i}-X_{meas,i})/\ X_{meas}), \quad (12)$$

$$\text{NMAE (\%)} = \text{mean}\ (|100\times(X_{esti,i}-X_{meas,i})/\ X_{meas,i}|), \quad (13)$$

where $X_{esti,i}$ and $X_{meas,i}$ are the estimated and measured SD values, respectively; N is the number of samples. The RMSE denotes the absolute scattering of estimated SD values. The MNB represents the average bias in the estimation, and the NMAE means the average relative error in the estimations. I also calculate the correlation between the measured and estimated values (R^2).

I also used R language (R Core Team, 2018) for several statistical analyses. First, I used an R package named "hydroGOF" (Mauricio et al., 2017) to calculate Willmott Index of Agreement (WIA) and Nash–Sutcliffe model efficiency (NSME) to enhance the accuracy assessment of the developed model. The WIA value is a measure of modeled errors and varies between 0 and 1. A WIA value closer to 1 represents a better match between in situ data and modeled data (Willmott, 1981). The NSME value indicates how well the in situ data versus modeled data fits the 1:1 line, and a value closer to 1 indicates a better match of the modeled data

to the in situ data (Nash et al., 1970). Second, I made a Taylor diagram using the "openair" package in R language to compare the performance between different SD estimation models (Carslaw et al., 2012). The correlation coefficient (R), root-mean-square (RMS) difference, and the standard deviations of different models can be simultaneously shown in this diagram (Taylor, 2001). Third, I used an R package named "ggplot2" (Wickham, 2016) to obtain long-term trends based on in situ-measured and satellite estimated SD values by using the Locally wEighted Scatterplot Smoothing (LOESS) method. LOESS uses Savitzky–Golay filter to obtain a trend line from scattered points by local polynomial regression. It has been widely used in time-series data analyses (e.g., Christina et al., 2016; Lu et al., 2003; Jiang et al., 2010).

2.3. Results

2.3.1. Improved Landsat Data Quality by Filtering

The filtering procedures aimed to replace the extremely low and extremely high pixels with the specified box's median values. The filter will calculate the median value from that specified box rather than produce a new value. In this study, the box size is 3 by 3 and 5 by 5. The calculations were done iteratively until no further change in pixel value was observed. Figure 2.3. showed the comparison of non-filtered and filtered reflectance of the visible band of Lake Maninjau acquired in 2008-08-14. Fluctuated reflectance values of neighboring pixels were observed. Figure 2.4. shows more considerable reflectance fluctuation between adjacent pixels of Lake Towuti acquired 1994-11-10, which is known as the clear lakes (SD >15 m). Generally, over clear water, the reflectance values are relatively lower than over turbid water. The weaker signal consequently resulted in the more dominant noise captured by the sensor. The unstable pixel values will influence further calculation results such as converting DN to radiance, atmospheric correction and may lead to inaccurate SD estimation. Figures 2.3. (b) and 2.4. (b) shows the filtering results (red line). It indicated that the filter was necessary to be applied to obtain more stable and reliable reflectance for both Landsat TM and ETM+ data.

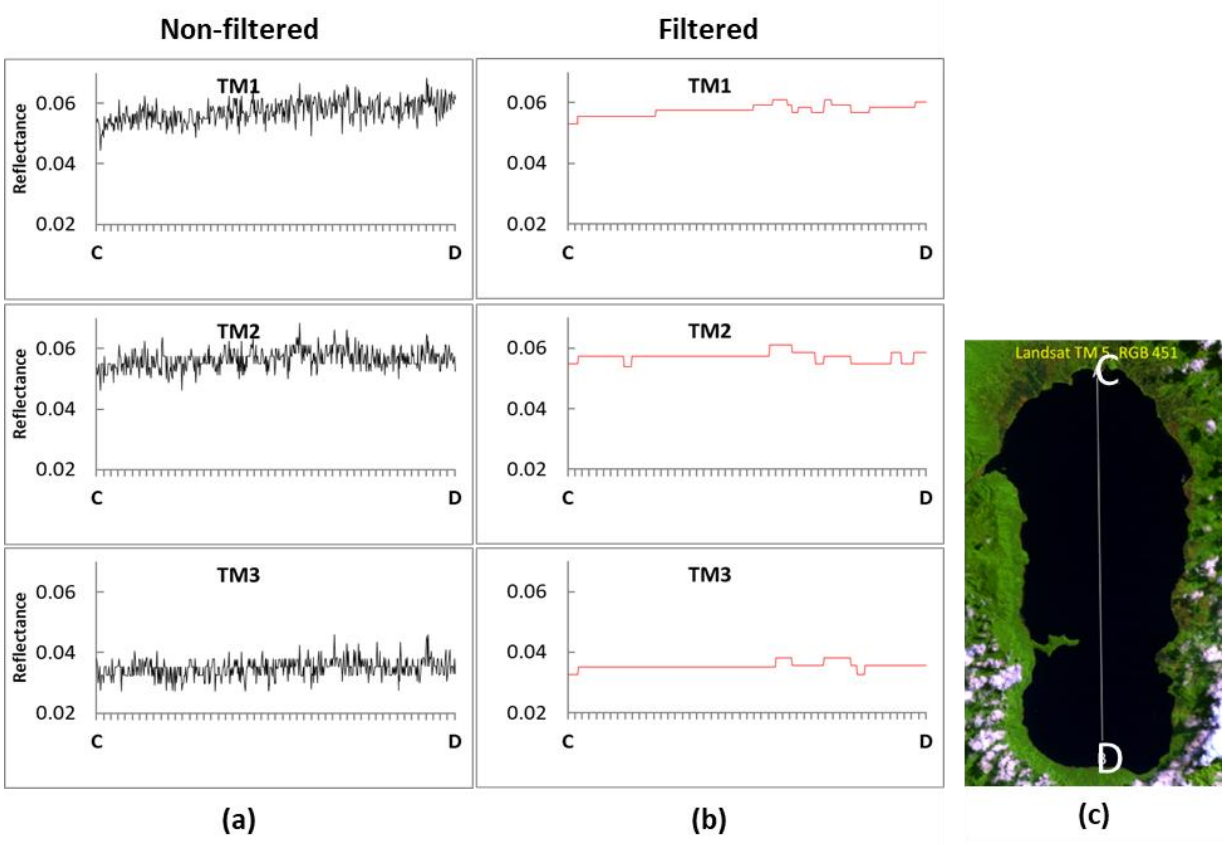

Figure 2.3. Comparing Transects of (a) Non-Filtered Reflectance and (b) Filtered Reflectance in Lake Maninjau. (c) Landsat Path = 127, row = 60, date acquired 2008-08-14, the average corresponding SD = 3 m.

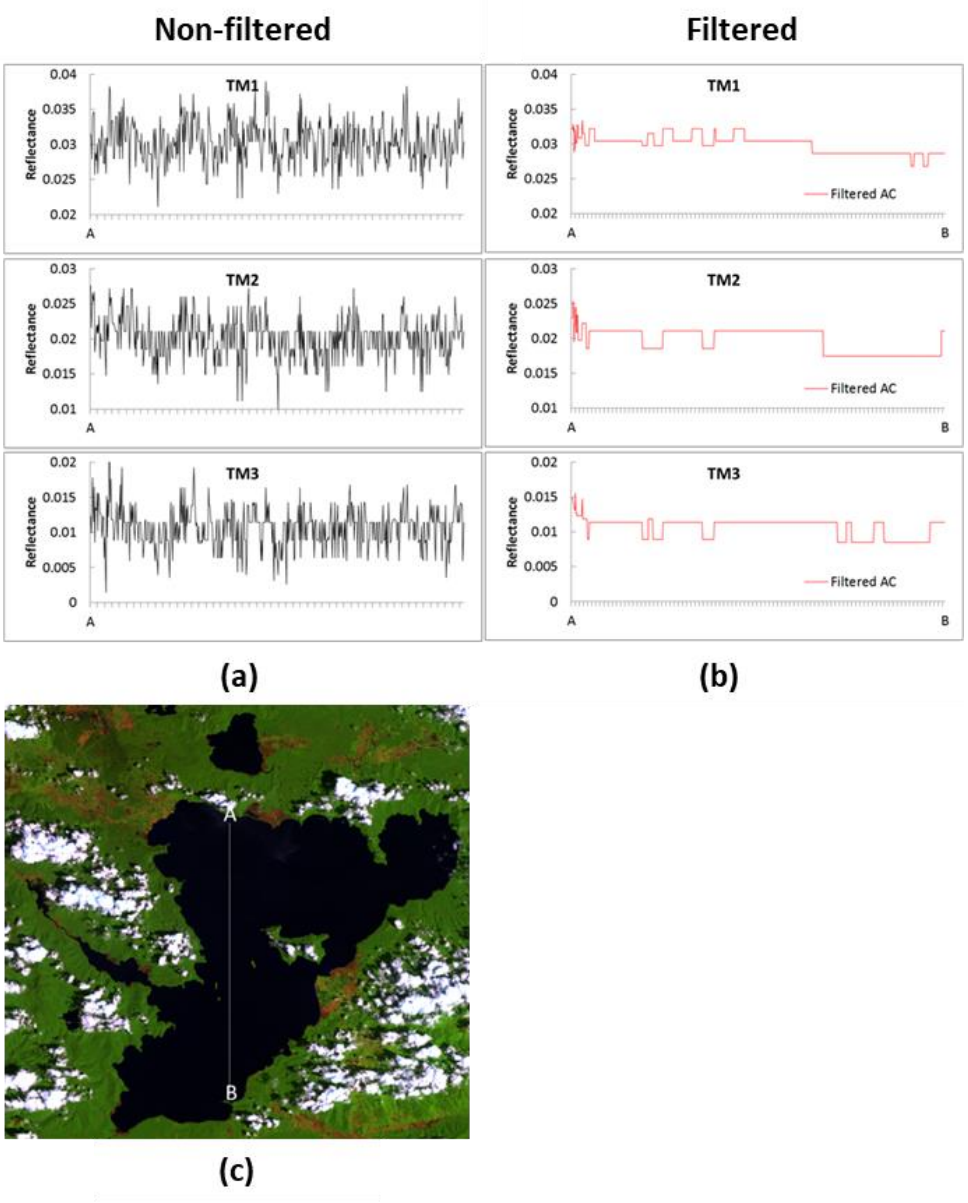

Figure 2.4. Comparing Transects of (a) Non-Filtered Reflectance and (b) Filtered Reflectance in Lake Towuti. (c) Landsat Path = 113, row = 62, date acquired 1994-11-10, the average in situ SD = 20 m.

2.3.2. Atmospherically Corrected Reflectance

The atmospheric corrections aimed to obtain comparable reflectance data acquired from different time and location. The atmospheric corrections in this study consist of two steps. The first step is for Rayleigh scattering effect correction, and the second step is to mitigate the aerosol scattering effect in visible bands. I applied two-step atmospheric correction because the information about the aerosol thickness or visibility data were not available. Figure 2.5. shows the comparison of atmospherically corrected reflectance (blue line), uncorrected reflectance (dashed lines), and Surface reflectance product from the USGS website (red lines) of nine lakes data, which were used for SD calibration.

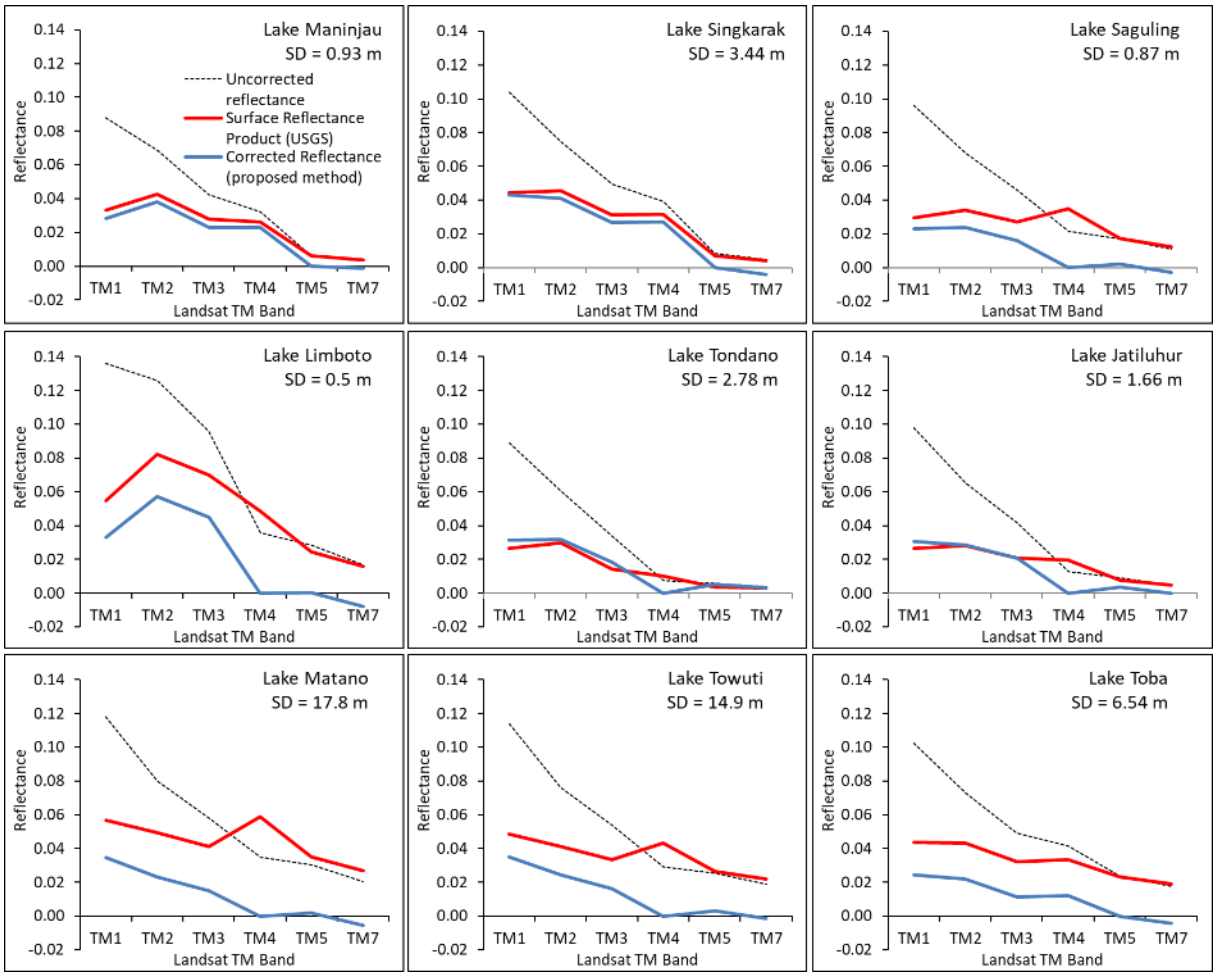

Figure 2.5. Comparison of the Uncorrected reflectance (black dashed line), Surface Reflectance product from USGS (Red solid line), and Corrected Reflectance using the proposed method (solid blue line) for Seven Landsat TM/ETM+ images corresponding with "In situ SD Dataset I".

Results demonstrated that the proposed atmospheric correction method has a better spectra profile than the USGS standard product. The USGS product often fails to remove the aerosol at the longer wavelength (band 4, band 5, and band 7). The reflectance over the water surface should be very close to zero at these longer wavelengths due to the very strong water absorption. The proposed atmospheric correction successfully removed the Rayleigh effect and mitigated the Aerosol effect for both turbid and clear lakes pixel by pixel.

2.3.3 Empirical Models for Estimating the SD from Landsat TM/ETM+ Data

Table 2.5 shows all of the developed SD estimation models and their performances based on In situ SD Dataset I and the preprocessed Landsat Dataset I. I excluded the SD estimation models with the worse performance from the further analyses using thresholds of R^2 values <0.9 and RMSE values >2.5 m. SD estimation models remained (models in bold in Table 2.5): Two band-ratio-based models (A and B), six band-ratio with single-band-based models (A1–A3 and B1–B3), and nine two-band ratio-based models (AB–AF and BC–BF). Since all 17 remaining SD estimation models contained band ratio of TM1 and TM3 (TM1/TM3) or band ratio of TM1 and TM2 (TM1/TM2), I refer to the models with TM1/TM3 as "A-type models" and the models with TM1/TM2 as "B-type models" hereafter for convenience. In addition, all 17 remaining SD estimation models showed WIA and NSME values larger than 0.96 and 0.87, respectively.

Figure 2.6. provides the scatterplots of the in situ SD measurements and the corresponding estimated SD values using the selected 17 models in the model calibration procedures. The A-type models generally showed better performances than the B-type models. The A-type models' determination's coefficients ranged from 0.97 to 0.99, with RMSE values ranging from 0.8 to 1.6 m and NMAE values ranging from 24.3 to 34.7%. In contrast, the ranges of the coefficients of determination, RMSE, and NMAE of the B-type models were 0.91–0.96, 1.9–2.2 m, and 42–51.1%, respectively.

Table. 2.5. The developed SD estimation models and their performances based on In situ SD Dataset I and the preprocessed Landsat Dataset I.

Variable	Type	ln (SD) =	R^2	RMSE (m)	MNB (%)	NMAE (%)
Single band	1	-0.04 + 29.35(TM1)	0.021	6.6	89.7	140.5
	2	2.77 - 47.99(TM2)	0.317	5.9	58.8	111.0
	3	2.24 - 53.91(TM3)	0.330	5.9	55.2	107.5
Band ratio	**A**	**-2.45 + 1.81(TM1/TM3)**	**0.971**	**1.6**	**10.1**	**34.7**
	B	**-3.29 + 3.93(TM1/TM2)**	**0.914**	**2.1**	**16.6**	**50.7**
	C	-5.77 + 3.95(TM2/TM3)	0.270	5.6	43.2	86.9
	D	3.33 - 3.88(TM3/TM1)	0.782	4.6	29.3	74.5
	E	4.55 - 3.60(TM2/TM1)	0.845	4.0	28.2	68.3
	F	6.97 - 10.07(TM3/TM2)	0.293	5.6	45.7	91.1
Band ratio and single band	**A1**	**-4.36 + 1.87(TM1/TM3) + 49.01(TM1)**	**0.985**	**0.8**	**4.4**	**25.0**
	A2	**-4.48 + 2.33TM1/TM3) + 28.22(TM2)**	**0.983**	**0.8**	**5.4**	**24.3**
	A3	**-3.85 + 2.24(TM1/TM3) + 25.83(TM3)**	**0.982**	**0.9**	**6.6**	**27.2**
	B1	**-4.43 + 3.94(TM1/TM2) + 30.99(TM1)**	**0.919**	**1.9**	**12.5**	**46.7**
	B2	**-4.47 + 4.52(TM1/TM2) + 14.93(TM2)**	**0.915**	**1.9**	**13.9**	**49.4**
	B3	**-3.71 + 4.18(TM1/TM2) + 7.18(TM3)**	**0.912**	**2.0**	**15.8**	**50.3**
	C1	-13.60 + 5.85(TM2/TM3) + 124.11(TM1)	0.540	4.2	15.8	56.6
	C2	-4.17 + 3.28(TM2/TM3) -12.07(TM2)	0.339	5.5	42.9	88.9
	C3	-4.80 + 3.49(TM2/TM3) - 8.40(TM3)	0.297	5.6	43.3	88.2
	D1	0.21 - 4.84(TM3/TM1) + 100.49(TM1)	0.926	2.8	8.2	34.5
	D2	4.53 - 11.87(TM3/TM1) + 146.26(TM2)	0.936	3.1	17.5	50.5
	D3	4.27 - 10.20(TM3/TM1) + 125.67(TM3)	0.925	2.8	9.8	36.8
	E1	2.75 - 3.78(TM2/TM1) + 53.86(TM1)	0.899	3.2	17.4	53.4
	E2	4.80 - 5.10(TM2/TM1) + 33.83(TM2)	0.890	3.4	21.0	57.0
	E3	4.90 - 4.47(TM2/TM1) + 22.52(TM3)	0.866	3.7	25.4	63.9
	F1	5.46 - 16.59(TM3/TM2) + 146.02(TM1)	0.679	3.6	10.3	42.9
	F2	6.63 - 9.10(TM3/TM2) - 6.16(TM2)	0.327	5.6	45.5	92.3
	F3	7.11 - 10.37(TM3/TM2) + 2.01(TM3)	0.287	5.6	45.7	90.9
Two band ratios	**AB**	**-2.49 + 1.76(TM1/TM3) + 0.12(TM1/TM2)**	**0.971**	**1.6**	**10.2**	**34.6**
	AC	**-1.80 + 1.95(TM1/TM3) - 0.53(TM2/TM3)**	**0.973**	**1.4**	**10.2**	**34.3**
	AD	**-4.34 + 2.35(TM1/TM3) + 1.45(TM3/TM1)**	**0.979**	**1.0**	**8.1**	**26.4**
	AE	**-4.17 + 2.22(TM1/TM3) + 0.96(TM2/TM1)**	**0.974**	**1.3**	**8.6**	**30.5**
	AF	**-3.94 + 2.00(TM1/TM3) + 1.89(TM3/TM2)**	**0.974**	**1.3**	**9.9**	**33.7**
	BC	**-4.84 + 3.37(TM1/TM2) + 1.26(TM2/TM3)**	**0.957**	**2.0**	**13.0**	**42.0**
	BD	**-3.05 + 3.80(TM1/TM2) - 0.16(TM3/TM1)**	**0.916**	**2.2**	**16.7**	**51.1**
	BE	**-6.78 + 5.60(TM1/TM2) + 1.70(TM2/TM1)**	**0.905**	**1.9**	**14.2**	**48.8**
	BF	**-1.18 + 3.45(TM1/TM2) - 2.67(TM3/TM2)**	**0.946**	**2.1**	**14.4**	**45.2**
	CD	2.53 + 0.38(TM2/TM3) - 3.62(TM3/TM1)	0.769	4.6	28.6	73.8
	CE	1.48 + 1.41(TM2/TM3) - 2.94(TM2/TM1)	0.861	3.9	22.3	60.8
	CF	-10.31 + 5.34(TM2/TM3) + 3.64(TM3/TM2)	0.260	5.6	42.6	86.6
	DE	4.49 - 0.28(TM3/TM1) - 3.36(TM2/TM1)	0.846	4.0	28.0	67.9
	DF	2.72 - 4.27(TM3/TM1) + 1.43(TM3/TM2)	0.790	4.6	29.9	74.4
	EF	5.65 - 3.07(TM2/TM1) - 2.74(TM3/TM2)	0.865	3.9	24.7	64.1

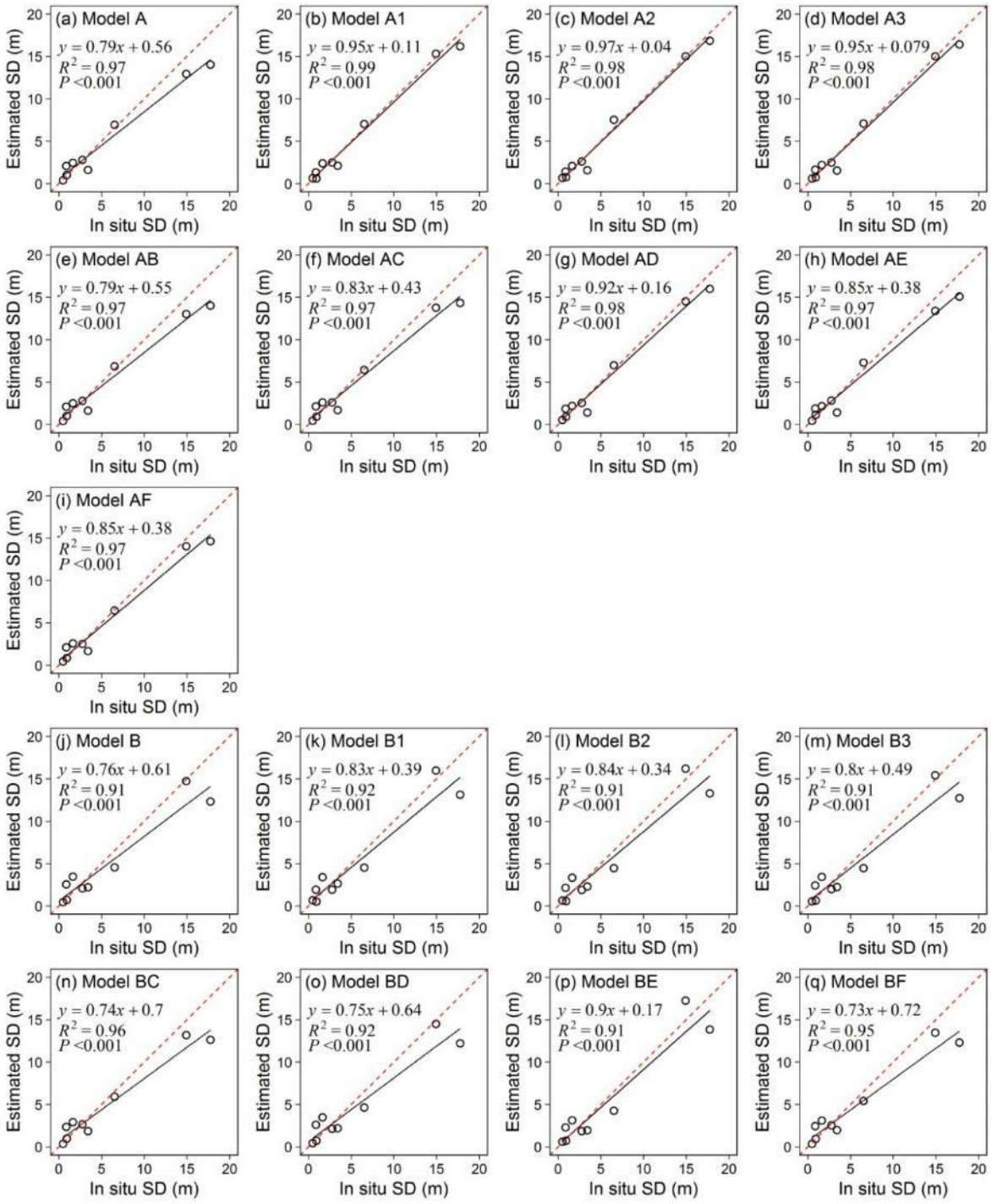

Figure 2.6. Comparison of the in situ SD measurements and the corresponding estimated SD values using the 17 selected models in the model calibration procedures.

2.3.4. Validation of the 17 Selected SD Estimation Models in Lake Maninjau

Figure 2.7 and Table 2.6 illustrate the results of our comparisons of the in situ-measured SD values (In situ SD Dataset III) and the corresponding estimated SD values from the preprocessed Landsat images (Landsat Dataset III) using the 17 selected SD estimation models. The figure and table reveal that the B-type models generally outperformed the A-type models in Lake Maninjau. All of the A-type models showed larger overestimations with RMSE values ranging from 1.64 to 2.55 m (average 1.94 m) and lower R^2 values ranging from 0.25 to 0.44 (Figure 2.7 a–i). In contrast, the B-type models showed smaller RMSE values (0.92–1.52 m, with an average of 1.07 m) and higher R^2 values (0.35–0.60; Figures 2.7 j–q).

Figure 2.8 shows the performances of the 17 selected SD estimation models using the Taylor diagram, which also reveals that the B-type models have better performance than the A-type models in Lake Maninjau (higher R values and smaller RMS errors). Among the B-type models, since the BF model showed the highest R^2 value (0.60; Table 2.6), the closest distance to the observed point (Figure 2.8), the highest WIA value (0.83; Table 2.6), a smaller RMSE value (1.01 m; Table 2.6), I chose this model for further analysis.

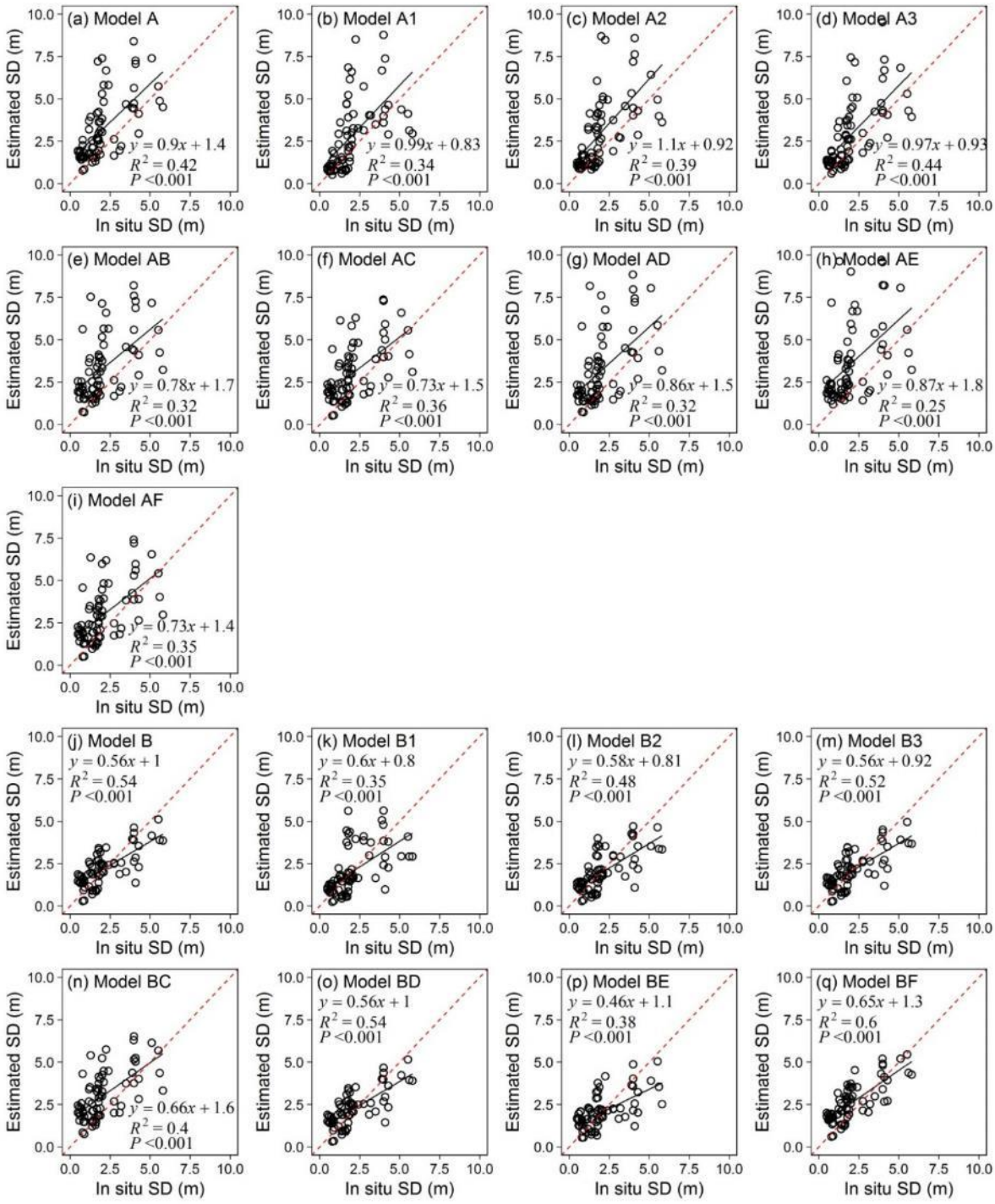

Figure 2.7. Comparisons of the in situ-measured SD values (In situ SD Dataset III) and the corresponding estimated SD values from the preprocessed Landsat images (Landsat Dataset III) using the 17 selected SD estimation models (n = 74).

Table 2.6. The developed SD estimation models and their performances based on In situ SD Dataset III and the preprocessed Landsat Dataset III (n=74)

Name	ln (SD) =	R2	WIA *	NSME **	RMSE (m)	MNB (%)	NMAE (%)
A	**-2.45 + 1.81(TM1/TM3)**	**0.42**	**0.68**	**-0.88**	**1.83**	**83.46**	**89.83**
A1	**-4.36 + 1.87(TM1/TM3) + 49.01(TM1)**	**0.34**	**0.65**	**-1.29**	**2.02**	**45.98**	**63.67**
A2	**-4.48 + 2.33TM1/TM3) + 28.22(TM2)**	**0.39**	**0.66**	**-1.35**	**2.05**	**61.35**	**73.23**
A3	**-3.85 + 2.24(TM1/TM3) + 25.83(TM3)**	**0.44**	**0.72**	**-0.61**	**1.70**	**57.25**	**69.72**
AB	**-2.49 + 1.76(TM1/TM3) + 0.12(TM1/TM2)**	**0.32**	**0.62**	**-1.24**	**2.00**	**98.44**	**106.40**
AC	**-1.80 + 1.95(TM1/TM3) - 0.53(TM2/TM3)**	**0.36**	**0.69**	**-0.52**	**1.65**	**81.22**	**93.08**
AD	**-4.34 + 2.35(TM1/TM3) + 1.45(TM3/TM1)**	**0.32**	**0.63**	**-1.37**	**2.06**	**88.98**	**99.28**
AE	**-4.17 + 2.22(TM1/TM3) + 0.96(TM2/TM1)**	**0.25**	**0.54**	**-2.63**	**2.55**	**115.41**	**122.65**
AF	**-3.94 + 2.00(TM1/TM3) + 1.89(TM3/TM2)**	**0.36**	**0.69**	**-0.51**	**1.64**	**76.59**	**90.17**
B	**-3.29 + 3.93(TM1/TM2)**	**0.54**	**0.83**	**0.53**	**0.92**	**30.67**	**54.19**
B1	**-4.43 + 3.94(TM1/TM2) + 30.99(TM1)**	**0.35**	**0.76**	**0.16**	**1.23**	**13.44**	**48.66**
B2	**-4.47 + 4.52(TM1/TM2) + 14.93(TM2)**	**0.48**	**0.82**	**0.46**	**0.98**	**14.80**	**45.81**
B3	**-3.71 + 4.18(TM1/TM2) + 7.18(TM3)**	**0.52**	**0.83**	**0.52**	**0.93**	**22.72**	**50.20**
BC	**-4.84 + 3.37(TM1/TM2) + 1.26(TM2/TM3)**	**0.40**	**0.71**	**-0.29**	**1.52**	**84.90**	**92.43**
BD	**-3.05 + 3.80(TM1/TM2) - 0.16(TM3/TM1)**	**0.54**	**0.83**	**0.53**	**0.92**	**33.19**	**55.38**
BE	**-6.78 + 5.60(TM1/TM2) + 1.70(TM2/TM1)**	**0.38**	**0.76**	**0.37**	**1.07**	**26.62**	**55.97**
BF	**-1.18 + 3.45(TM1/TM2) - 2.67(TM3/TM2)**	**0.60**	**0.83**	**0.43**	**1.01**	**56.47**	**67.43**

Note: *: Willmott Index of Agreement, **: Nash-Sutcliffe model efficiency.

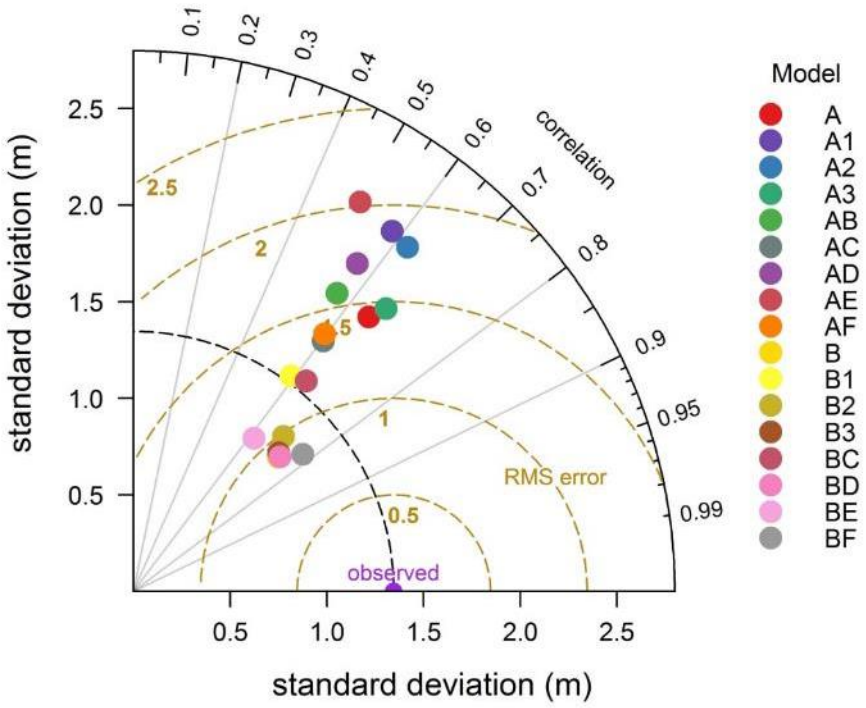

Figure 2.8. Comparison of the 17 selected SD estimation models using the Taylor diagram in terms of their correlation coefficients, root-mean-square differences, and standard deviations.

2.3.5. Long-term SD Changes in Lake Maninjau from the Landsat TM/ETM+ Time Series

I applied the BF model to the preprocessed Landsat Dataset II to observe the long-term SD change in Lake Maninjau (1987–2018). To maintain the representativeness of the SD of the entire lake, I excluded Landsat images with <50% available water pixels in Lake Maninjau (see Section 2.2.3.1 above). I also removed two Landsat images (acquired on July 2, 2004, and July 5, 2005) due to a large area of clouds and cloud shadows that failed to be masked by the BQA, NDWI, MNDWI values. I thus used only 230 Landsat images for the long-term SD change analysis.

Figure 2.9 provides the averaged SD values estimated from the 230 preprocessed Landsat images using the BF model. The averaged in situ SD measurements of each field survey in Lake Maninjau are also shown in Figure 2.9 for visual comparison. From the long-term Landsat-based SD estimations, it can be seen that low SD values (1–1.5 m) occurred four times during the years from 2001 to 2018 (around 1989, 1999, 2011, and 2018). Around 2004, the water transparency in Lake Maninjau increased notably, as the SD values changed from 1.5 m (around 1999) to approx. 6 m. The lake's water transparency then showed a continuous decrease until 2011, a smaller

tendency to increase in 2011–2015, and a decreasing trend again in 2015–2018. These water transparency variations observed from the Landsat-based SD estimations can be validated by the In situ SD dataset II after 2001 (Figure 2.9, blue points, and trend line), which showed a similar fluctuation pattern of SD values.

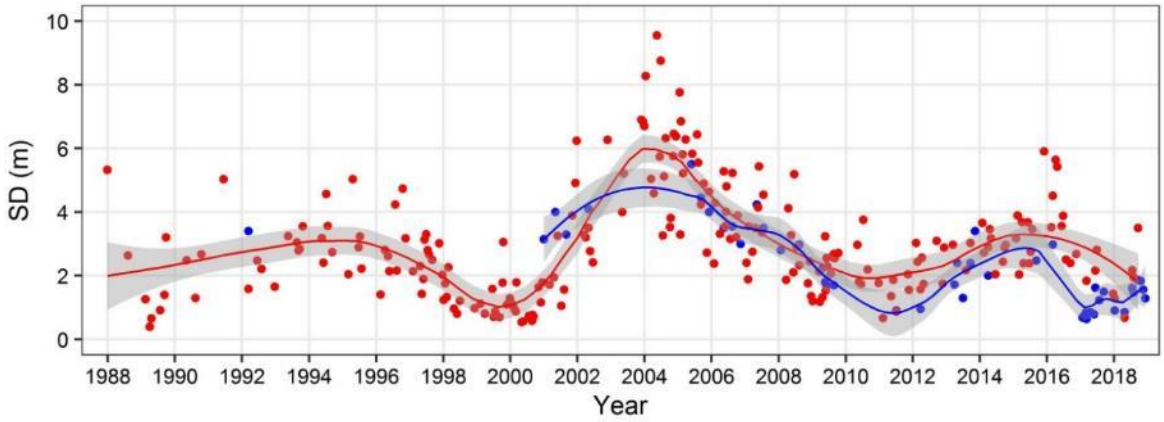

Figure 2.9. Long-term changes in water transparency in Lake Maninjau from 1987 to 2018. Red points: The averaged SD values estimated from the preprocessed Landsat Dataset II using the BF model. Blue points: The averaged in situ SD values for each field survey (In situ SD Dataset II). Redline: obtained from the red points via a trend analysis in the R language. Blueline: obtained from the blue points via a trend analysis in the R language. Gray areas: 95% confidence intervals of the trend analysis.

2.4. Discussion

2.4.1 Atmospheric Correction Caused Unstable TM1/TM3

Previous research directly used Digital Number (DN) and calibrated the model using in situ data then estimated SD for whole water pixels in the corresponding scenes (Kloiber et al., 2002; Brezonik et al., 2005; Olmanson et al., 2008 and Olmanson et al., 2016). In situ data were available to calibrate the corresponding image one by one, and thus it possible to use the Digital Number (DN) data format. In my research, the number of corresponding in situ data with Landsat images was very limited, and it also comes from different lakes, locations, and time of image acquisition. The atmospheric effect should be corrected to make a standard data set. After atmospheric correction, I found that the band ratio of reflectance TM1/TM3 becomes very volatile in contrast to the DN ratio at the same band, as shown in Figure 2.10 (red line). Even though a series of the median filter was applied, the band ratio of TM1/TM3 still showed a larger magnitude between neighboring pixels, especially in Lake Towuti (a clear lake).

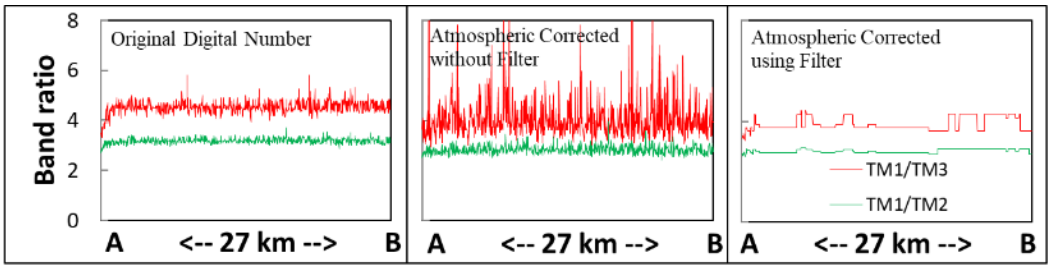

(a) Lake Towuti

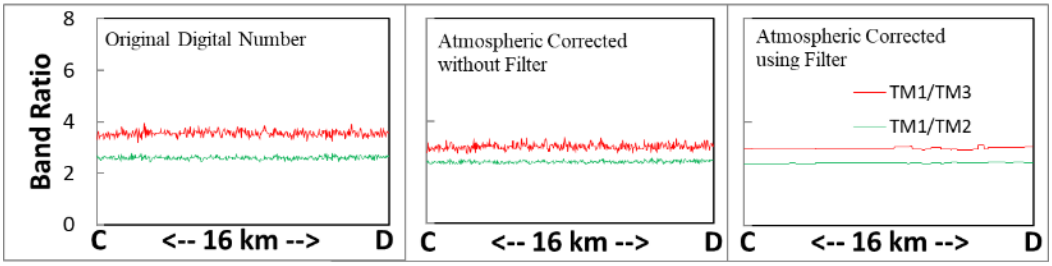

(b) Lake Maninjau

Figure 2.10. Comparing transects of Digital Number, Non-filtered atmospheric corrected reflectance, and Filtered Atmospheric corrected reflectance of Lake Towuti, a clear lake with an SD = 20 m (a), and Lake Maninjau, a medium turbid lake with SD = 3 m (b).

After performing atmospheric correction, the TM1/TM3 becomes unstable; using this band ratio as an SD predictor will estimate unstable SD values. On the other hand, after performed atmospheric correction, the band ratio of TM1/TM2 showed smaller fluctuation between neighboring pixels compares to TM1/TM3. The stable band ratios of atmospherically corrected reflectance of TM1/TM2 indicate that the model contains TM1/TM2 will have more robust SD estimations. Figure 2.11 shows the spectra of three neighbor pixels extracted from Lake Maninjau, the same Images as Figure 2.10 (b).

The original DN data shows similar spectra profile (Figure 2.11. (a)) and a more stable band ratio (Figure 2.11. (c)). In detail, the DN value of band_3 of these three pixels is 14, 15, and 16, respectively. Contrary, after the atmospheric correction, the pixel's absolute values become very small, and the relative difference between neighboring pixels becomes more explicit, especially for band_3 (Figure 2.11. (b)). Consequently, using atmospherically corrected data resulted in an unstable band ratio of TM1/TM3 (Figure 2.11. (d)).

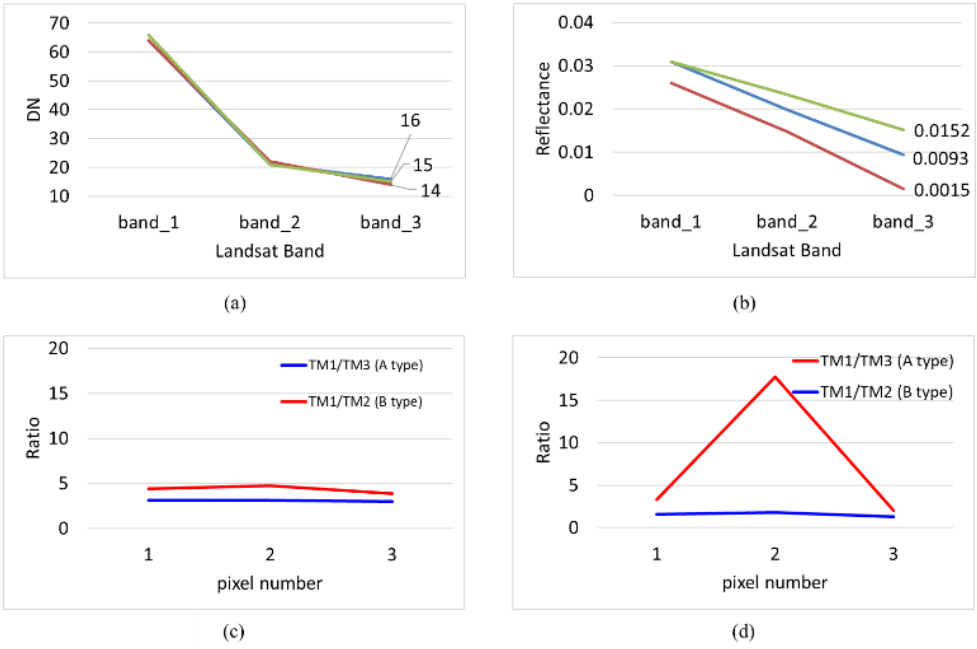

Figure 2.11. Spectra of three neighbor pixels and their band ratios in Lake Maninjau; (a) in original DN format, (b) after atmospheric correction, (c) band ratio of original DN, (d) band ratio after atmospheric correction.

2.4.2. Benefit of Using TM2 as the Denominator in Band Ratios

Many researchers have suggested that the use of the band ratio of TM1/TM3 with the single band of TM1 as the SD predictor (i.e., the A1 model in Table 2.5; [e.g., Bonansea et al., 2015; Brezonik et al., 2005; Kloiber et al., 2002; Olmanson et a., 2008, 2016; Zhao et al., 2011; Sriwongsitanon et al., 2011]). Their suggestion differed from the recommendation in my study. The two band ratios of TM1/TM2 and TM3/TM2 are suggested as independent variables in the SD estimation model (i.e., the BF model in Table 2.5). The A1 model showed the best performance in the calibration procedure with the highest R^2 value of 0.99 and the smallest RMSE of 0.8 m (Figure 2.6.b). However, the A1 model showed a lower R^2 value (0.34) and larger error (RMSE=2.0 m) in the validation procedure (Figure 2.7.b). I observed many outliers in the SD estimations when the A1 model was applied to the Landsat Dataset II to estimate long-term SD changes (data not shown). Similar results were observed in all A-type and B-type models (Figs. 2.7 and 2.8). These findings indicate that the A-type models present considerable uncertainty, whereas the B-type models are more robust in many applications.

2.4.3. Advantages of Using Two-Band Ratio Models

Another difference between my model and the previous models is that I used the band ratio instead of a single band for the second independent variable (i.e., I used TM3/TM2 instead of TM1). The merit of using the band ratio is that effects due to imperfect atmospheric correction can be mitigated (Doxaran et al., 2002, 2003). In addition, since water-leaving reflectance at the green band (TM2) does not change as much as that at the blue and red bands (TM1 and TM3) in various waters, using this value to normalize water-leaving reflectance at blue and red bands can avoid a large fluctuation of the ratios. The BF model thus showed the greatest robustness in Lake Maninjau (Fig. 2.7).

2.4.4. Applicability of the Developed SD Estimation Model

In this chapter, I developed an empirical model for estimating SD values from Landsat data. Although the number of data pairs is small, the reflectance and SD data pairs were collected from nine Indonesian lakes with a wide dynamic range of SD values (0.5–18.6 m). I also conducted a series of preprocessing steps, including removing contaminated water pixels, filtering the images, and mitigating the atmospheric effects before the Landsat data were used. These efforts enable the developed SD estimation model to be applied to different Landsat images across time and space (Bonansea et al., 2015; Kloiber et al., 2002; Sriwongsitanon et al., 2011). In contrast, since the fewer available bands and the broad bandwidths of Landsat TM and ETM+ sensors, the changed IOPs in different water bodies are probably not the main cause to affect the robustness and universality of the developed SD estimation model. Nevertheless, the developed SD estimation model is still needed to be further validated by using more comprehensive data pairs collecting from various waters or simulation experiments.

2.5. Conclusions

In this chapter, I developed an empirical model to estimate SD values from Landsat TM/ETM+ data. The developed model suggested using the two-band ratios of TM1/TM2 and TM3/TM2 as the SD predictor to reduce uncertainties in the model. This suggestion differs from the recommendations in previous studies. The preprocessing procedure for Landsat data is essential for improving the robustness of the developed model. The model has the potential to generate an SD database for Indonesian lakes.

Chapter III Application of the Developed Model to Indonesian Lakes

3.1. Introduction

Routine monitoring of the water environment is necessary to ensure the management practices for achieving sustainability (Blake et al., 2013). In addition, long-term water quality information on a broad regional and spatial scale is also essential for effective lake management (Olmanson et al., 2008). However, monitoring data for evaluating water quality is very limited in Indonesia due to a lack of a field survey budget. A combination of field surveys and remote sensing techniques can provide comprehensive data solutions to address sustainability issues because satellite sensors have the potential to provide better spatial and temporal coverage compared with traditional field surveys (Blake et al., 2013).

Relating to global concerns, the Sustainable Development Goal (SDG) 6.3.2 of the United Nations (UN) focuses on ambient water quality (UN, 2015). For SDG 6.3.2 water quality evaluation, the UN-Water Group proposed five water quality parameters: nitrogen, phosphorus, pH, dissolved oxygen, and electrical conductivity as the global scale indicator (UN-Water, 2017). However, these parameters are mainly based on field measurements and laboratory analysis, limited by the number of monitoring stations or data and laboratory analysis costs. As a result, many countries are unable to provide global-level evaluation reports for SDG 6.3.2 (UN-Water, 2018). On the other hand, water clarity (SD) simplistically and visually reflects water quality and can potentially support SDG 6.3.2 reporting (Shen et al., 2020).

Shen et al. (2020) proposed a simple SDG 6.3.2 indicator evaluation scheme established from remote sensing derived Secchi Disk Depth (SD). The proposed scheme has higher spatiotemporal coverage data and effectively evaluates water quality in inland lake waters over a

large area, and demonstrates a significant increase in data availability and continuity for the SDG 6.3.2 evaluation.

In Chapter II, a robust model to estimate SD using Landsat TM/ETM+ data was developed. The Landsat-based SD estimations using the developed model well captured the changes in water transparency in Lake Maninjau. The developed model has the potential to generate an SD database for other Indonesian lakes. However, the reliability of the estimated SD and the generated SD database should be verified. Accordingly, the specific objectives of this chapter were to: (1) confirm the model can estimate reasonable SD in Indonesian lakes, (2) check the reasonableness of the generated SD database, (3) show the SD changes of large Indonesian lakes using the generated database.

3.2. Material and Methods

3.2.1. Study Area

According to Hamzah (2019), Indonesia has 60 lakes with an area larger than 10 km^2, including 50 natural lakes and ten reservoirs. Considering the Landsat Images availability, I studied 35 lakes. The 35 lakes including ten reservoirs and 25 natural lakes. Table 3.1 provides the lakes coordinate, surface area, and the number of usable Landsat images. Lake Towuti is the clearest lake with a surface area of 561 km^2. The maximum SD was observed as 20 m in 1992 (Lehmusluoto et al., 1997). Lake Limboto is the most turbid lake in Indonesia; with a surface area of 56 km^2, the SD was observed as 0.4 m in 1993 (Lehmusluoto et al., 1997). Lake Toba is the largest lake with a surface area of 1,121 km^2. The maximum SD was observed as 15.5 m in the Northern part and 13.5 m in the Southern part in 1992 (Lehmusluoto et al., 1997). In 2009, SD was observed as around 11 m in the Northern part and 9.5 m in the Southern part (Nomosatryo and Lukman, 2012). Lake Dibawah is the smallest lakes among the 35 selected lakes, with a surface area of 11 km^2. SD was observed as 5.5 m in 1992 (Lehmusluoto et al., 1997). Figure 3.1 shows the locations of the selected lakes.

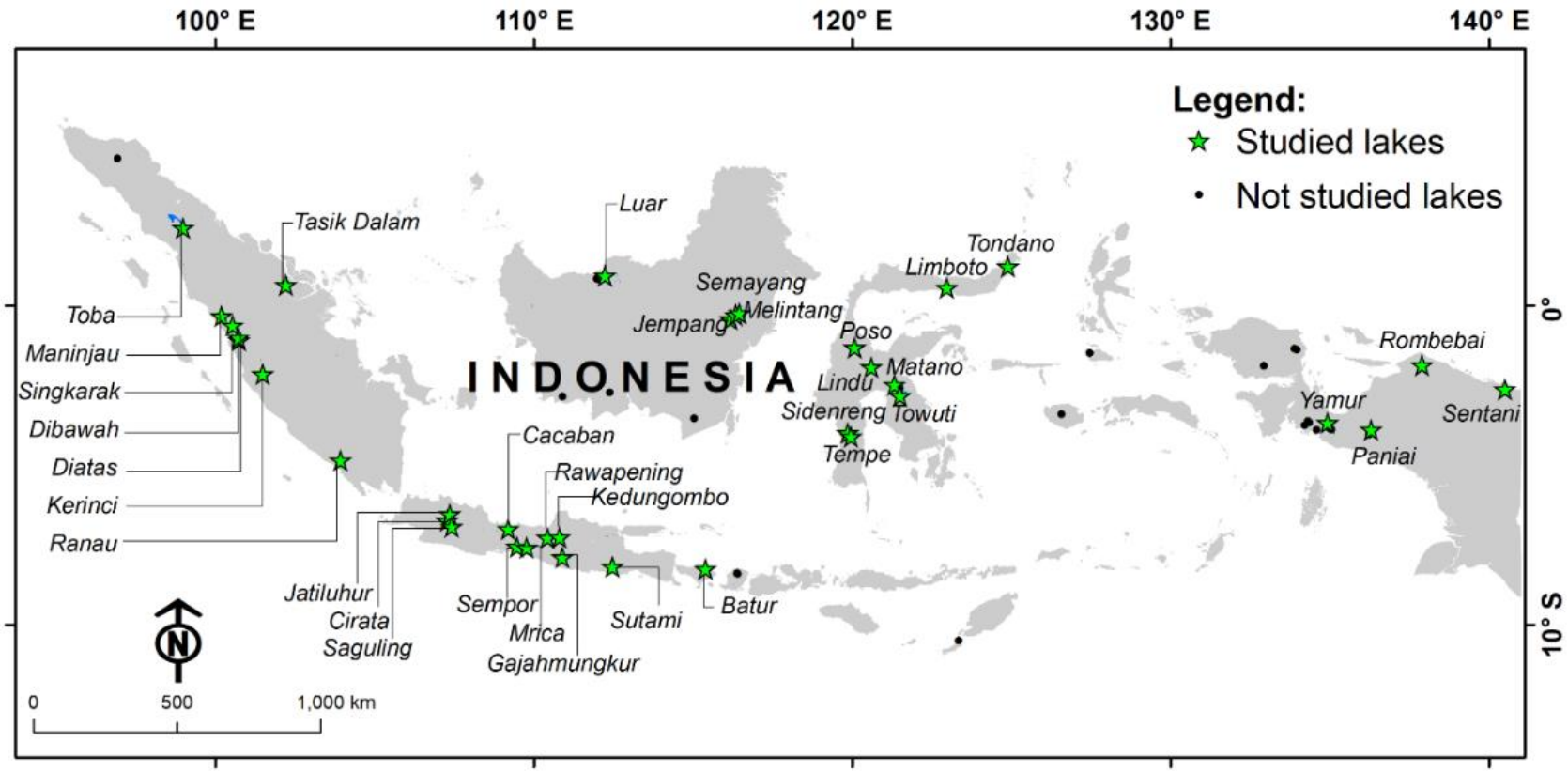

Figure 3.1. The locations Indonesian lakes with an area larger than 10 km2, thirty-five lakes were selected considering the amount of usable Landsat images (Green stars). In contrast, the other 25 lakes were not studied (Black points).

Table 3.1. List of 35 Selected Indonesian Lakes with an area larger than 10 km^2 and the amount of usable Landsat images

No.	Name	Island	Latitude (° N)	Longitude (° E)	Area (km^2)	Amount of Landsat (scene)
1	Toba	Sumatera	2.4347	98.9949	1,121	327
2	Maninjau	Sumatera	-0.3266	100.1924	96	230
3	Singkarak	Sumatera	-0.6122	100.5410	107	201
4	Dibawah	Sumatera	-1.0105	100.7310	11	192
5	Diatas	Sumatera	-1.0762	100.7548	12	200
6	Kerinci	Sumatera	-2.1476	101.4920	44	176
7	Tasik Dalam	Sumatera	0.6565	102.2243	18	286
8	Ranau	Sumatera	-4.8478	103.9392	125	196
9	Cirata (R)	Jawa	-6.7339	107.2843	62	329
10	Jatiluhur (R)	Jawa	-6.5343	107.3724	83	313
11	Saguling (R)	Jawa	-6.9306	107.4267	53	310
12	Cacaban (R)	Jawa	-7.0081	109.2105	59	281
13	Sempor (R)	Jawa	-7.5604	109.4845	12	328
14	Merica (R)	Jawa	-7.3854	109.6210	13	224
15	Wadaslintang (R)	Jawa	-7.5819	109.7865	15	303
16	Rawapening	Jawa	-7.2834	110.4333	27	320
17	Kedungombo (R)	Jawa	-7.2659	110.8240	65	158
18	Gajahmungkur (R)	Jawa	-7.8958	110.9053	88	214
19	Sutami (R)	Jawa	-8.1795	112.4753	15	258
20	Luar	Kalimantan	0.9360	112.2452	70	266
21	Jempang	Kalimantan	-0.4322	116.1837	85	227
22	Melintang	Kalimantan	-0.2966	116.3409	71	234
23	Semayang	Kalimantan	-0.2320	116.4567	99	238
24	Sidenreng	Sulawesi	-3.9879	119.8706	37	129
25	Tempe	Sulawesi	-4.1006	119.9627	75	124
26	Lindu	Sulawesi	-1.3166	120.0808	39	277
27	Poso	Sulawesi	-1.9179	120.6135	423	309
28	Matano	Sulawesi	-2.4830	121.3435	188	82
29	Towuti	Sulawesi	-2.8203	121.5181	657	140
30	Limboto	Sulawesi	0.5641	122.9818	21	152
31	Tondano	Sulawesi	1.2281	124.8973	53	151
32	Yamur	Papua	-3.6730	134.9357	52	316
33	Paniai	Papua	-3.8851	136.3100	213	254
34	Sentani	Papua	-2.6194	140.5085	156	186
35	Batur	Bali	-8.2588	115.4073	17	183
	Note: (R) = Reservoir					**Total: 8,114**

3.2.2. In situ SD Data Collection

The first in situ SD data set was collected from 23 lakes during 1992-1993 by the Finnish researcher (Lehmusluoto et al., 1997). The SD values ranged from 0.4 m to 20 m. For the second in situ SD data set, I measured 75 SD values from 14 lakes during 2014-2018. The SD values ranged from 0.03 m to 17.5 m. These two in situ SD data sets (Table 3.2) were used to evaluate the developed model in estimating SD in Indonesian lakes in different periods.

Table 3.2. Two-periods of in situ SD Dataset for Further Evaluate the Developed Model

Dataset	Number of lakes	Number of data	SD range (m)	Period	Sources
I	23	23	0.4 – 20	1992-1993	Lehmusluoto et al., 1997
II	14	75	0.03 – 17.5	2014-2018	My Surveys

3.2.3. Landsat Data collection

I downloaded Landsat TM/ETM+ images from the USGS website (https://earthexplorer.usgs.gov/). Theoretically, Landsat images were available globally from 1984 until now (until 2019 in this research). However, the images are not always available or downloadable. I used the same "Data Range" from January 1st, 1984 to December 31st, 2019, for the "Search Criteria" and download all available Landsat 5 TM and Landsat 7 ETM+ images. The "Cloud Cover Range" was not considered; later, the cloudy pixel will be removed in the Landsat Data Preprocessing procedure.

3.2.4. SD estimation

I carried out the same image preprocessing (i.e., removing contaminated water pixels, filtering images, and mitigating atmospheric effects) as in Chapter II before the Landsat TM/ETM+ data were used to estimate SD using the developed model. The SD equation of the developed model in Chapter II is rewritten as:

$$SD = \exp \{ -1.18 + 3.45(TM1/TM2) - 2.67(TM3/TM2)\}, \quad (14)$$

TM1, TM2, and TM3 are the preprocessed reflectance at Landsat TM/ETM+ Band 1, Band 2, and Band 3.

3.2.5. Data Postprocessing

I carried out data postprocessing to ensure the representativeness of the SD in each lake. I excluded Landsat images with the available water pixels less than 50% of a lake surface. I removed the 5% highest and the 5 % lowest SD values to avoid the outlier. Afterward, I averaged remained pixels. To improve the reliability of the historical data, I performed the Savitzky–Golay filter on the averaged data. Finally, I applied LOESS (the Locally wEighted Scatterplot Smoothing) to obtain long-term trends using the R program (R Core Team, 2018) with the *ggplot2* library (Wickham, 2016).

3.2.6. Relating Data Collections from Other Lakes

Since the available in situ SD data are minimal, to further confirm the reliability of the generated SD, I also collected data in other lakes from literature. These data include the number of fish cages and fish production in Lake Maninjau (Junaidi et al., 2014; *Badan Pusat Statistik Kabupaten Agam.;* 2016, 2017, 2018, 2019). Other data or information from previous studies or reports were collected to investigate factors related to water quality changes. Figure 3.2 shows the number of fish cages and fish production in Lake Maninjau from 1992 to 2016.

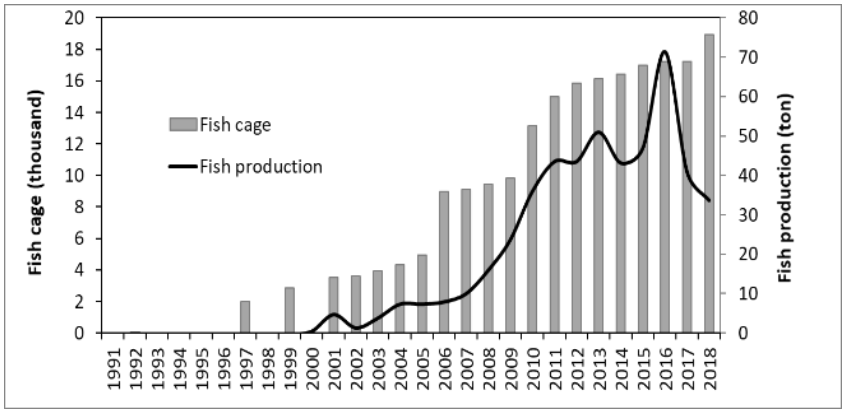

Figure 3.2. Number of fish cages and fish production in Lake Maninjau from 1992 to 2016

3.3. Results

3.3.1. Validation of the Developed SD Estimation Model in Various Waters

SD of 35 Indonesian lakes was estimated by the model BF (Eq. (14)) using pre-processed Landsat TM/ETM+ data. Figure 3.3. shows the number of usable images in 35 lakes for each year. I compare the estimated SD with corresponding available in situ data from various lakes in two different periods to confirm the reliability. The first comparison is between estimated SD and in situ SD in 23 lakes during 1992-1993, and the second comparison is between estimated SD and in situ SD in 14 lakes during 2014-2018.

Figure 3.4 shows the comparison of in situ SD data collected from 23 Indonesian lakes during 1992-1993 (in situ SD data set I) and the estimated SD using the developed model. As the coordinate data of in situ SD data set I collected from Lehmusluoto et al. (1997) was not available, the boxplot data representation method was used. Boxplot displays a range of SD values from a whole lake. It can be observed that the model has reasonable SD estimations in extremely turbid and highly turbid lakes (Lake Limboto, Kedungombo reservoir, Saguling reservoir, Lake Tempe, and Lake Rawapening). However, slightly underestimated SD were observed in Lake Dibawah, Lake Tondano, Lake Singkarak, Mrica Reservoir, and Lake Ranau. Remarkably underestimated SD was found in clear lake (i.e., Lake Maninjau, Lake Poso, and Lake Toba). For the very clear lakes (i.e., Lake Matano and Lake Towuti), even though the in situ SD were within the estimated

range, it was located in the higher percentile range. The time gap between in situ measurement and the satellite acquisition may influence the accuracy. Overall, the estimated SD shows reasonable values in 23 lakes in the 1990s, except for the SD estimations from the low-quality images & large time gaps.

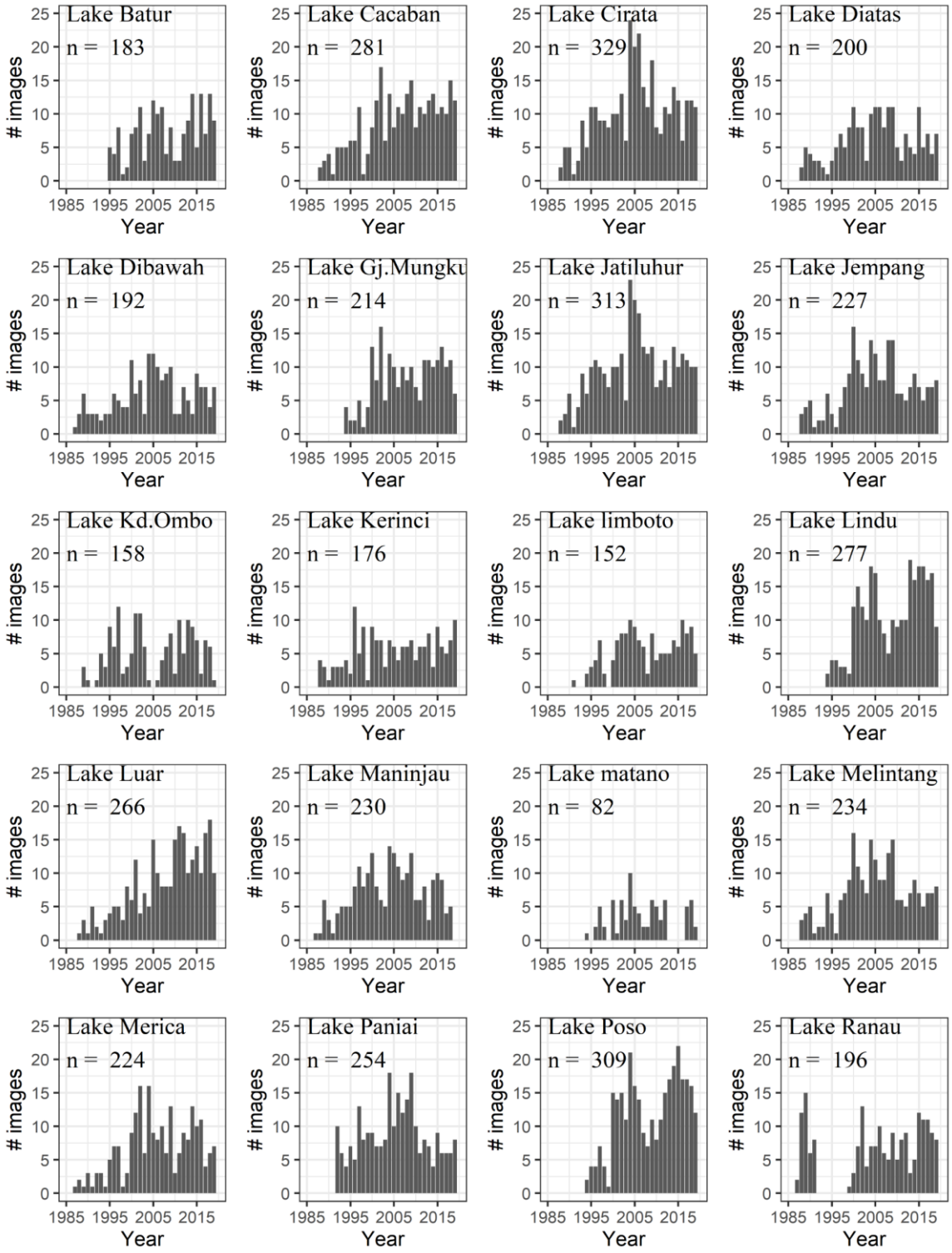

continued

continuation

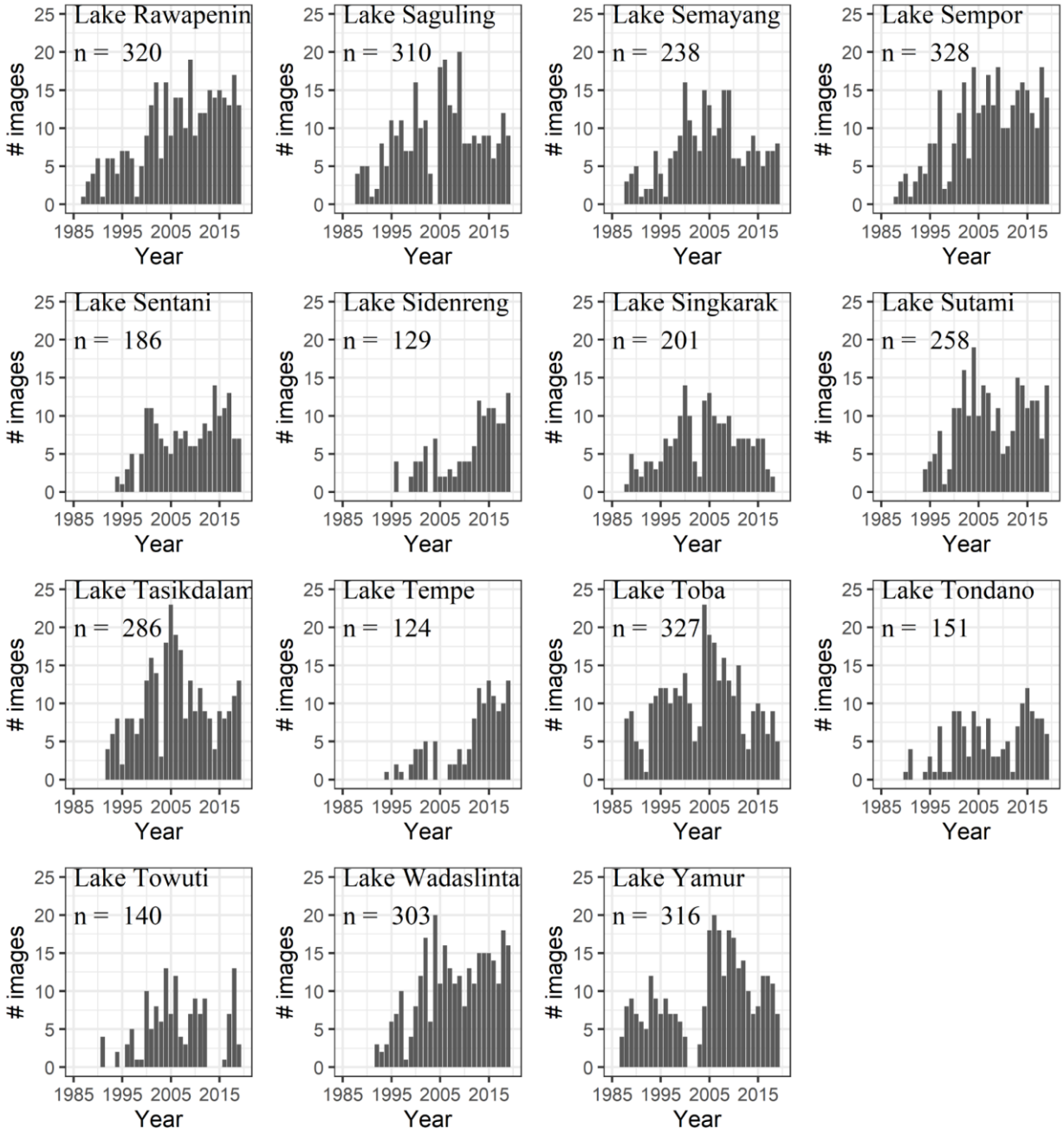

Figure 3.3. The number of usable images for 35 lakes from 1985 to 2019

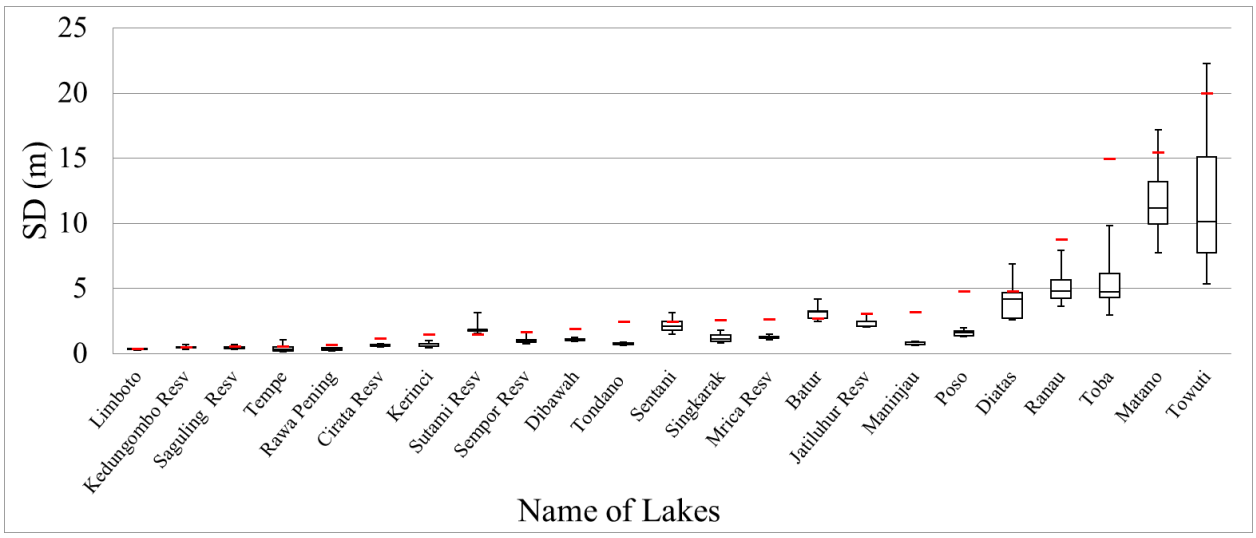

Figure 3.4. Comparison of in situ SD data (red line) collected from 23 lakes in the 1990s and the range of estimated SD using the developed model

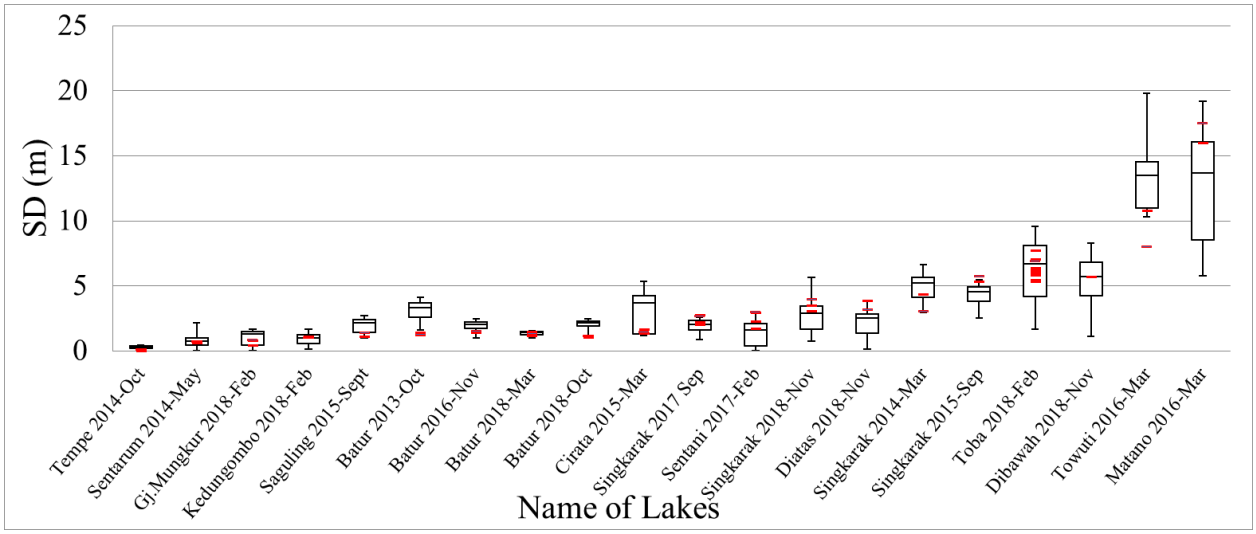

Figure 3.5. Comparison of in situ SD data (red line) collected from 14 lakes during 2014-2018 and the range of estimated SD using the developed model

Figure 3.5 shows the in situ SD data collected from 14 Indonesian lakes during 2014-2018 (in situ SD data set II) and the estimated SD using the developed model. The time gap between in situ measurement and the satellite acquisition was narrower compared to in Figure 3.4. Overall, the estimated SD generally show reasonable values in 14 Indonesian lakes during 2014-2018.

3.3.2. Further Validation of the Generated Long-Term SD Database

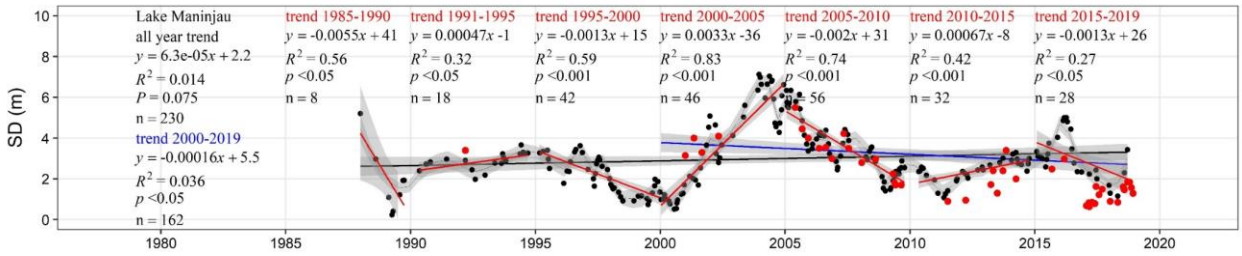

Figure 3.6. Long-term change of SD in Lake Maninjau

Febrianti (2000) and Sulastri (2002) reported a heavy algal bloom occurred in 2000 in Lake Maninjau. This event was also detected by my Landsat-based SD estimations, which showed low SD values during that period (Figure 3.6). To weaken the algal bloom effects on Lake Maninjau, residents around the lake asked the power company to open the secondary watergate in March 2001 to flush the surface waters (Fakhrudin et al., 2002). After that, the water transparency in Lake Maninjau increased significantly. The RCL (LIPI) observed the highest SD values of 4.1 m in May 2002 and 5.8 m in May 2005 (Henny et al., 2016). The trend of increased water transparency was also revealed by the Landsat time-series data (Figure 3.6). These results indicate that water management is effective in improving water quality.

The continuous decrease of SD values during 2004 and 2012 from both the in situ-measured and Landsat-based SD values can be explained by the dramatically increased number of fish cages in Lake Maninjau. In 2005, the number of fish cages in the lake was 4,920 units, and this number increased to 8,955 units in 2006 and 13,129 units in 2010 (Figure 3.2). I observed a strong correlation between the number of fish cages and the Landsat-based SD values during 2004–2012 (R^2=0.88, Figure 3.7).

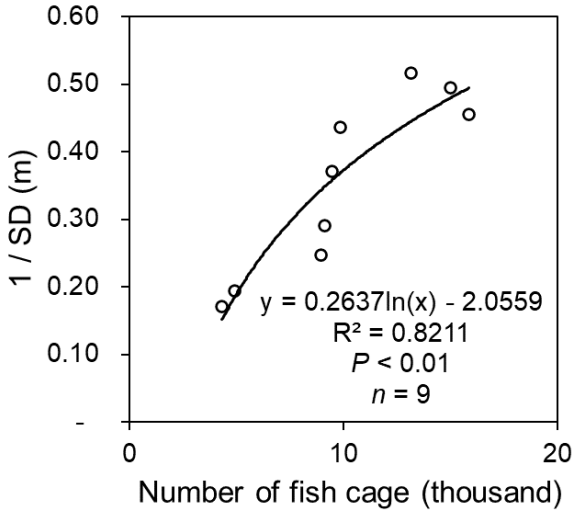

Figure 3.7. The relationship between the number of fish cages and 1/ SD generated from Landsat during 2004-2012 in Lake Maninjau shows a positive correlation.

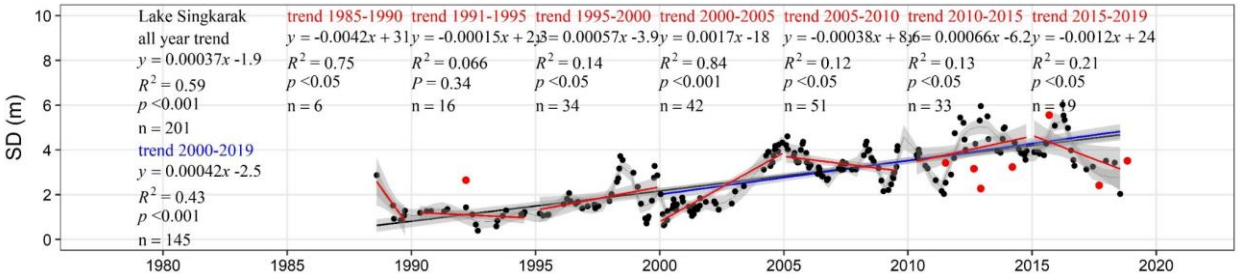

Figure 3.8. Long-term change of SD in Lake Singkarak

Lake Singkarak is a lake close to Lake Maninjau. In early 1990, fish aquaculture was also introduced in Lake Singkarak as that in Lake Maninjau. However, the profit was not as good as in Lake Maninjau. Risdawati (2011) reported that a fish parasite (*Cirolana. sp*) probably caused the low fish productivity in Lake Singkarak. Therefore, fish cages culture is not popular in the lake.

The Singkarak Hydroelectric Power Plant (HEPP) began operation in May 1998, and in a certain sense, it changed the water balance in Lake Singkarak. Previously, the outlet of Lake Singkarak was located at the north-east (*Batang Ombilin* River) and flowed to the east direction. After the operating of HEPP, the outflows were shifted to the west direction through an artificial tunnel for hydropower purposes. This water management probably removed the upper layer of turbid water and was supposed to trigger a gradual SD increased during 2000-2005 (Figure 3.8).

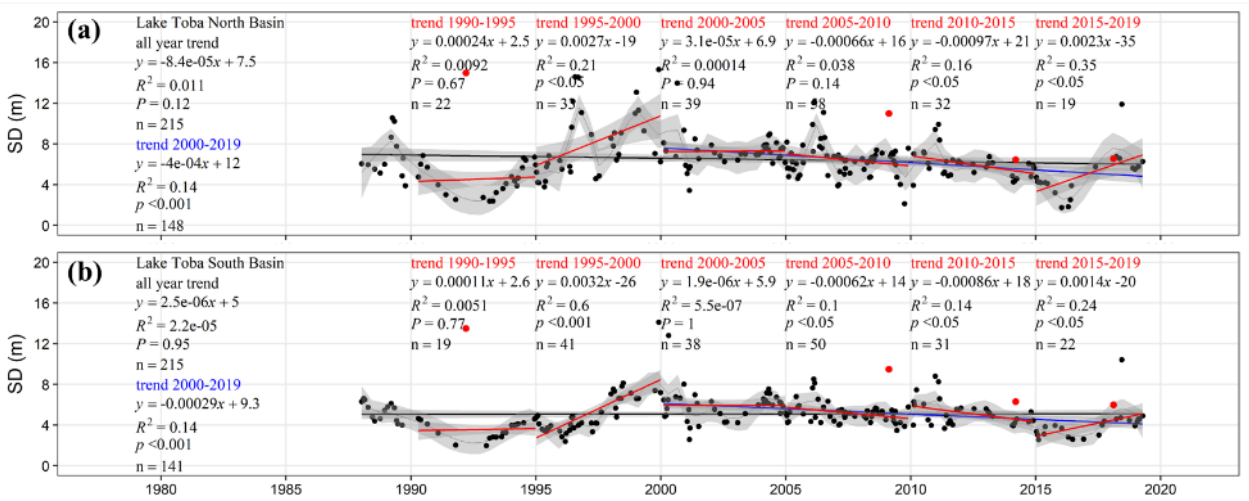

Figure 3.9. Long-term change of SD in Lake Toba North Basin (a) and South Basin (b)

Decreasing Rainfall (El Niño) during 1991-1992,1995,1997-1998 & 2015 is probably associating with the decreased SD in Lake Toba during corresponding periods (Figure 3.9). I measured three SD at three sites in Lake Toba in March 2014; the values are 6.54 m, 6.50 m, and 6.22 m, respectively. These values are relatively close to the Landsat-based SD shown in Figure 3.9. My other field surveys in February 2018 found SD is 6.5 m (averaged from 10 measurements); this value was slightly lower than Landsat-based SD.

A report by the World Bank (2019) pointed out the degrading water quality in Lake Toba. This trend agrees with the significant decreased SD shown by Landsat TM/ETM+ data from 2000 to 2019 (Figure 3.9 blue line). World Bank (2019) reported that fish culture, land use, landcover changes, and short-term weather dynamics are the main drivers regulating water quality in Lake Toba. This result demonstrates the reliability of the Model BF based long-term SD database.

3.3.3. Long-Term SD Database for 35 Indonesian Lakes

Figures 3.6, 3.8, and 3.9 show that the generated SD database is reliable enough to capture water transparency's change tendency in Lake Maninjau, Lake Singkarak, and Lake Toba. These results increase the confidence to apply the developed model to generate an SD database for other Indonesian lakes. Figures 3.10 to 3.41 show the generated SD database for the remaining 32 Indonesian lakes. The black points are the averaged SD values estimated from the preprocessed Landsat using the developed SD estimation model in Chapter II. The black tin line was obtained from the black points using the LOESS trend analysis method (the **L**ocally w**E**ighted **S**catterplot **S**moothing) using the R language. Gray areas represent 95% confidence intervals of the LOESS trend analysis. The solid black line is the linear trend of averaged estimated SD using all data. Considering the data availability, I select data from 2000 to 2019 to perform SD changing trend comparison. The solid blue line is the linear trend of averaged estimated SD using data from 2000 to 2019. The red line was the linear trend of averaged estimated SD of five-year periods (1985-1990, 1990-1995, 1995-2000, 2000-2005, 2005-2010, 2010-2015, and 2015-2019).

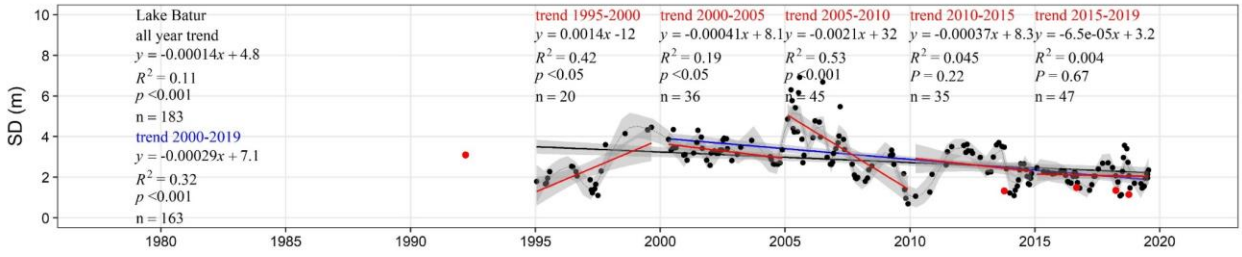

Figure 3.10. Long-term of change SD in Lake Batur

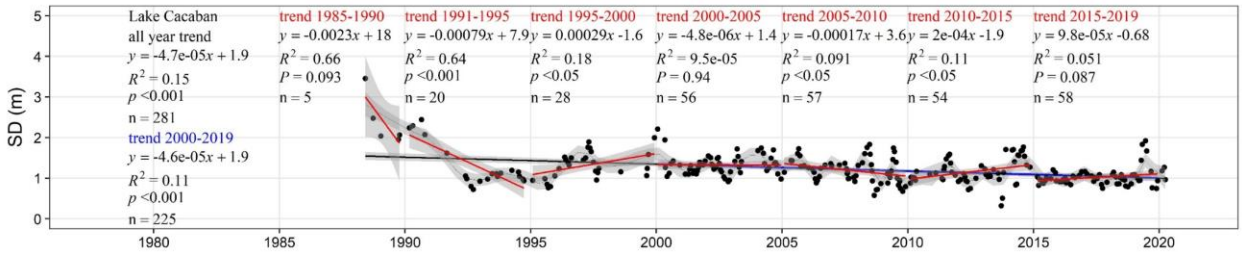

Figure 3.11. Long-term of change SD in Lake Cacaban (reservoir)

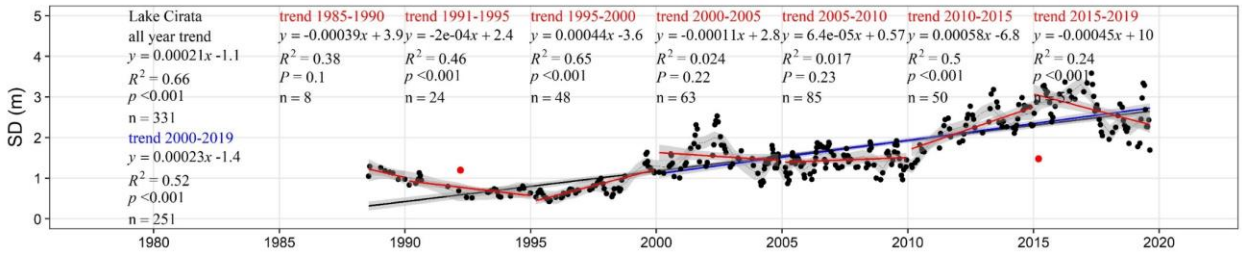

Figure 3.12. Long-term change of SD in Lake Cirata (reservoir)

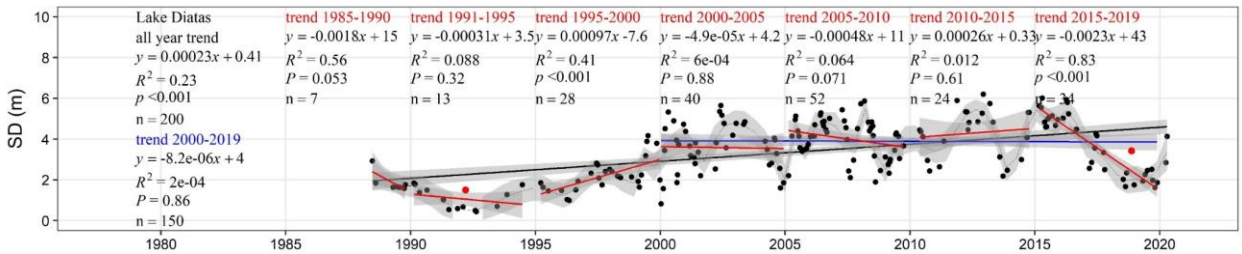

Figure 3.13. Long-term change of SD in Lake Diatas

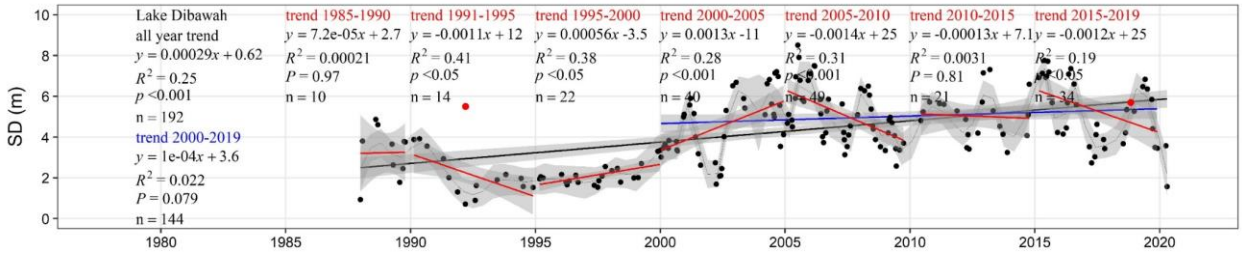

Figure 3.14. Long-term change of SD in Lake Dibawah

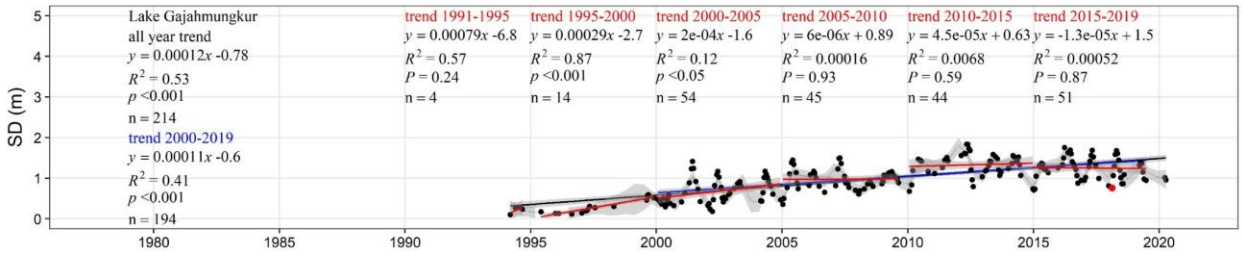

Figure 3.15. Long-term change of SD in Lake Gajahmungkur (reservoir)

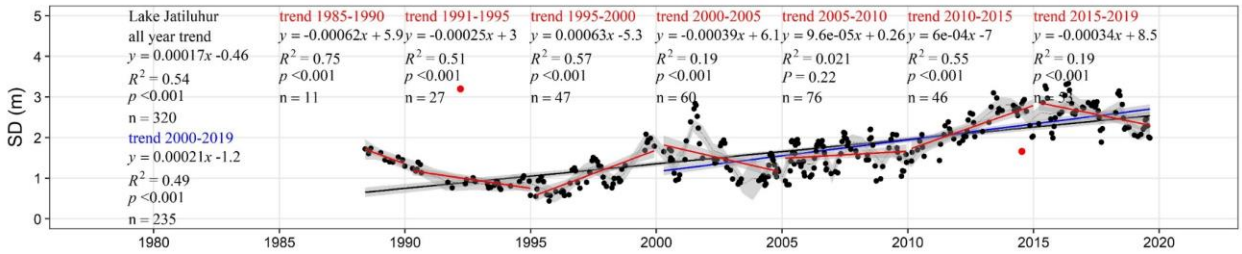

Figure 3.16. Long-term change of SD in Lake Jatiluhur (reservoir)

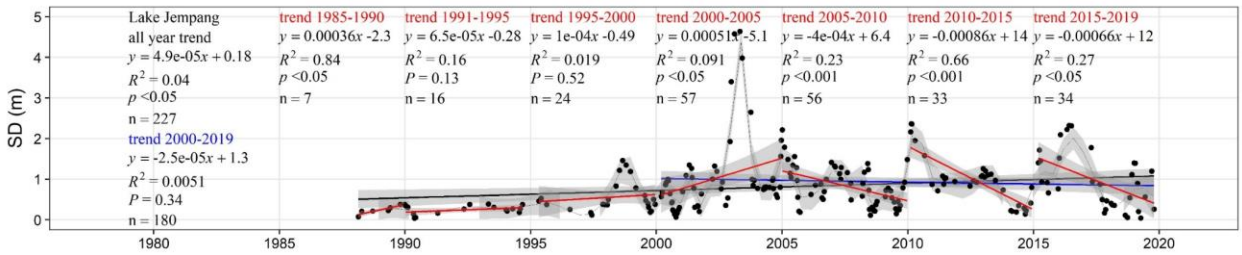

Figure 3.17. Long-term change of SD in Lake Jempang

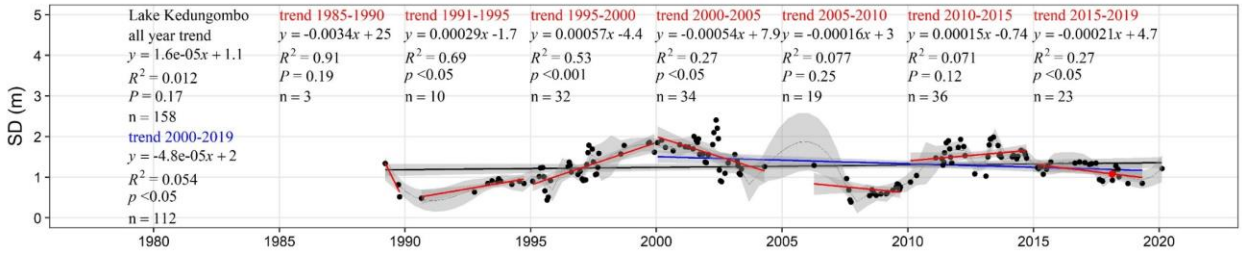

Figure 3.18. Long-term change of SD in Lake Kedungombo (reservoir)

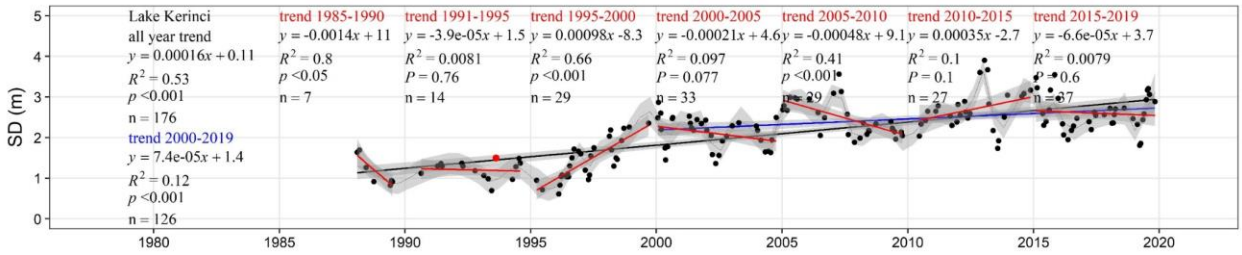

Figure 3.19. Long-term change of SD in Lake Kerinci

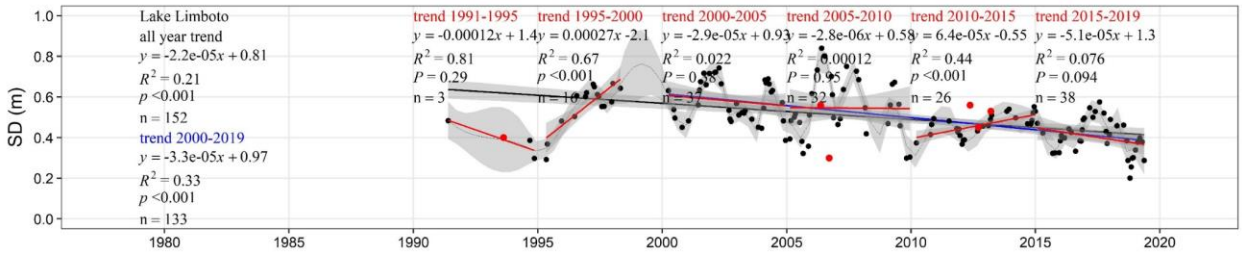

Figure 3.20. Long-term change of SD in Lake Limboto

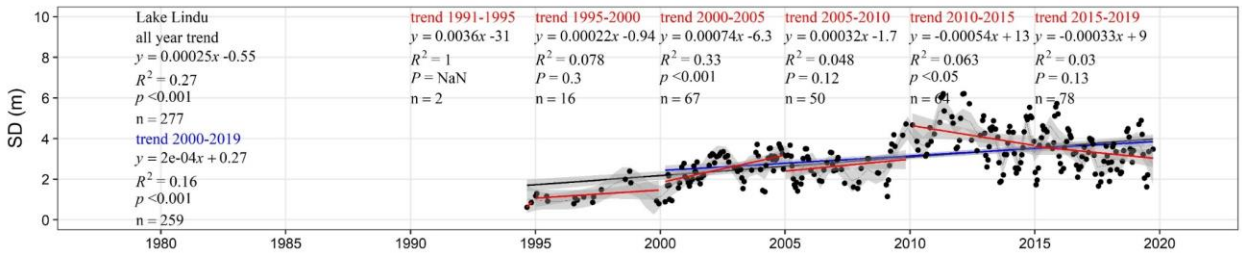

Figure 3.21. Long-term change of SD in Lake Lindu

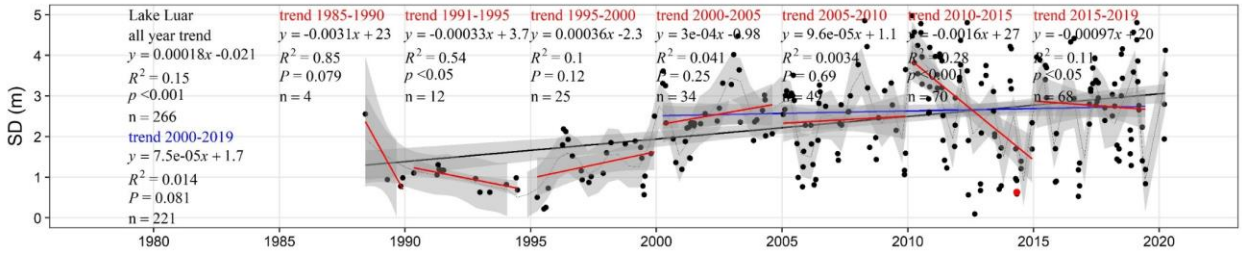

Figure 3.22. Long-term change of SD in Lake Luar

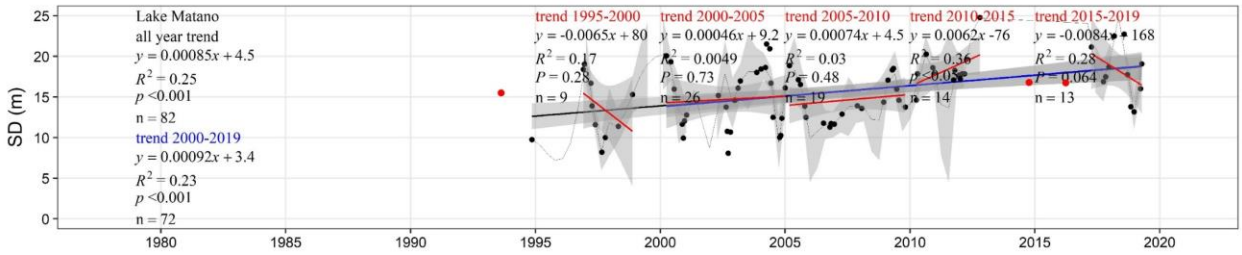

Figure 3.23. Long-term change of SD in Lake Matano

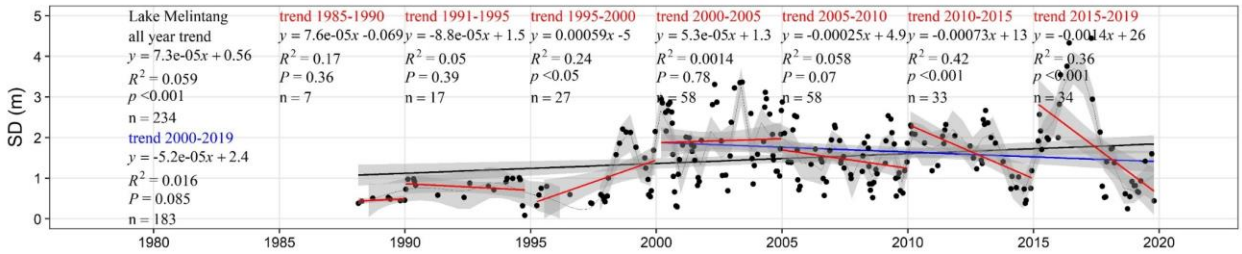

Figure 3.24. Long-term change of SD in Lake Melintang

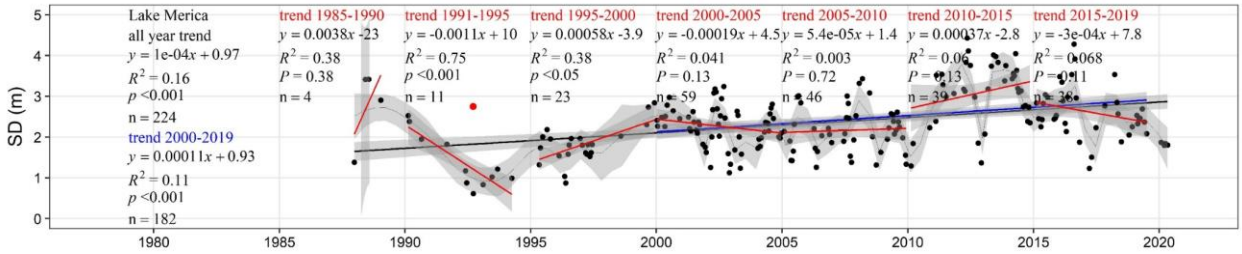

Figure 3.25. Long-term change of SD in Lake Merica (reservoir)

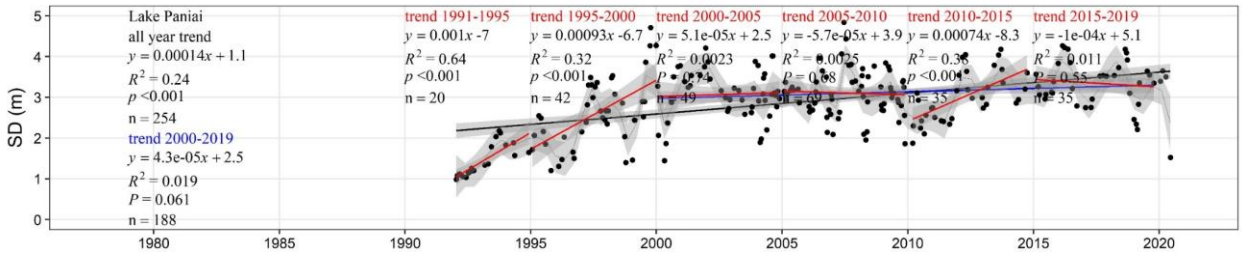

Figure 3.26. Long-term change of SD in Lake Paniai

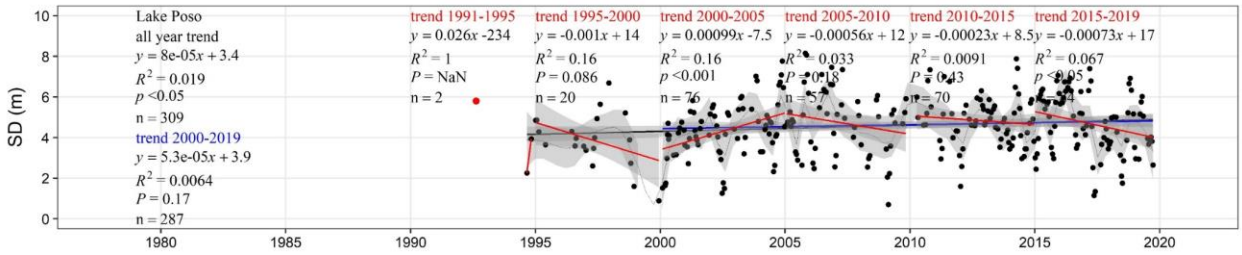

Figure 3.27. Long-term change of SD in Lake Poso

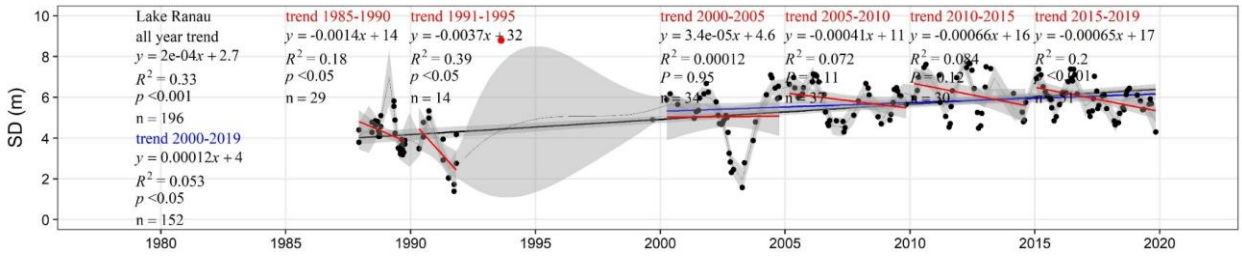

Figure 3.28. Long-term change of SD in Lake Ranau

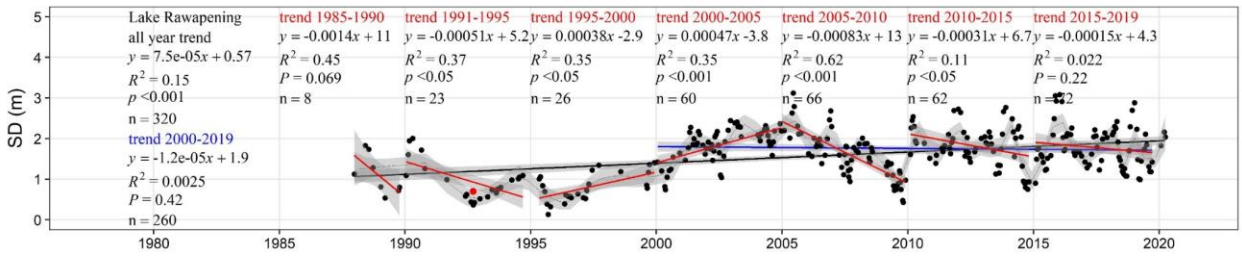

Figure 3.29. Long-term change of SD in Lake Rawapening

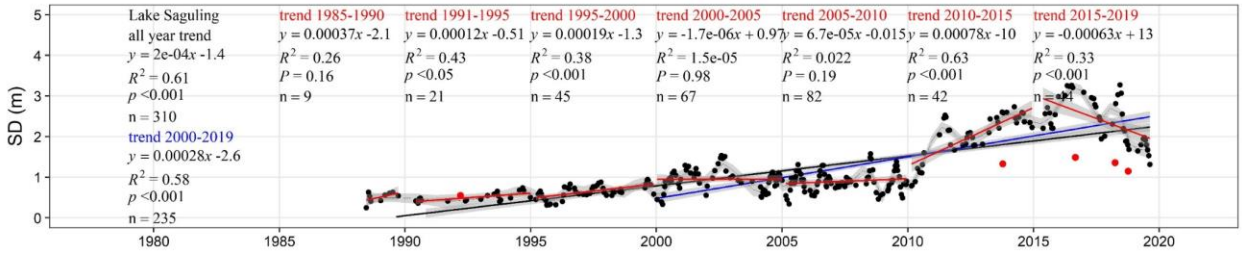

Figure 3.30. Long-term change of SD in Lake Saguling (reservoir)

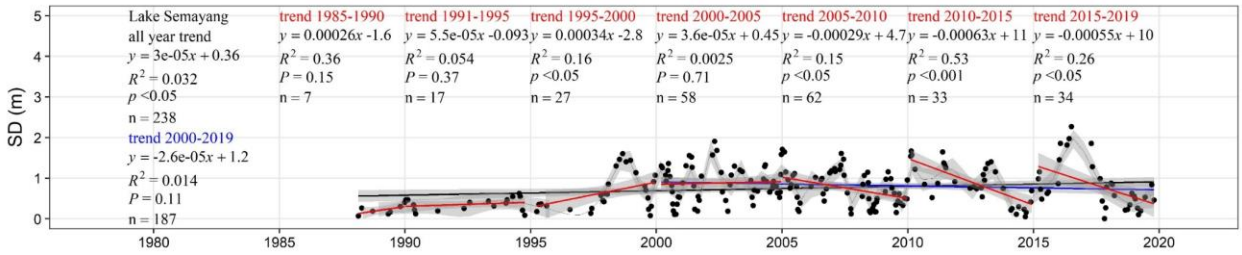

Figure 3.31. Long-term change of SD in Lake Semayang

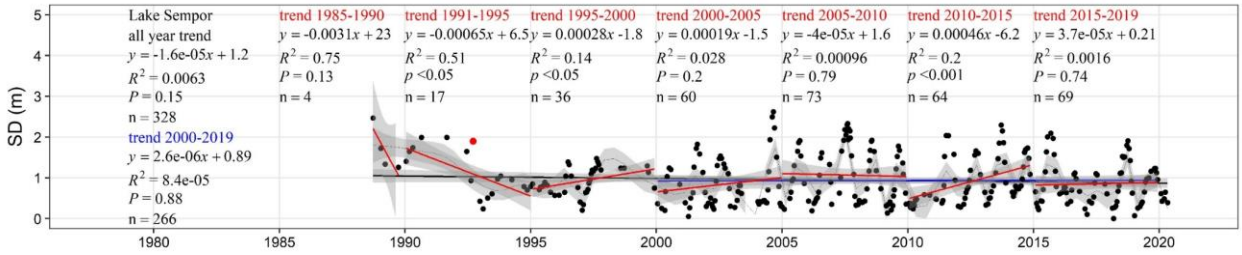

Figure 3.32. Long-term change of SD in Lake Sempor (reservoir)

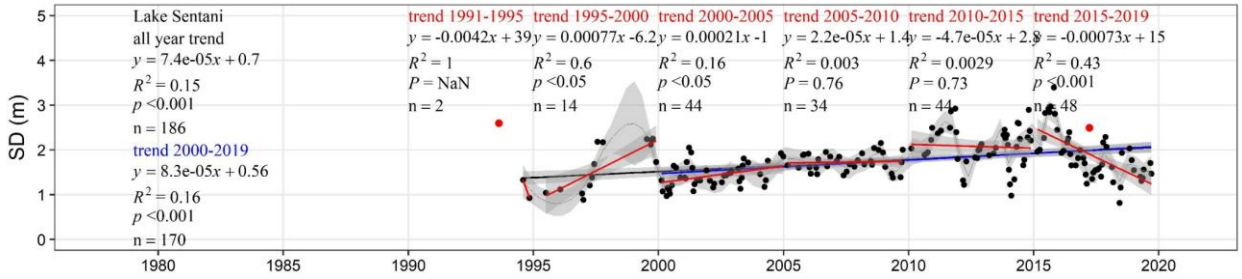

Figure 3.33. Long-term change of SD in Lake Sentani

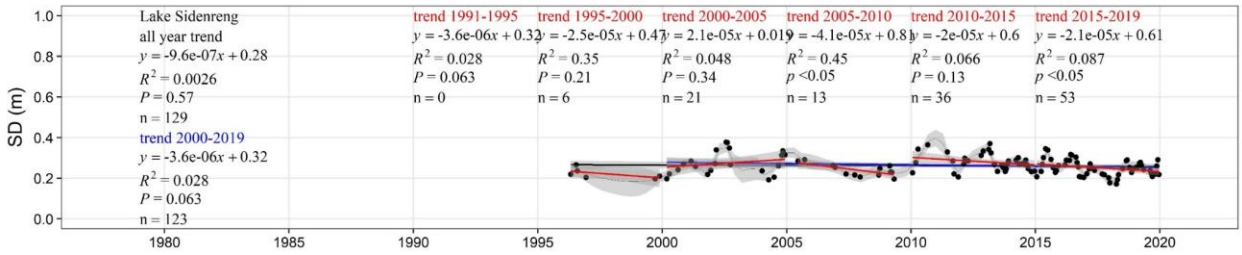

Figure 3.34. Long-term change of SD in Lake Sidenreng

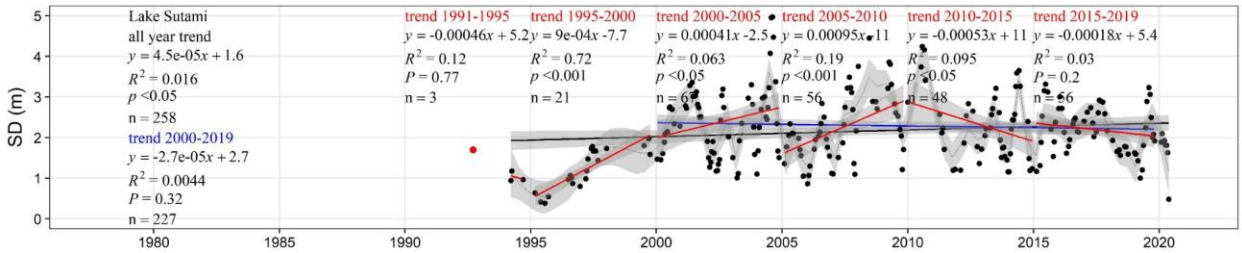

Figure 3.35. Long-term change of SD in Lake Sutami (Reservoir)

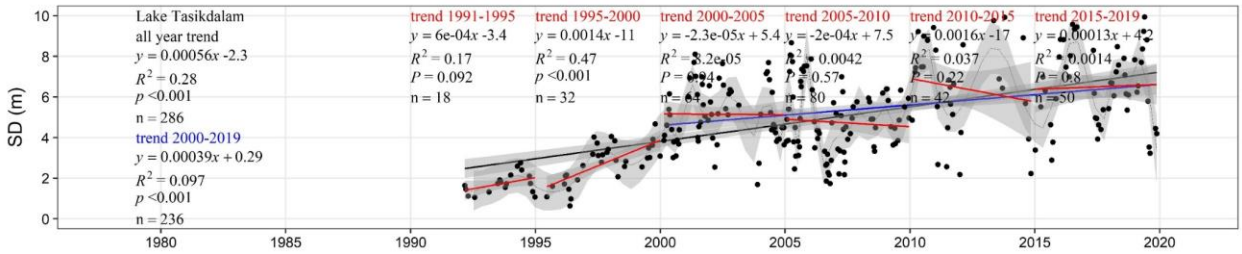

Figure 3.36. Long-term change of SD in Lake Tasikdalam

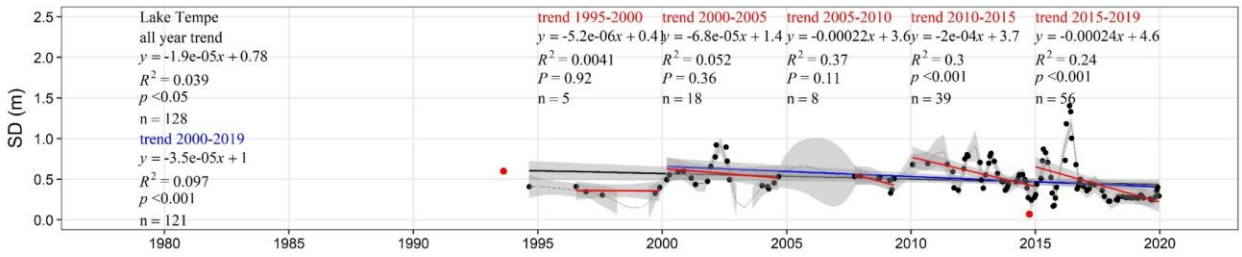

Figure 3.37. Long-term change of SD in Lake Tempe

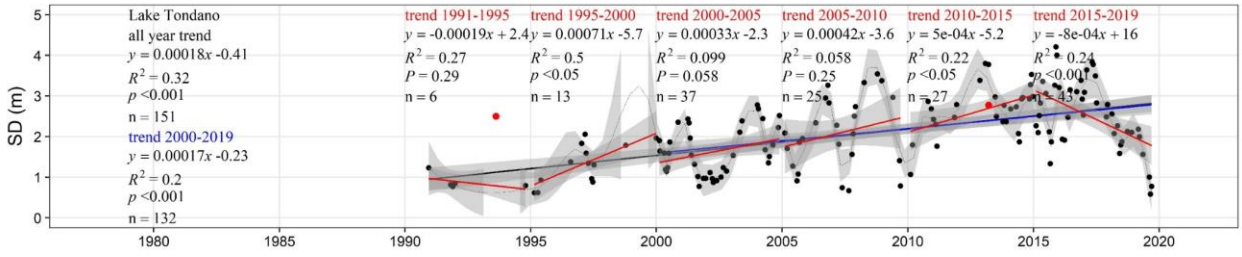

Figure 3.38. Long-term change of SD in Lake Tondano

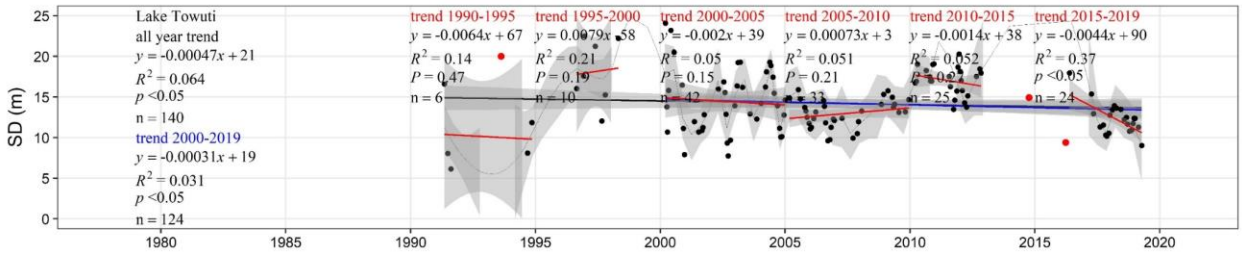

Figure 3.39. Long-term change of SD in Lake Towuti

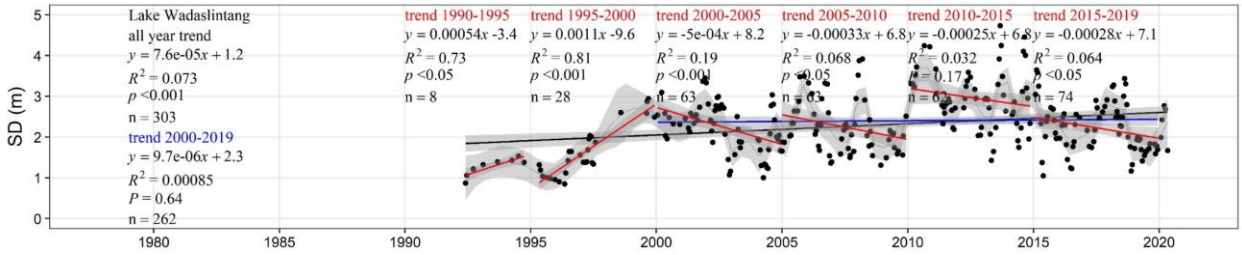

Figure 3.40. Long-term change of SD in Lake Wadaslintang (reservoir)

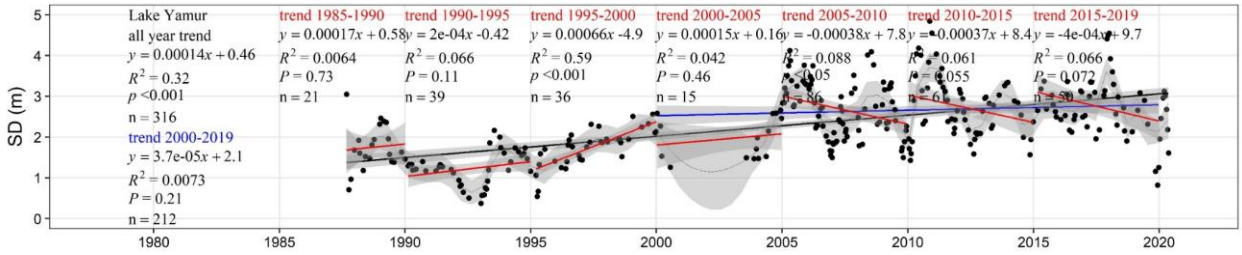

Figure 3.41. Long-term change of SD in Lake Yamur

3.3.4. Spatial distribution of SD in 35 Indonesian Lakes

Figures 3.42 to 3.76 show the spatial distribution of a five-year averaged SD estimated from Landsat TM/ETM+ in the 35 selected Indonesian lakes. The five-year periods are 1987-1990, 1990-1995, 1995-2000, 2000-2005, 2005-2010, 2010-2015 and 2015-2019. Each pixel is the average of the whole pixel during the corresponding period. In the case of no data, I ignore it in the averaging calculation.

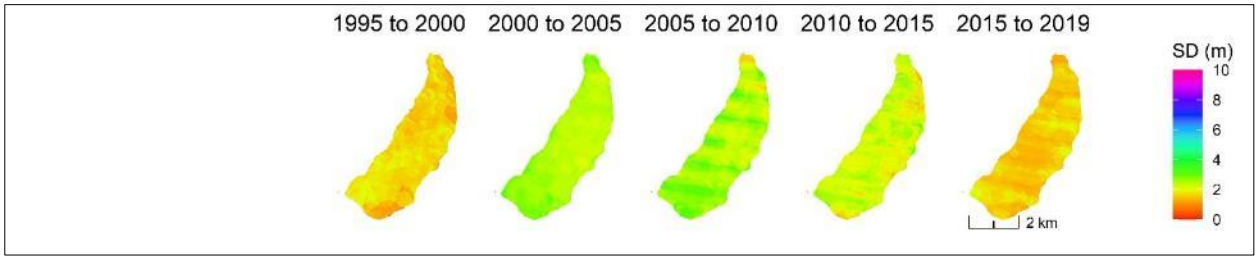

Figure 3.42. Spatial distribution of 5-year averaged SD in Lake Batur

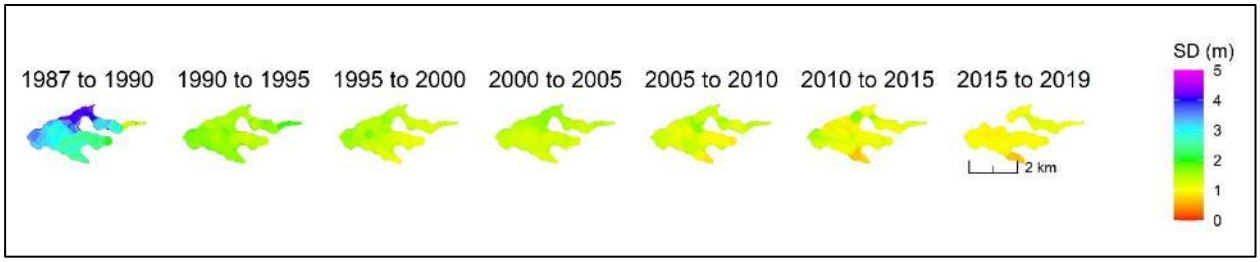

Figure 3.43. Spatial distribution of 5-year averaged SD in Lake Cacaban (reservoir)

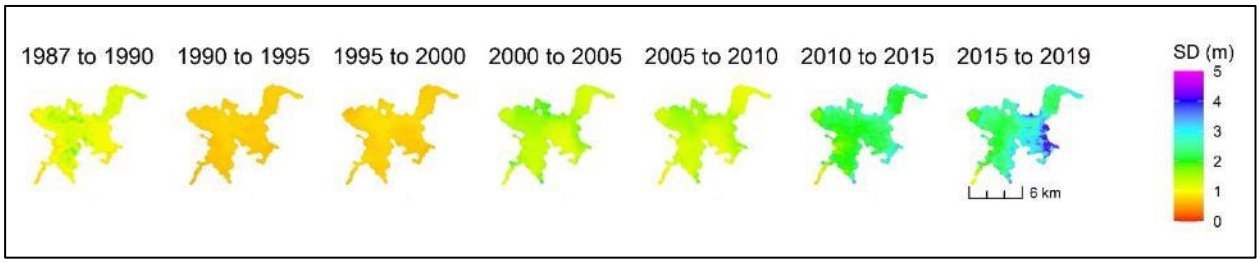

Figure 3.44. Spatial distribution of 5-year averaged SD in Lake Cirata (reservoir)

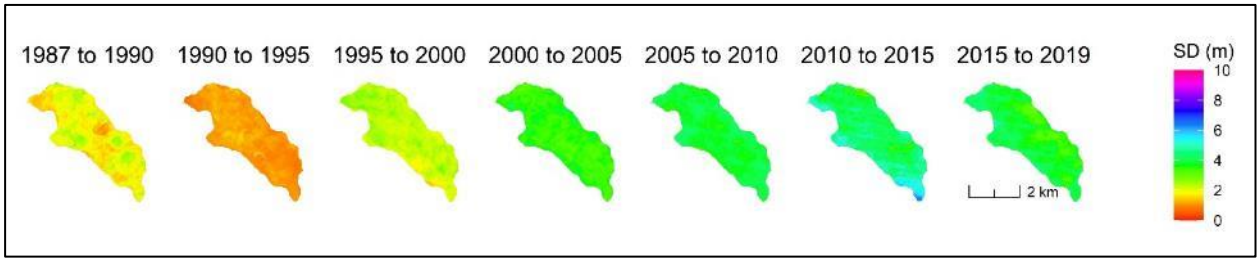

Figure 3.45. Spatial distribution of 5-year averaged SD in Lake Diatas

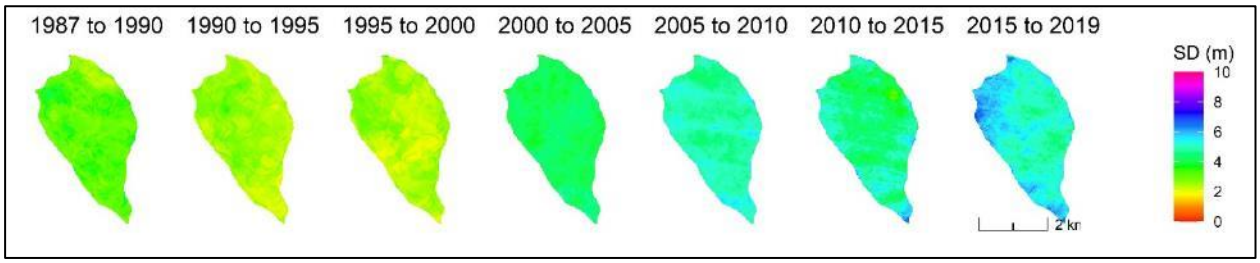

Figure 3.46. Spatial distribution of 5-year averaged SD in Lake Dibawah

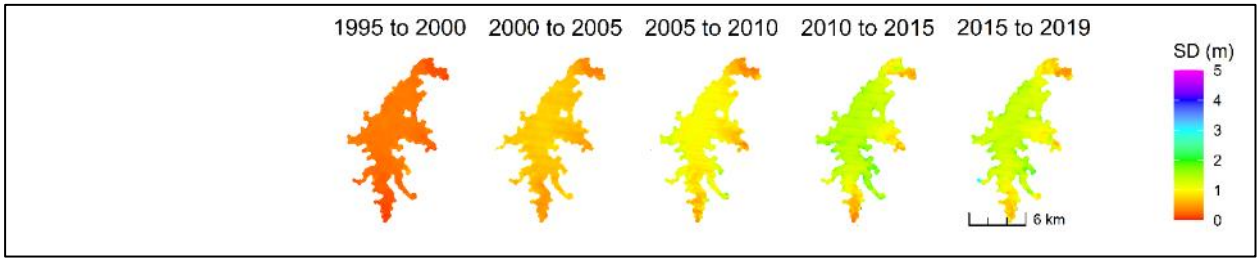

Figure 3.47. Spatial distribution of 5-year averaged SD in Lake Gajahmungkur (reservoir)

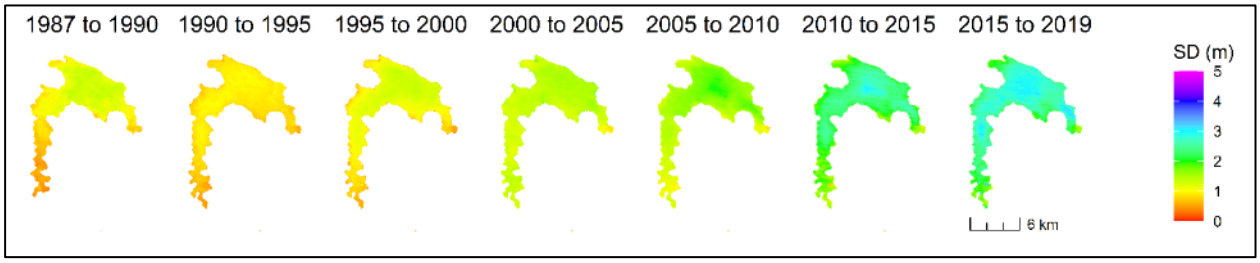

Figure 3.48. Spatial distribution of 5-year averaged SD in Lake Jatiluhur (reservoir)

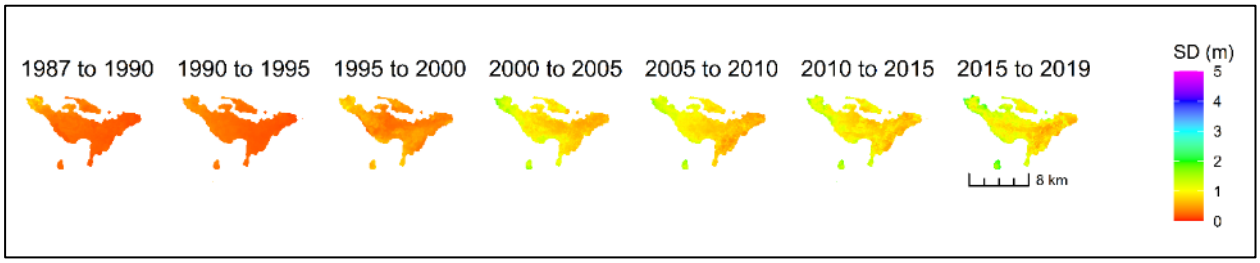

Figure 3.49. Spatial distribution of 5-year averaged SD in Lake Jempang

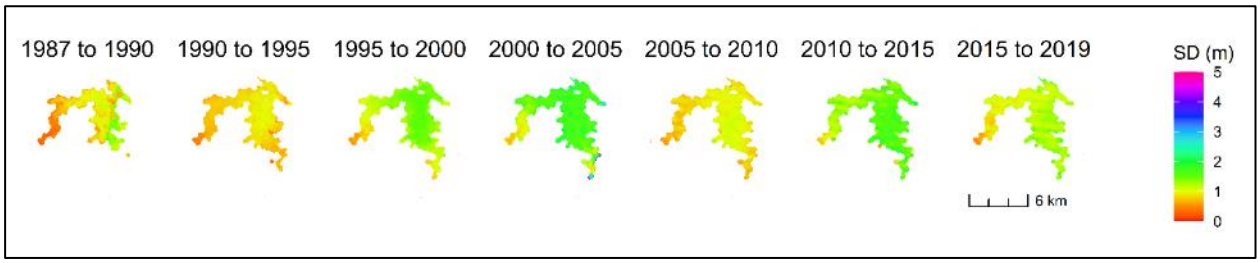

Figure 3.50. Spatial distribution of 5-year averaged SD in Lake Kedungombo (reservoir)

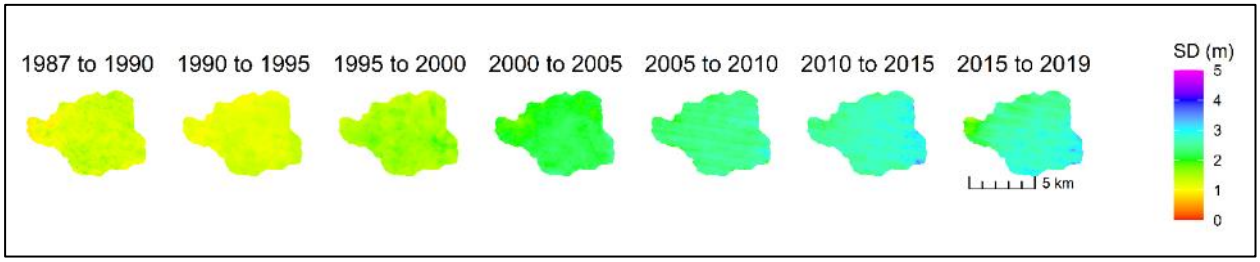

Figure 3.51. Spatial distribution of 5-year averaged SD in Lake Kerinci

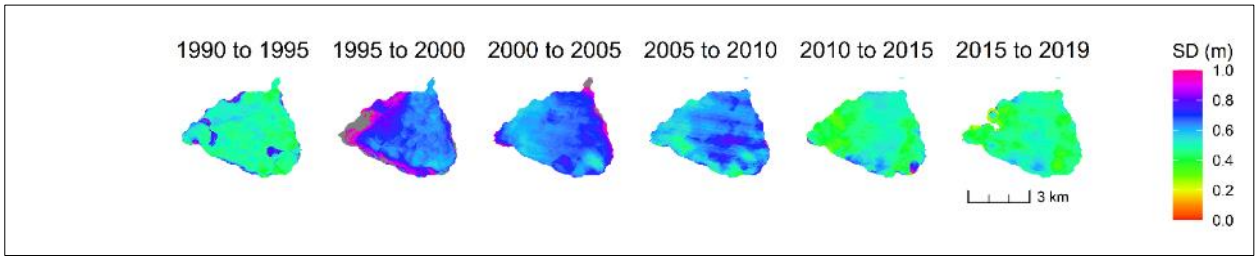

Figure 3.52. Spatial distribution of 5-year averaged SD in Lake Limboto

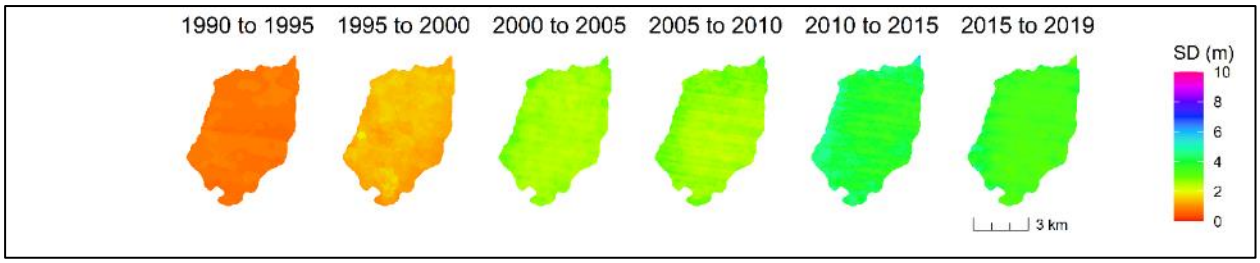

Figure 3.53. Spatial distribution of 5-year averaged SD in Lake Lindu

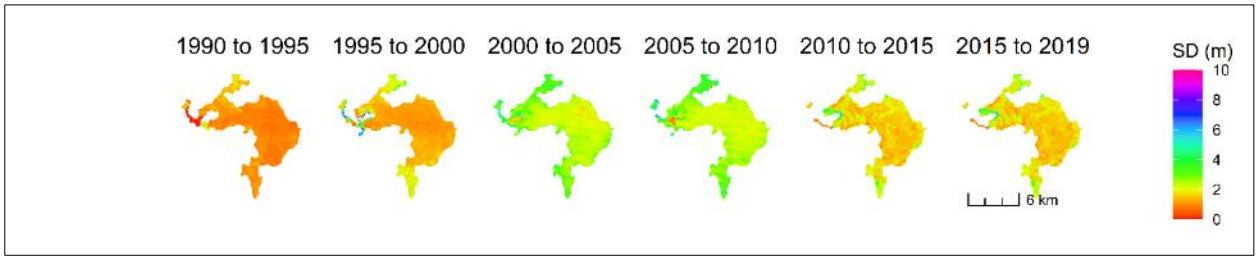

Figure 3.54. Spatial distribution of 5-year averaged SD in Lake Luar

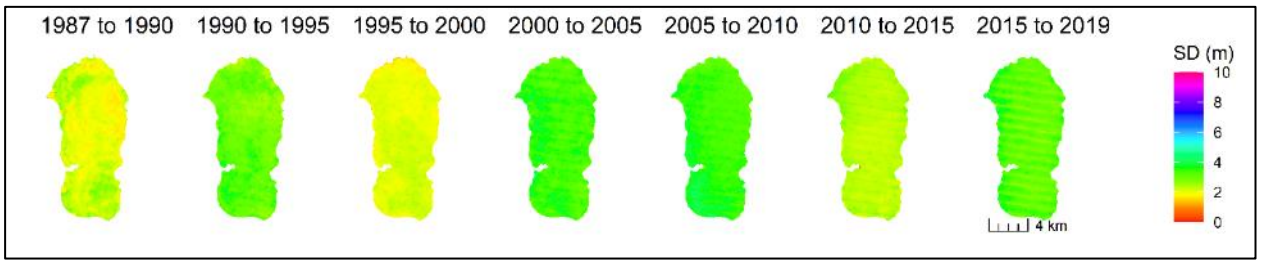

Figure 3.55. Spatial distribution of 5-year averaged SD in Lake Maninjau

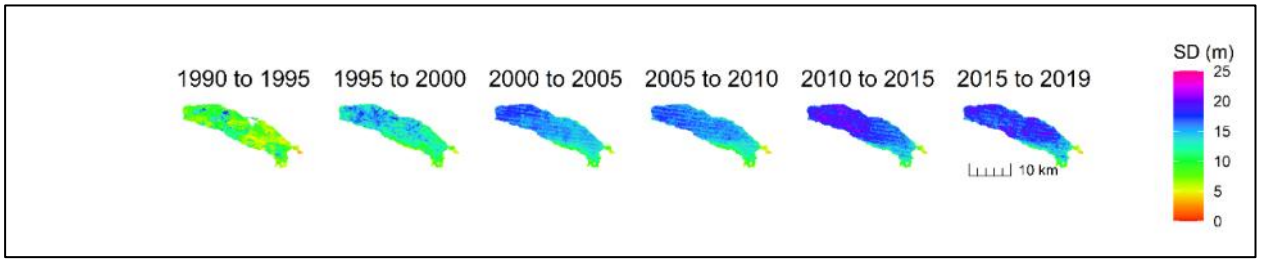

Figure 3.56. Spatial distribution of 5-year averaged SD in Lake Matano

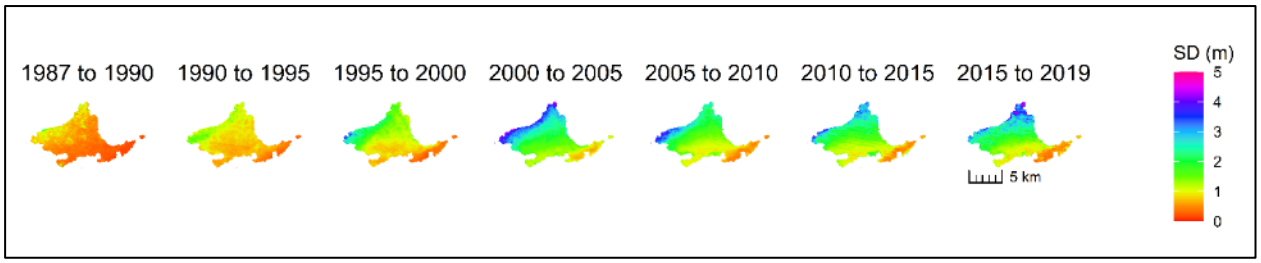

Figure 3.57. Spatial distribution of 5-year averaged SD in Lake Melintang

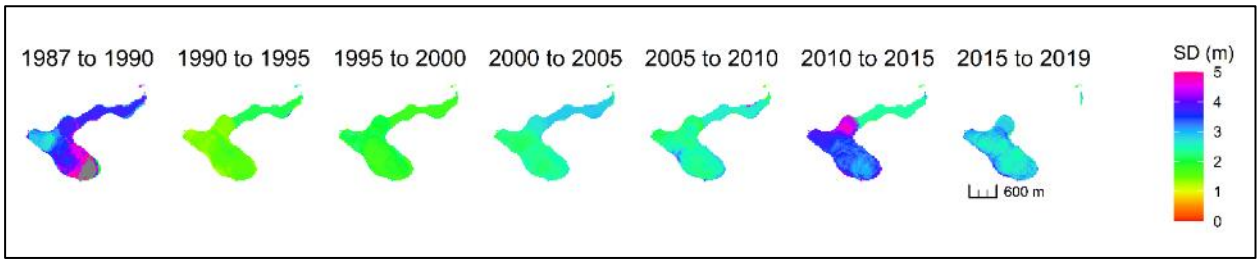

Figure 3.58. Spatial distribution of 5-year averaged SD in Lake Merica (reservoir)

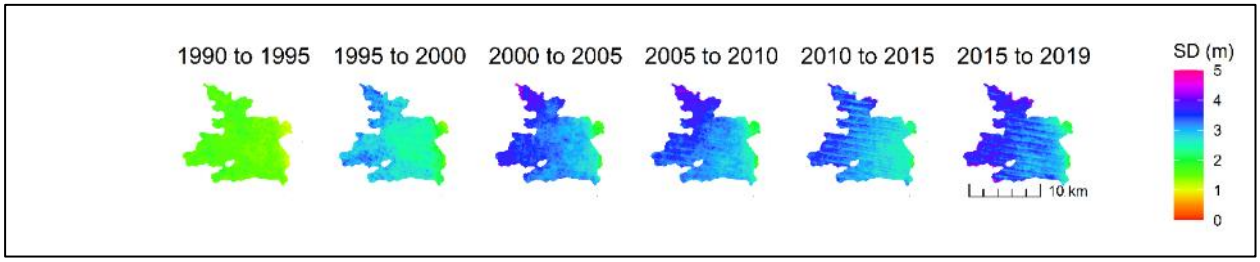

Figure 3.59. Spatial distribution of 5-year averaged SD in Lake Paniai

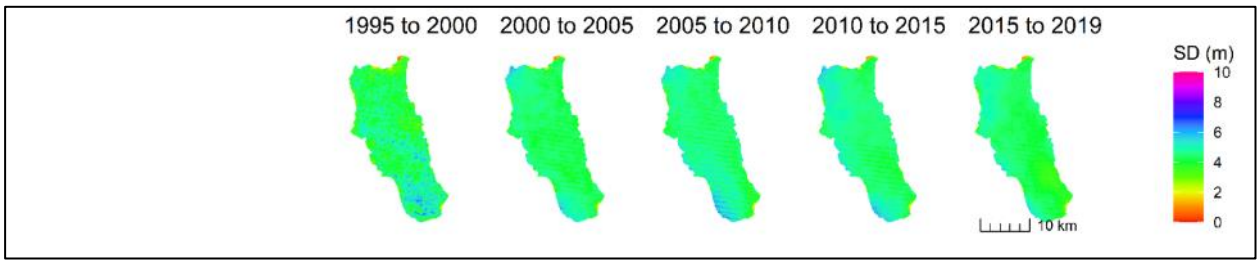

Figure 3.60. Spatial distribution of 5-year averaged SD in Lake Poso

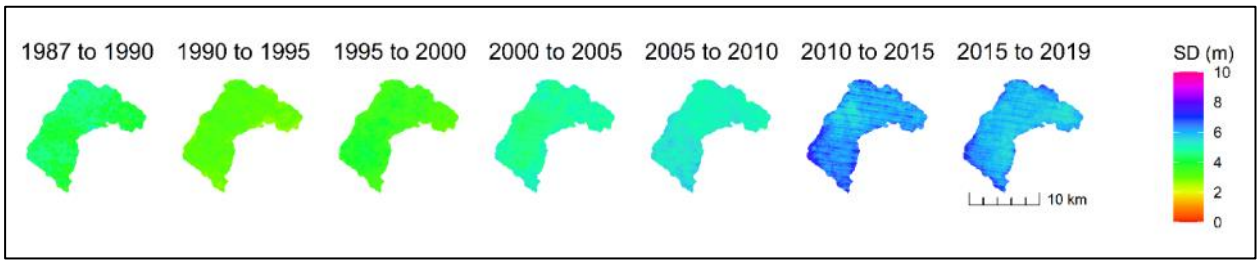

Figure 3.61. Spatial distribution of 5-year averaged SD in Lake Ranau

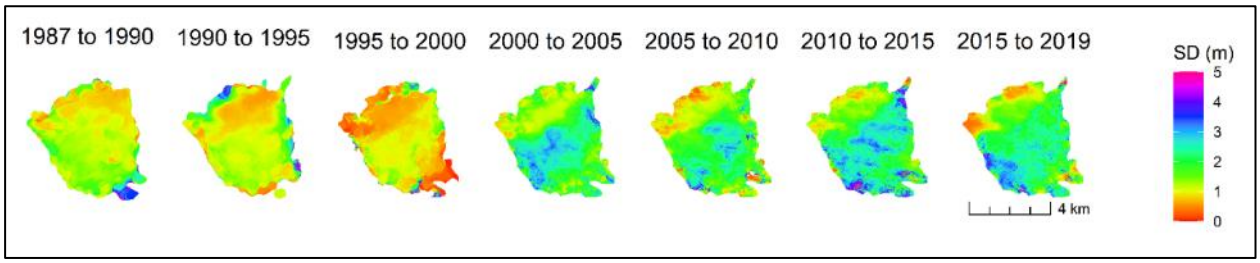

Figure 3.62. Spatial distribution of 5-year averaged SD in Lake Rawapening

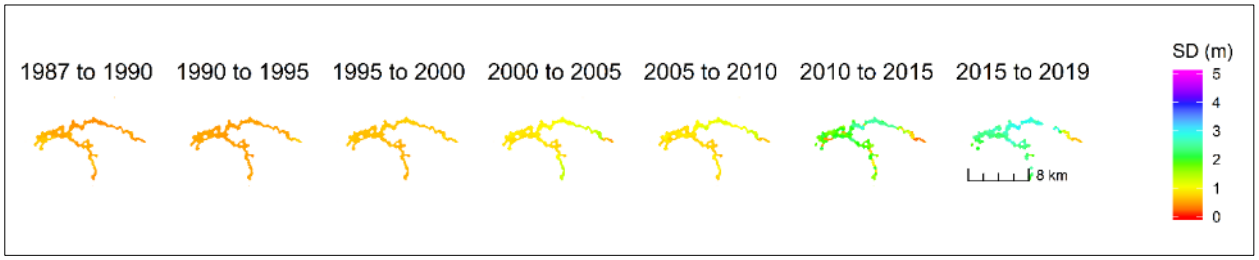

Figure 3.63. Spatial distribution of 5-year averaged SD in Lake Saguling (reservoir)

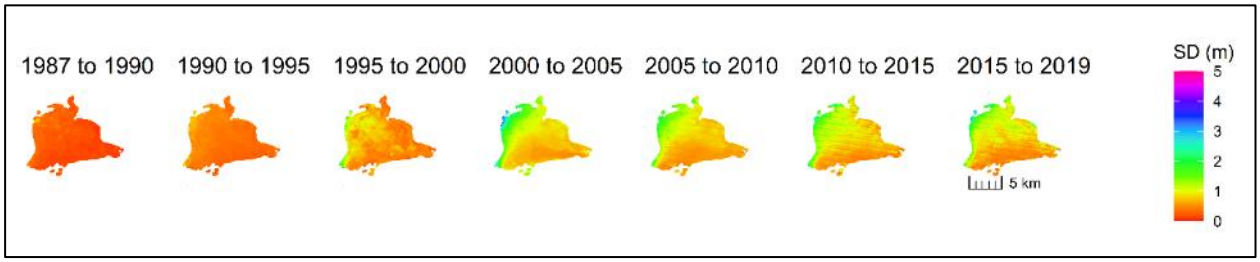

Figure 3.64. Spatial distribution of 5-year averaged SD in Lake Semayang

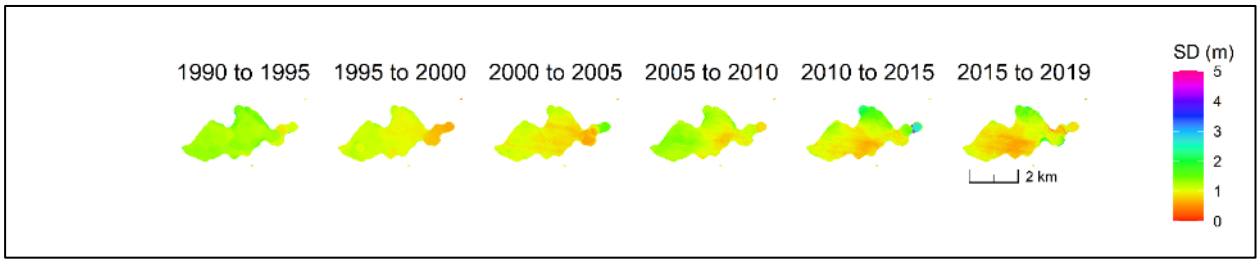

Figure 3.65. Spatial distribution of 5-year averaged SD in Lake Sempor (reservoir)

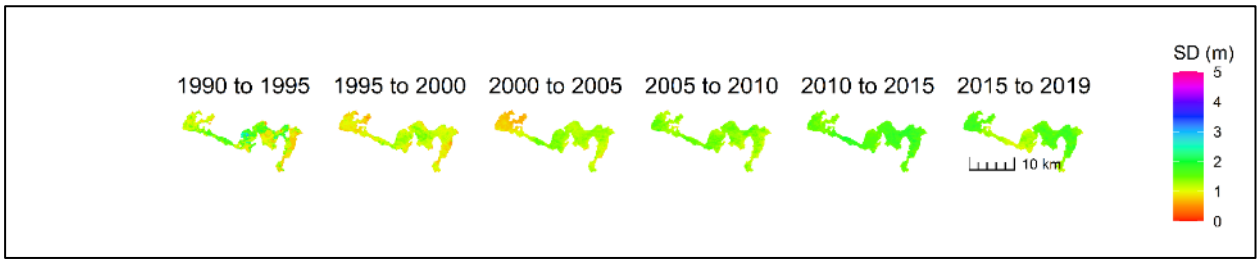

Figure 3.66. Spatial distribution of 5-year averaged SD in Lake Sentani

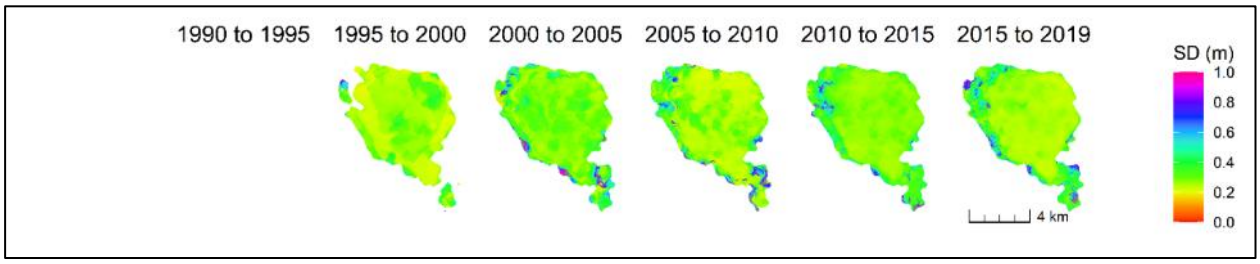

Figure 3.67. Spatial distribution of 5-year averaged SD in Lake Sidenreng

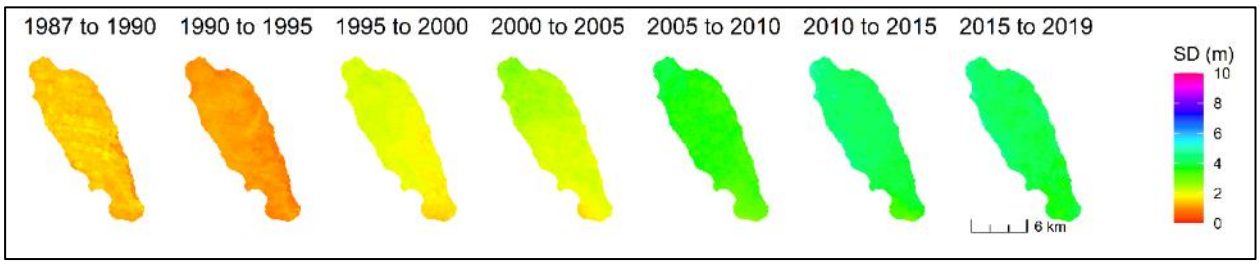

Figure 3.68. Spatial distribution of 5-year averaged SD in Lake Singkarak

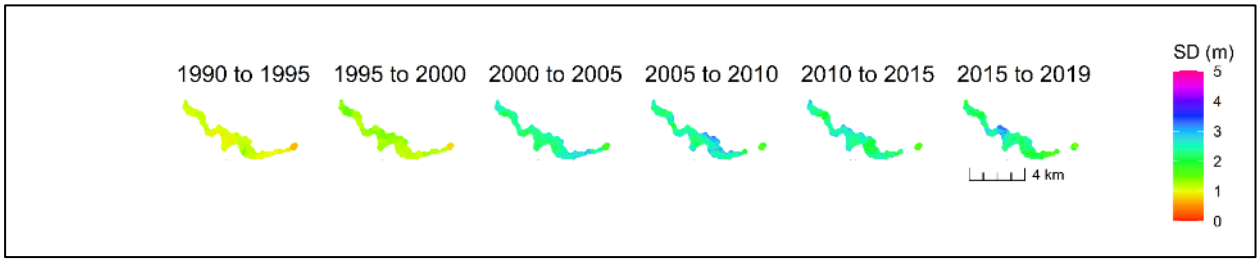

Figure 3.69. Spatial distribution of 5-year averaged SD in Lake Sutami (reservoir)

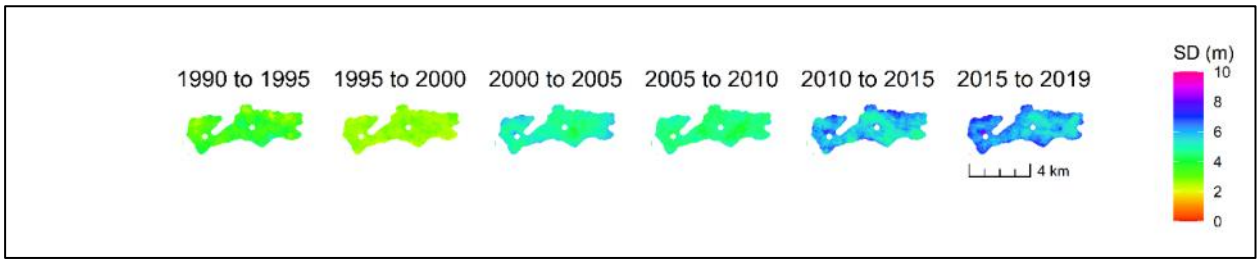

Figure 3.70. Spatial distribution of 5-year averaged SD in Lake Tasikdalambesar

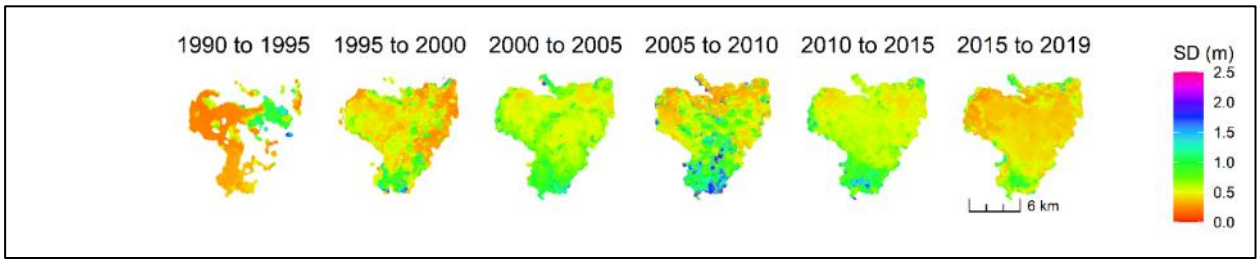

Figure 3.71. Spatial distribution of 5-year averaged SD in Lake Tempe

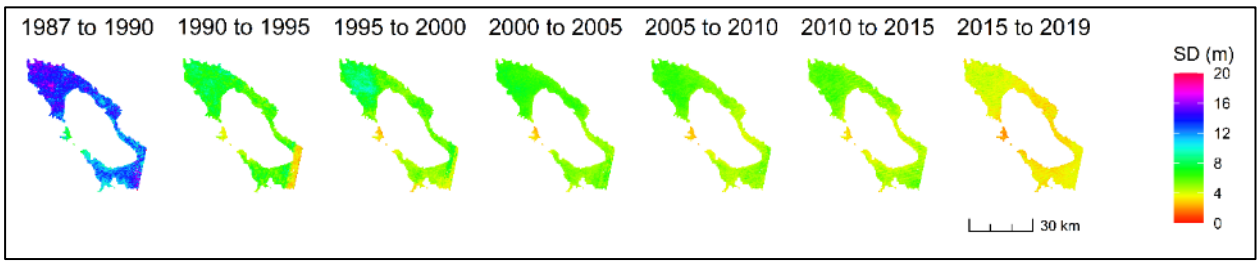

Figure 3.72. Spatial distribution of 5-year averaged SD in Lake Toba

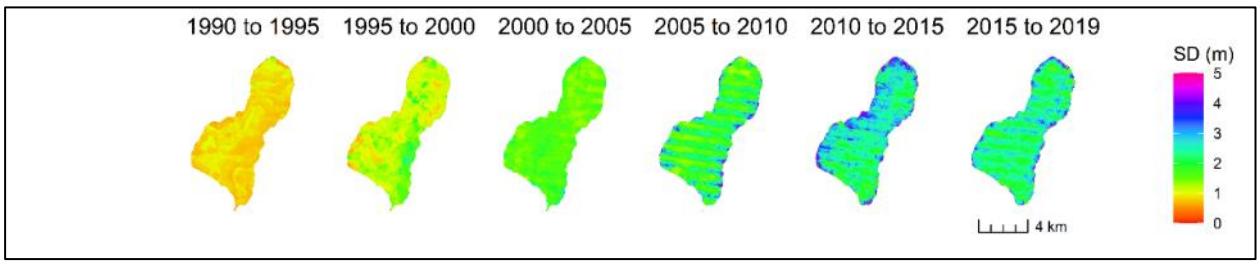

Figure 3.73. Spatial distribution of 5-year averaged SD in Lake Tondano

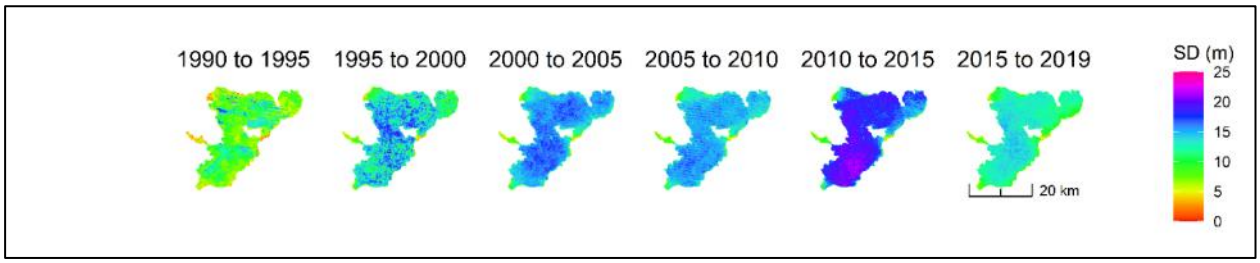

Figure 3.74. Spatial distribution of 5-year averaged SD in Lake Towuti

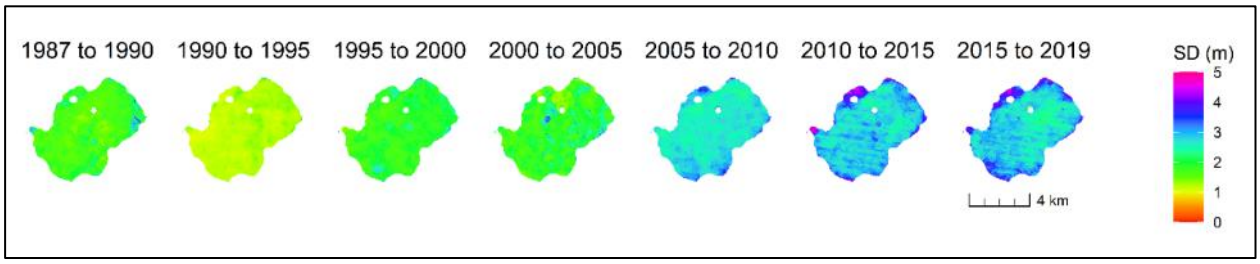

Figure 3.75. Spatial distribution of 5-year averaged SD in Lake Yamur

3.3.5. 20-year SD changes in 35 Indonesian Lakes (2000-2019)

To analyze the temporal variation in SD for Indonesian lakes, I selected the period from 2000 to 2019 and compared the lakes' SD changes. By calculating the linear trend of long-term change SD in Figures 3.6, 3.8 – 3.41, I found three SD changing trends. In which 14 lakes showed no significant changes ($P > 0.05$), 13 lakes showed significantly increased SD (positive slope, $P < 0.05$), and eight lakes showed significantly decreased SD (negative slope, $P < 0,05$) during 2000-2019. Table 3.3. provide the name of lakes grouped by the SD changing trend.

Table 3.3. SD changing trends in 35 Indonesian lakes

No.	SD changing trend		
	No significant change	Significantly Increased (change degree in %)	Significantly decreased (change degree in %)
1.	Diatas	Kerinci (16.20)	Batur (-39.12)
2.	Dibawah	Lindu (39.12)	Limboto (-53.97)
3.	Jempang	Matano (32.25)	Maninjau (-23.59)
4.	Luar	Ranau (11.82)	Tempe (-21.31)
5.	Melintang	Sentani (54.14)	Toba (-35.18)
6.	Paniai	Singkarak (119.02)	Towuti (-5.11)
7.	Poso	Tasikdalam (28.62)	Cacaban Resv. (-56.25)
8.	Rawapening	Tondano (63.48)	Kedungombo Resv. (-34.39)
9.	Semayang	Cirata Resv. (47.38)	
10.	Sidenreng	Gajahmungkur Resv. (99.74)	
11.	Yamur	Jatiluhur Resv. (20.16)	
12.	Sempor (R)	Merica Resv. (38.10)	
13.	Sutami (R)	Saguling Resv. (213.75)	
14.	Wadaslintang (R)		

Among the lakes with a significantly increased SD, the Saguling reservoir has the highest increased degree (SD increased 213.75 %). In comparison, Lake Ranau has the lowest increased degree (SD increased 11.82 %). Among the lakes with a significantly decreased SD, the Cacaban reservoir has the highest decreased degree (SD decreased -56.25 %). In comparison, Lake Ranau has the lowest decreased degree (SD decreased -5.11 %).

3.4. Discussion

The developed model was applied to different Indonesian lakes across time and space. The results demonstrate that SD can be reasonably estimated over various waters, spanning over a wide range of SD values (0.03 – 17.5 m) using the developed model (Figures 3.4 and 3.5). These results increase the confidence to enhance the Landsat image's usefulness along with the developed model to estimate time-series SD in Indonesian lakes. The developed model was then used to generate a long-term SD database in Lake Maninjau, Lake Singkarak, and Lake Toba for further validation. The generated long-term SD database well capture water transparency's change tendency in these three lakes (Figures 3.6, 3.8, and 3.9) and further demonstrate the reliability of the Landsat based long-term SD database.

Thus, in this research, it was created the first long-term SD database in 35 Indonesian lakes. This database enables to monitor water quality changes in Indonesian inland waters and provides higher spatial and temporal coverage to address data scarcity issues using remote sensing data as suggested by previous researches (Olmanson et al., 2008; Kutser., 2012; Blake et al., 2013; Lobo et al., 2015). Therefore, this database can provide useful information for lake managers and policymakers to support inland water's sustainable management. This SD database is also expected to provide a global level evaluation report for SDG 6.3.2, as proposed by Shen et al. (2020).

Binding et al. (2015) reported remarkable and complex changes in SD in North America's Great Lakes from multi-sensor satellite observations. Over the last several decades, the change was driven by invasive species, eutrophication, and implemented nutrient management practices. Meanwhile, in my research, I found three patterns of SD change trend: significantly increased SD, significantly decreased SD, and no significant change SD during the period between 2000-2019.

Visual observation on the generated SD database from figure 3.6, 3.8 – 3.41 identified three SD seasonal changes: noticeable seasonal changes, disguised (not so clear) seasonal changes, and no seasonal SD changes. Lakes with noticeable seasonal SD changes, including nine reservoirs (i.e., Cacaban, Cirata, Gajahmungkur, Jatiluhur, Merica, Saguling, Sempor, Sutami,

Wadaslintang) and 17 natural lakes (i.e., Batur, Diatas, Dibawah, Jempang, Limboto, Lindu, Luar, Melintang, Paniai, Poso, Ranau, Rawapening, Semayang, Tasikdalam, Tempe, Towuti and Yamur). Lakes with disguised seasonal SD changes, including one reservoir (Kedungombo) and five natural lakes (i.e., Kerinci, Matano, Sentani, Sidenreng, Tondano). Meanwhile, three natural lakes showed no seasonal SD changes (i.e., Maninjau, Singkarak, Toba).

Visual observation on the generated 5-year averaged SD map from figure 3.42, 3.75 identified two spatial SD homogeneity: homogenous and inhomogeneous. Lakes with apparent homogenous spatial SD spatial distribution, including three reservoirs (i.e., Merica, Saguling, Wadaslintang) and ten natural lakes (i.e., Diatas, Dibawah, Lindu, Maninjau, Matano, Poso, Ranau, Singkarak, Tondano, Towuti). Lakes with apparent inhomogeneous spatial SD spatial distribution, including seven reservoirs (i.e., Cacaban, Cirata, Gajahmungkur, Jatiluhur, Kedungombo, Sempor, Sutami) and 15 natural lakes (i.e., Batur, Jempang, Kerinci, Limboto, Luar, Melintang, Paniai, Rawapening, Semayang, Sentani, Sidenreng, Tasik Dalam, Tempe, Toba, Yamur).

Low SD regions identified at the inflow river of eight reservoirs (i.e., Cacaban, Cirata, Gajahmungkur, Jatiluhur, Kedungombo, Saguling, Sempor and Wadaslintang), and 12 natural lakes (i.e., Batur, Jempang, Kerinci, Limboto, Luar, Melintang, Poso, Rawapening, Semayang, Sentani, Singkarak, Toba). Generally, high SD regions are located in the lake offshore.

3.5. Conclusions

This chapter aimed to confirm whether the developed model can estimate reasonable SD, verify the reasonableness of the generated SD database, and show the SD changes of large Indonesian lakes using the generated database. Based on the boxplot analysis, it is concluded that the developed model can estimate reasonable SD values in various waters. The qualitative analysis in three selected lakes further confirmed the reasonableness of the generated SD database. Therefore, the SD database of large Indonesian lakes has been generated reliably, and the SD changes can be shown.

Chapter IV General Conclusions

A robust empirical model for estimating SD from Landsat TM/ETM+ data was developed in this research. The Landsat data preprocessing procedure and the use of two-band ratios are the main efforts to improve the robustness of the developed model. The developed model suggested the use of the two-band ratios of TM1/TM2 and TM3/TM2 as the SD predictor to reduce uncertainties in the model. This suggestion differs from the recommendations in previous studies.

I confirmed that the developed model could estimate a reasonable SD for several lakes and verify the reasonableness of the generated SD database. Next, I generated the first long-term SD database for 35 large Indonesian lakes and showed the SD changes. This information is expected to be useful to support inland water sustainable management. In the future, I will analyze what determinants regulate the changes in SD in Indonesian lakes.

Overall, although the Landsat TM and ETM+ were designed as Land specific sensors, by several efforts, this research demonstrates the high values of TM/ETM+ as data sources for historical water quality studies. For future studies, a Semi-Analytical model for estimating SD using medium resolution sensors (e.g., MERIS and or Sentinel-3) and newer sensors (Landsat-8 OLI and Sentinel-2 MSI) is expected to be used to validate the generated SD database further. The use of various remote sensing data will increase the data density and allow a more comprehensive understanding of the aquatic environment.

Acknowledgment

I would like to express my gratitude to my supervisor, Prof. Matsushita Bunkei, for his full scientific support for assisting my research at the University of Tsukuba, Japan. He allowed me to join in various field surveys, International Academic Conferences, and many scientific events. He always encourages me to boost up my skill and knowledge in the Remote sensing field. He always allocates his time to discuss my research, well-read my manuscript. His patient guidance, suggestion, and shared knowledge are beneficial for my future work.

I want to express gratitude to the thesis committee members, Prof. Fukushima Takehiko, Prof. Nasahara Kenlo, and Prof. Kato Hiroaki, for their valuable-constructive questions, comments, and suggestions.

I always debt to Mrs. Suzuki Mika for her help in the laboratory work and many administrative documents. Many thanks to Dr. Kawamura Shimako for her support in PC and related software, Mr. Rossi Hamzah, and Dr. Jiang Dalin for their help in programming. Also, Dr. Pok Sophak, Dr. Vundo Augusto, and all Laboratory members for their valuable time for discussion.

I would like to thank the United States Geological Survey (USGS) for providing Landsat data, Dr. Luki Subehi, from the Indonesian Institute of Sciences (LIPI) for helping me collect the in situ data of Indonesian lakes.

I appreciate the Government of Japan, the Ministry of Education, Culture and Sports, Sciences, and Technology (MEXT) for providing me the scholarship.

I express special gratitude to my parents, my wife, and my daughters, for their love and kind support.

References

Badan Pusat Statistik Kabupaten Agam. (2016). Agam in Figures 2015. Available online: https://agamkab.bps.go.id/publication/2016/01/27/9e1bdfeacc59787c00e6a53e/kabupaten-agam-dalam-angka-2015.html (accessed on 15 February 2019)

Badan Pusat Statistik Kabupaten Agam. (2017). Agam in Figures 2016. Available online: https://agamkab.bps.go.id/publication/2016/07/15/3a4ed5ae43c41906b939bf50/kabupaten-agam-dalam-angka-2016.html (accessed on 15 February 2019)

Badan Pusat Statistik Kabupaten Agam. (2018). Agam in Figures 2017. Available online: https://agamkab.bps.go.id/publication/2017/08/11/2ef8e1564e24faf29cd9ebd4/kabupaten-agam-dalam-angka-2017.html (accessed on 15 February 2019)

Badan Pusat Statistik Kabupaten Agam. (2019). Agam in Figures 2018. Available online: https://agamkab.bps.go.id/publication/2018/08/16/61f234670dec4ca6f38c0024/kabupaten-agam-dalam-angka-2018.html (accessed on 15 February 2019)

Blake A. Schaeffer, Kelly G. Schaeffer, Darryl Keith, Ross S. Lunetta, Robyn Conmy & Richard W. Gould. (2013). Barriers to adopting satellite remote sensing for water quality management. International Journal of Remote Sensing, 34:21, 7534-7544, DOI: 10.1080/01431161.2013.823524

Blondeau-Patissier, D.; Gower, James F.R.; Dekker, Arnold G.; Phinn, Stuart R.; Brando, Vittorio E. (2014). A review of ocean color remote sensing methods and statistical techniques for the detection, mapping and analysis of phytoplankton blooms in coastal and open oceans. Progress in Oceanography, 123, 123-144. http://dx.doi.org/10.1016/j.pocean.2013.12.008

Bonansea, M.; Ledesma, C.; Rodríguez, C.; Pinotti, L.; Antunes, H.M. (2015). Effects of atmospheric correction of Landsat imagery on lake water clarity assessment. Advances In Space Research, 56, 2345-2355. https://doi.org/10.1016/j.asr.2015.09.018

Bonansea, M.; Rodríguez, C.; Pinotti, L.; Ferrero., S. (2016). Using multi-temporal Landsat imagery and Linear mixed models for assessing water quality parameters in Rio Tercero reservoir (Argentina). Remote Sens. Environ. 158, 28-41. https://doi.org/10.1016/j.rse.2014.10.032

Brezonik, P.; Menken, K, D.; Bauer, Ma. (2005). Landsat-based Remote Sensing of Lake Water Quality Characteristics, Including Chlorophyll and Colored Dissolved Organic Matter (CDOM). Lake and Reservoir Management, 21 (4), 373-382. https://doi.org/10.1080/07438140509354442

Brönmark, C., & Hansson, L. (2002). Environmental issues in lakes and ponds: Current state and perspectives. Environmental Conservation, 29(3), 290-307. doi:10.1017/S0376892902000218

Butt, M.J and Nazeer, M. (2015). Landsat ETM+ Secchi Disc Transparency (SDT) retrievals for Rawal Lake, Pakistan. Advances in Space Research, 56, 1428-1440. http://dx.doi.org/10.1016/j.asr.2015.06.041

Carlson, R.E. (1977). A trophic state index for lakes. Limnology and Oceanography, 22,361-369.

Carslaw, D. C., and Ropkins, K. (2012). Openair - an R package for air quality data analysis. Environmental Modelling & Software, Volume 27-28, 52-61.

Chander, G., Markham, B., and Dennis, D, L. (2009). Summary of current radiometric calibration coefficients for Landsat MSS, TM, ETM+, and EO-1 ALI sensors. Remote Sens. Environ, 113, 893-903 https://doi.org/10.1016/j.rse.2009.01.007

Cox, R.M.; Forsythe, R.D.; Vaughan, G.E.; Olmsted, L. L. (1998). Assessing water quality in the Catawba river reservoirs using Landsat thematic mapper satellite data. Lake Reservoir Management 1998, 14, 405–416. https://doi.org/10.1080/07438149809354347

Cristina, S., Cordeiro, C., Lavender, S., Costa Goela, P., Icely, J., & Newton. (2016). A. MERIS phytoplankton time series products from the SW Iberian Peninsula (Sagres) using seasonal-trend decomposition based on loess. Remote Sensing, 8(6), 449.

Dall'Olmo, G., Gitelson, A., & Rundquist, D. C. (2003). Towards a unified approach for remote estimation of chlorophyll-a in both terrestrial vegetation and turbid productive waters. Geophys. Res. Lett., 30.

Devlin, M. J., Barry, J., Mills, D. K., Gowen, R. J., Foden, J., Sivyer, D., et al. (2008). Relationships between suspended particulate material, light attenuation and Secchi depth in UK marine waters. Estuar. Coast. Shelf Sci. 79, 429–439. doi: 10.1016/j.ecss.2008.04.024

Dörnhöfer, K., and Oppelt, N. (2016). Remote sensing for lake research and monitoring. Recent advances. Ecological Indicators, 64, 105-122. https://doi.org/10.1016/j.ecolind.2015.12.009

Doron, M., Babin, M., Hembise, O., Mangin, A., Garnesson, P. (2011). Ocean transparency from space: validation of algorithms using MERIS, MODIS and SeaWiFS data. Remote Sens. Environ. 115, 2986-3001.

Doxaran, D., Froidefond, JM., and Castaing, P. (2002). A reflectance band ratio used to estimate suspended matter concentrations in sediment-dominated coastal waters. Int. J. Remote Sens, 23, 5079–5085 https://doi.org/10.1080/0143116021000009912

Doxaran, D., Froidefond, JM., and Castaing, P. (2003). Remote-sensing reflectance of turbid sediment-dominated waters. Reduction of sediment type variations and changing illumination conditions effects by use of reflectance ratios. Applied Optics, 42 (15), 2623-2634 https://doi.org/10.1364/AO.42.002623

Duan, H., MA, R., Zhang, Y. and Zhang, B. (2009). Remote-sensing assessment of regional inland lake water clarity in northeast China. Limnology, 10, pp. 135–141.

Duntley, S. Q. (1952). The visibility of submerged objects; Visibility Lab., Mass. Inst. Tech. San Diego, CA, USA.74.

Fakhrudin, M.; Wibowo, H.; Subehi, L and Ridwansyah, I. (2002) Karakterisasi Hidrologi Danau Maninjau Sumatera Barat. Prosiding Seminar Nasional Limnologi 2002, Bogor, Indonesia, 22 April 2002, Pusat Penelitian Limnologi – LIPI, Bogor, Indonesia, 65 – 75.

Febrianti. (2000). Attack of the Algae at Lake Maninjau. Tempo: Indonesia's Weekly News Magazine; Jakarta, 19 November 2000.

Gholizadeh, M, H.; Melesse, A, M.; Reddi, L. (2016). A Comprehensive Review on Water Quality Parameters Estimation Using Remote Sensing Techniques. Sensors, 16, 1298. https://doi.org/10.3390/s16081298

Giardino, C.; Pepe, M.; Brivio, P.A.; Ghezzi, P.; Zilioli, E. (2001). Detecting chlorophyll, Secchi disk depth and surface temperature in a sub-alpine lake using Landsat imagery. Science of the Total Environment, 268, 19–29. DOI: 10.1016/S0048-9697(00)00692-6

Gilerson, A., Gitelson, A., Zhou, J., Gulrin, D., Moses, W., Ioannou, I., & Ahmed, S. (2010). Algorithms for remote sensing of chlorophyll-a in coastal and inland waters using red and near infrared bands. Optics Express, 18, 24109–24125.

Gitelson, A., Dall'Olmo, G., Moses, W., Rundquist, D. C., Barrow, T., Fisher, T. R. et al. (2008). A simple semi-analytical model for remote estimation of chlorophyll-a in turbid waters: Validation. Remote Sensing of Environment, 112, 3582–3593.

Gower, J., King, S., Borstad, G., & Brown, L. (2005). Detection of intense plankton blooms using the 709 nm band of the MERIS imaging spectrometer. International Journal of Remote Sensing, 26, 2005–2012.

Hamzah, R. (2019). 'Long-Term Monitoring of Lake Surface Area Change in Indonesia from Global Surface Water Data', Master thesis, University of Tsukuba, Tsukuba

Henny, C., and Nomosatryo, S. (2016). Changes in water quality and trophic status associated with aquaculture in Lake Maninjau, Indonesia. IOP Conf. Ser.: Earth Environ. SCi. 31 022027, doi: 10.1088/1755-1315/31/1/012027

Jiang, B., Liang, S., Wang, J., and Xiao, Z. (2010). Modeling MODIS LAI time series using three statistical methods. Remote Sens. Environ, 114(7), 1432-1444.

Junaidi.; Syandri, H., and Azrita. (2014). Loading and Distribution of Organic Materials in Maninjau Lake West Sumatra Province-Indonesia. J. Aquac. Res. Development, 5:7, 1-4. doi:10.4172/2155-9546.1000278

Kallio, K., Attila, J., Harma, P., Koponen, S., Pullianen, J., Hyytiainen, U.M., and Pyhalahti, T. (2008). Landsat ETM images in the estimation of seasonal lake water quality in boreal river basins. Environmental Management, 42, pp. 511–522.

Karydis, M. (2009). Eutrophication assessment of coastal waters based on indicators: a literature review. Global Nest J., 11,373–90. Available online at: https://pdfs.semanticscholar.org/b9f3/8d962258fd7426ed07352c5829c7e1380a2e.pdf

Kloiber, S. M., Brezonik, P.L., and Bauer, ME. (2002). Application of Landsat imagery to regional-scale assessment of lake clarity. Water Research, 26, 4330-4340.

Kutser, T. (2012). The possibility of using the Landsat image archive for monitoring long time trends in coloured dissolved organic matter concentration in lake waters. Remote Sens. Environ, 123, 334-338. https://doi.org/10.1016/j.rse.2012.04.004

Kutser, T., Metsamaa, L., Strombeck, N., & Vatmae, E. (2006). Monitoring cyanobacterial blooms by satellite remote sensing. Estuarine, Coastal and Shelf Science, 67, 303–312.

Landsat Science-Landsat 5. (n.d.). Last Accessed January 9, 2021, from https://landsat.gsfc.nasa.gov/landsat-5/landsat-8-overview

Landsat Science-Landsat 7. (n.d.). Last Accessed January 9, 2021, from https://landsat.gsfc.nasa.gov/landsat-7/landsat-8-overview

Landsat Science-Landsat 8. (n.d.). Last Accessed January 9, 2021, from https://landsat.gsfc.nasa.gov/landsat-8/landsat-8-overview

Lathrop, R.G. (1992). Landsat thematic mapper monitoring of turbid inland water quality. Photogramm. Eng. Remote Sens, 58, 465–470.

Lavery, P; Pattiaratchi, C.; Wyllie, A.; Hick, P. (1993). Water quality monitoring in estuarine waters using the Landsat thematic mapper. Remote Sens. Environ, 46.3, 268-280. https://doi.org/10.1016/0034-4257(93)90047-2

Lee, Z., Shang, S., Hu, C., Du, K., Weidemann, A., Hou, W., Lin, J., Lin, G. (2015). Secchi disk depth: a new theory and mechanistic model for underwater visibility. Remote Sens. Environ, 169, 139–149. http://dx.doi.org/10.1016/j.rse.2015.08.002.

Lee, Z.; Carder, K.L.; Arnone, R.A. (2002). Deriving inherent optical properties from water color: a multiband quasi-analytical algorithm for optically deep waters. Appl. Opt., 41 (27), 5755–5772. https://doi.org/10.1364/AO.41.005755

Lee, Z.; Shang, S.; Qi, L.; Yan, J.; Lin, G. (2016). A semi-analytical scheme to estimate Secchi-disk depth from Landsat-8 measurements. Remote Sens. Environ, 177, 101–106. http://dx.doi.org/10.1016/j.rse.2016.02.033

Lehmusluoto, P.; Machbub, B, Terangna, N.; Rusmiputro, S.; Achmad, F.; Boer, L.; Brahmana, S.; Priadi, B.; Setiadji, B.; Sayuman, O.; Margana. (1997). National inventory of the major lakes and reservoirs in Indonesia. General Limnology. Revised Edition.; Bandung and Helsinki; pp. 1-71.

Lobo, Felipe L.; Costa, Maycira P.F.; Novo, Evlyn M.L.M. (2015). Time-series analysis of Landsat-MSS/TM/OLI images over Amazonian waters impacted by gold mining activities. Remote Sens. Environ, 157, 170-184. http://dx.doi.org/10.1016/j.rse.2014.04.030

Lu, H., Raupach, M. R., McVicar, T. R., & Barrett, D. J. (2003). Decomposition of vegetation cover into woody and herbaceous components using AVHRR NDVI time series. Remote Sens. Environ, 86(1), 1-18.

Matthews, M.W. (2011). A current review of empirical procedures of remote sensing in inland and near-coastal transitional waters, International Journal of Remote Sensing, 32:21, 6855-6899, DOI: 10.1080/01431161.2010.512947

Mauricio, Z. B. (2017). hydroGOF: Goodness-of-fit functions for comparison of simulated and observed hydrological time series, R package version 0.3-10. http://hzambran.github.io/hydroGOF/. DOI:10.5281/zenodo.840087.

McFeeters, S. K. (1996). The use of normalized difference water index (NDWI) in the delineation of open water features. International Journal of Remote Sensing, 17, 1425–1432 https://doi.org/10.1080/01431169608948714

Ministry of Environment of the Republic of Indonesia. (2011). Profil 15 Danau Prioritas Nasional; Kementerian Lingkungan Hidup Republik Indonesia, Indonesia; pp. 1-148.

Nash, J.E. and Sutcliffe, J.V. (1970). River Flow Forecasting Through Conceptual Models Part I: A Discussion of Prinicples. Journal of Hydrology, 10 (3), 282-290. http://dx.doi.org/10.1016/0022-1694(70)90255-6

Nichol, J.E and Vohora, V. (2004). Noise over water surface in Landsat TM images. International Journal of Remote Sensing, 25 (11), 2087-2094. http://dx.doi.org/10.1080/01431160310001618770

Nomosatryo, S. and Lukman. (2012). Klasifikasi Trofik Danau Toba, Sumatera Utara. LIMNOTEK, 19 (1), 13-21.

Ocean Color-GOCI. (n.d). Last Accessed January 9, 2021, from https://oceancolor.gsfc.nasa.gov/data/goci/

Ocean Color-MODIS Aqua. (n.d.). MODIS Aqua, Last Accessed January 9, 2021, from https://oceancolor.gsfc.nasa.gov/data/aqua/

Ocean Color-SeaWiFS. (n.d.). SeaWiFS, Last Accessed January 9, 2021, from https://oceancolor.gsfc.nasa.gov/data/seawifs/

Olmanson, L. G.; Bauer, M. E.; & Brezonik, P. L. (2008). A 20-year Landsat water clarity census of Minnesota's 10,000 Lakes. Remote Sensing of Environment, 112, 4086–4097. https://doi.org/10.1016/j.rse.2007.12.013

Olmanson, L. G.; Brezonik, P. L.; Bauer, M. E. (2011). Evaluation of medium to low resolution satellite imagery for regional lake water quality assessments. Water Resour. Res, 47, W09515. https://doi.org/10.1029/2011WR011005.

Olmanson, L. G.; Brezonik, P. L.; Finlay, J.C.; and Bauer, M. E. (2016). Comparison of Landsat 8 and Landsat 7 for regional measurements of CDOM and water clarity in lakes. Remote Sens. Environ, 185, 119-128. https://doi.org/10.1016/j.rse.2016.01.007

Oyama, Y.; Matsushita, B.; Fukushima, T.; Matsushige, K.; Imai, (2009). A. Application of spectral decomposition algorithm for mapping water quality in a turbid lake (Lake Kasumigaura, Japan) from Landsat TM data. ISPRS Journal of Photogrammetry and Remote Sensing, 64(1), 73-85. https://doi.org/10.1016/j.isprsjprs.2008.04.005

Pattiaratchi, C., Lavery, P., Wyllie, A., and Hick, P. (1994). Estimates of water quality in coastal waters using multi-date Landsat Thematic Mapper data. International Journal of Remote Sensing, 15, pp. 1571–1584

Poros, D.J., and Petersen, C.J. (1985). A method for destriping Landsat Thematic Mapper images: a feasibility study for an online destriping process in the Thematic Mapper image processing System (TIPS). Photogrammetric Engineering and Remote Sensing, 51, 1371–1378.

Preisendorfer, R. W. (1986). Secchi Disk Science: Visual Optics of Natural Waters. Limnology and Oceanography, 31(5), 909-926

R Core Team. (2018). R: A language and environment for statistical computing. R Foundation for Statistical Computing, Vienna, Austria. https://www.R-project.org/.

Risdawati, Renny. (2011). Cirolana sp Salah Satu Endoparasit Di Danau Singkarak Sumatera Barat. Jurnal Pelangi, Vol. 3 No.2 Juni 2011 (103-108). http://dx.doi.org/10.22202/jp.2011.v3i2.24

Rodrigues, T.; Alcantara, E.; Watanabe, F.; Imai, N. (2017). Retrieval of Secchi disk depth from a reservoir using a semi-analytical scheme. Remote Sens. Environ, 198, 213–228. https://doi.org/10.1016/j.rse.2017.06.018

Ruttner, F. (1930). Hydrographische und Hydrochemishe Beobachtungen auf Java, Sumatera und Bali. Arch. Hydrobiol. Suppl, 8: pp. 197-454.

Ryu, J. H., Han, H. J., Cho, S., Park, Y. J., & Ahn, Y. H. (2012). Overview of Geostationary Ocean Color Imager (GOCI) and GOCI Data Processing System (GDPS). Ocean Science Journal, 47, 223–233.

Secchi, P. A. (1864). Relazione delle esperienze fatte a bordo della Pontificia pirocorvetta Imacolata Concezione per determine la transparenza del mare. Memoria del PA Secchi. Il nuovo Cimento Giornale de Fisica, Chimica e Storia Naturale, Ottobre 1864, Published 1865, 20, 205-237

Shen, M.; Duan, H.; Cao, Z.; et al. (2020) Sentinel-3 OLCI observations of water clarity in large lakes in eastern China: Implications for SDG 6.3.2 evaluation. Remote Sensing of Environment, 247, 111950. https://doi.org/10.1016/j.rse.2020.111950

Sriwongsitanon, N.; Surakit, K.; Thianpopirug, S. (2011). Influence of atmospheric correction and number of sampling points on the accuracy of water clarity assessment using remote sensing application. J. Hydrol, 401 (3–4), 203–220. https://doi.org/10.1016/j.jhydrol.2011.02.023

Sulastri. (2002). Spatial and Temporal Distribution of Phytoplankton in Lake Maninjau, West Sumatera. Proceeding of the International Symposium on Land Management and Biodiversity in South East Asia. Bali, Indonesia, 17-20 September; 403-408.

Sulastri. (2006). Inland water resources and limnlology in Indonesia. Tropics, 15 (3), pp.285-295 https://doi.org/10.3759/tropics.15.285

Taylor, K.E. (2001). Summarizing multiple aspect of model performance in a single diagram. Journal of Geophysical Research: Atmospheres, 106 (D7), 7183 -7192.

The European Space Agency-MERIS. (n.d.). Last Accessed January 9, 2021, from https://earth.esa.int/eogateway/instruments/meris/

The European Space Agency-Sentinel-2. (n.d.). Last Accessed January 9, 2021, from https://sentinel.esa.int/web/sentinel/missions/sentinel-2

The European Space Agency-Sentinel-3. (n.d.). Last Accessed January 9, 2021, from https://sentinel.esa.int/web/sentinel/missions/sentinel-3

UN, 2015. Transforming our World: The 2030 Agenda for Sustainable Development. United Nations, New York.

UN-Water, 2017. Integrated Monitoring Guide for SDG 6 - Targets and Global Indicators. New York.

UN-Water, 2018. Piloting the Monitoring Methodology and Initial Findings for SDG Indicator 6.3.2. UN-Water, New York.

USGS Earth Explorer. (2019). Available online: https://earthexplorer.usgs.gov/ (last accessed on 11 March 2019)

Vermote, E.F., Tanré, D., Deuzé, J.L., Herman, M., Morcrette, J.L. (1997). Second Simulation of the Satellite Signal in the Solar Spectrum, 6S: An Overview. IEEE Transactions on Geoscience and Remote Sensing 1997, 35(3), 675-686.

Wang, Shenglei., Lia, Junsheng., Zhanga, Bing., Spyrakos, Evangelos., Tyler, Andrew N., Shena, Qian., Zhanga, Fangfang., Kusterd Tiit., Lehmanne Moritz K., Wua, Yanhong and Peng, Dailiang. (2018). Trophic state assessment of global inland waters using a MODIS-derived Forel-Ule index. Remote Sens. Environ, 217, 444-460

Wickham, H. (2016). ggplot2: Elegant Graphics for Data Analysis. Springer-Verlag New York.

Willmott, C.J. (1981). On the Validation of Models. Physical Geography, 2, 184-194.

World Bank. (2019). "Better Data, Better Results: Remote Sensing as a Tool for Monitoring Water Quality in Lake Toba, Indonesia." World Bank, Washington, DC.

Wu, G.G., De-Leew, J., Skidmore, A.K., Prins, H.H.T. and Liu, Y. (2008). Comparison of Modis and Landsat TM5 images for mapping tempo-spatial dynamics of Secchi disk depths in Poyang Lake national nature reserve, China. International Journal of Remote Sensing, 29, pp. 2183–2198.

Xu, H. (2006). Modification of normalized difference water index (NDWI) to enhance open water features in remotely sensed imagery. International Journal of Remote Sensing, 27, 3025–3033. https://doi.org/10.1080/01431160600589179

Yang, W.; Matsushita, B.; Chen, J.; Yoshimura, K.; Fukushima, T. (2013). Retrieval of inherent optical properties for turbid inland waters from remote-sensing reflectance. IEEE Transactions on Geoscience and Remote Sensing, 51 (6), 3761–3773. https://doi.org/10.1109/TGRS.2012.2220147

Zhao, D.; Cai, Y.; Jiang, H.; Xu, D.; Zhang, W.; An, S. (2011). Estimation of water clarity in Taihu Lake and surrounding rivers using Landsat imagery. Adv. Water Resour., 34 (2), 165–173. https://doi.org/10.1016/j.advwatres.2010.08.010

Zheng, Z.; Li, Y.; Guo, Y.; Xu, Y.; Liu, G.; Du, C. (2015). Landsat-Based Long-Term Monitoring of Total Suspended Matter Concentration Pattern Change in the Wet Season for Dongting Lake, China. Remote Sensing, 7, 13975-13999. https://doi.org/10.3390/rs71013975